# Immunological and translational consequences of an altered $CD8^+$ T cell cytolytic activity

Inaugural-Dissertation
to obtain the academic degree
Doctor rerum naturalium (Dr. rer. nat.)

submitted to the Department of Biology, Chemistry and Pharmacy
of Freie Universität Berlin

by

**Anthea Wirges**

2018

Die vorliegende Arbeit wurde in der Zeit vom Juli 2014 bis Dezember 2018 in der Arbeitsgruppe „Translationale Tumorimmunologie“ unter der Leitung von Dr. Armin Rehm am „Max-Delbrück-Centrum für Molekulare Medizin“ in der Helmholtz-Gemeinschaft in Berlin angefertigt.

1. Gutachter: Dr. Armin Rehm
2. Gutachter: Prof. Dr. Oliver Daumke

Disputation: 06.05.2019

# I Abbrevations

| | |
|---|---|
| **-** | **--** |
| °C | Degree celsius |
| 7-AAD | 7-amino-actinomycin D |
| **A** | **--** |
| Ad | Up to |
| AF | Alexa Fluor |
| Ago | Argonaut |
| ALL | Acute lymphoblastic leukemia |
| AP-1 | Activator protein 1 |
| APC | Antigen-presenting cell |
| APC | Allophycocyanin |
| APC/Cy | Allophycocyanin/cyanin |
| ATT | Adoptive T cell transfer |
| **B** | **--** |
| B-NHL | B-cell non-Hodgkin lymphoma |
| BCL-2 | B cell lymphoma 2 |
| BCL-6 | B cell lymphoma 6 |
| BCMA | B cell maturation antigen |
| BCR | B cell receptor |
| BLIMP-1 | B lymphocyte-induced maturation protein 1 |
| BLOC-1 | Biogenesis of lysosome-related organelles complex 1 |
| BM | Bone marrow |
| BSA | Bovine serum albumin |
| BV | Brilliant violet |
| **C** | **--** |
| CAD | Caspase-activated DNase |
| CAR | Chimeric antigen receptor |
| Cbl-b | E3 ubiquitin ligase Casitas B-lineage lymphoma b |
| CCL | CC-chemokine ligand |
| CCR | CC-chemokine receptor |
| CD | Cluster of differentiation |
| cDNA | Complementary deoxyribonucleic acid |
| CMV | Cytomegalovirus |
| CRISPR | Clustered regularly interspaced short palindromic repeats |
| CRS | Cytokine release syndrome |

| | |
|---|---|
| CTL | Cytotoxic T cell |
| CTLA-4 | Cytotoxic T lymphocyte-associated protein 4 |
| **D** | **--** |
| d | Day |
| DC | Dendritic cell |
| DMEM | Dulbecco's Modified Eagle's Medium |
| DMSO | Dimethyl sulfoxide |
| DNA | Deoxyribonucleic acid |
| dNTP | Deoxynucleotide |
| dsRNA | double-stranded RNA |
| **E** | **--** |
| E:T | Effector to target |
| *E. coli* | *Escherichia coli* |
| EBAG9 | Estrogen receptor-binding fragment-associated antigen 9 |
| eGFP | Enhanced green fluorescent protein |
| ELISA | Enzyme-linked immunosorbent assay |
| Env | Envelope |
| EOMES | Eomesodermin |
| ER | Endoplasmic reticulum |
| *Et al.* | *Et alii* |
| **F** | **--** |
| FACS | Fluorescence-activated cell sorting |
| FasL | Fas Ligand |
| FCS | Fetal calf serum |
| FDA | U.S. Food and Drug Administration |
| FITC | Fluorescein isothiocyanate |
| FOXO1 | Forkhead box protein O1 |
| FSC | Forward scatter |
| **G** | **--** |
| Gag | Group-specific antigen |
| GalV | Gibbon ape leukemia virus |
| GAPDH | Glyceraldehyde 3-phosphate dehydrogenase |
| GDP | Guanosine diphosphate |
| gMFI | Geo mean fluorescence intensities |
| GTP | Guanosine triphosphate |
| GvHD | Graft-versus-host disease |
| **H** | **--** |

| | |
|---|---|
| h | Hour |
| HEPES | 4-(2-Hydroxyethyl)-piperazin-1-ethan-sulfonic acid |
| HLA | Human leukocyte antigen |
| HRP | Horseradish peroxidase |
| **I** | **--** |
| i.p. | Intraperitoneal |
| i.v. | Intravenously |
| ID | Inhibitor of DNA binding |
| IFN-γ | Interferon-γ |
| Ig | Immunoglobulin |
| IL | Interleukin |
| IVIS | *In vivo* imaging system |
| **J** | **--** |
| **K** | **--** |
| kDa | Kilodalton |
| KLRG1 | Killer cell lectin-like receptor 1 |
| **L** | **--** |
| LAG-3 | Lymphocyte-activation gene 3 |
| LCMV | Lymphocytic choriomeningitis virus |
| LPS | Lipopolysaccharide |
| LTR | Long terminal repeats |
| Luc | Luciferase |
| **M** | **--** |
| MACS | Magnetic activated cell sorting |
| mHag | Minor histocompatibility antigen |
| MHC | Major histocompatibility complex |
| min | Minutes |
| miRNA | micro RNA |
| MM | Multiple myeloma |
| mRNA | Messanger RNA |
| MTOC | Microtubule-organizing center |
| mTOR | Mammalian target of rapamycin |
| **N** | **--** |
| NK cell | Natural killer cell |
| NOD | Non-Obese Diabetic |
| ns | Not significant |
| NSG | NOD.Cg-Prkdcscid Il2rg tm1 Wjl/SzJ |

| | |
|---|---|
| **O** | **--** |
| OD | Optical density |
| **P** | **--** |
| P-Value | Probability-value |
| P/S | Penicillin-Streptomycin |
| PAMP | Pathogen-associated molecular pattern |
| PB | Pacific Blue |
| PBMC | Peripheral blood mononuclear cell |
| PBS | Phosphate buffered saline |
| PCR | Polymerase chain reaction |
| PD-1 | Programmed death protein 1 |
| PD-L1 | Programmed death ligand 1 |
| PE | Phycoerythrin |
| PerCP/Cy | Peridinin chlorophyll protein complex/cyanin |
| pH | Potential of hydrogen |
| PMA | Phorbol 12-myristate 13-acetate |
| Pol | Polymerase |
| **Q** | **--** |
| **R** | **--** |
| RAG | Recombinant-activating gene |
| RISC | RNA-induced silencing complex |
| RIN | RNA integrity number |
| RNA | Ribonucleic acid |
| RNAi | RNA interference |
| Rpm | Rounds per minute |
| RPMI 1640 | Roswell Park Memorial Institute 1640 |
| ROS | Reactive oxygen species |
| RUNX3 | Runt-related transcription factor 3 |
| **S** | **--** |
| scFV | Single chain variable fragment |
| SCID | Severe combined immunodeficient |
| SDS | Sodium dodecyl sulfate |
| SEM | Standard error of the mean |
| shRNA | Short hairpin RNA |
| siRNA | Small interfering RNA |
| SNAP | Soluble N-ethylmaleimide-sensitive fusion factor attachment protein |
| SNARE | SNAP receptor |

| | |
|---|---|
| SOCS | Suppressor of cytokine signaling |
| STAT | Signal transducer and activator of transcription |
| SSC | Side scatter |
| **T** | **--** |
| TAA | Tumor associated antigens |
| Tag | SV40 large T-antigen |
| TCM | Central memory T cell |
| TCF7 | Transcription factor 7 |
| TCR | T cell receptor |
| TEM | Effector memory T cells |
| TetIV | Tag-derived immunodominent Tetramer IV |
| $T_{FH}$ | Follicular T helper cells |
| TGF | Tumor growth factor |
| TGN | Trans golgi network |
| $T_H$ cells | T helper cells |
| TIL | Tumor-infiltrating lymphocytes |
| TIM-3 | T-cell immunoglobulin and mucin-domain containing-3 |
| TLR | Toll-like receptor |
| TNF-$\alpha$ | Tumor necrosis factor $\alpha$ |
| $T_{reg}$ | Regulatory T cell |
| TRIS | Tris(hydroxymethyl)aminomethane |
| $T_{SCM}$ | Stem memory T cells |
| Tween 20 | Polysorbate 20 |
| **U** | **--** |
| UT | Untransduced |
| UTR | Untranslated region |
| UV | Ultraviolet |
| **V** | **--** |
| VH | Variable heavy chain |
| VL | Variable light chain |
| **W** | **--** |
| w/o | Without |
| WL | Whitlow linker |
| **X** | **--** |
| X-SCID | X-linked severe combined immuno-deficiency |
| **Y** | **--** |
| **Z** | **--** |

# II Tables

# III Figures

# IV Zusammenfassung

Grundlage der adoptiven Immuntherapie ist die antigen-spezifische Stimulation, Aktivierung und Expansion autologer T-Zellen *ex vivo* und deren Reinfusion in den Patienten. Die gezielte genetische Veränderung der zu transferierenden T-Zellen ermöglicht es zum Beispiel ihre Avidität zu erhöhen, indem hochaffine T-Zell-Rezeptoren oder chimäre Antigenrezeptoren (CAR) eingebracht werden. Um jedoch die Etablierung eines immunologischen Gedächtnisses zu gewährleisten, ist es ebenso wichtig, dass diese T-Zellen zu langlebigen Gedächtniszellen differenzieren können. EBAG9 ist ein negativer Regulator der Sekretion von Effektormolekülen und kann die sekundäre Immunantwort beeinflussen. Es wird daher vermutet, dass die Modulierung des EBAG9-regulierten sekretorischen Signalweges eine alternative Strategie ist, um die Wirksamkeit von adoptiv transferierten T-Zellen zu erhöhen.

In der vorliegenden Arbeit konnte zunächst gezeigt werden, dass die verstärkte zytolytische Aktivität von T-Zellen in EBAG9-defizienten Mäusen mit einer präferentiellen Differenzierung zu Gedächtniszellen verbunden ist. Es wurden keine Unterschiede in der Frequenz von Effektor-T-Zellen oder in der Expression von spezifischen Oberflächenrezeptoren beobachtet. Im Gegensatz dazu konnte nachgewiesen werden, dass die mit einer Gedächtniszelldifferenzierung assoziierten Transkriptionsfaktoren EOMES, T-bet, ID3 und der IL-12Rβ Signalweg differentiell rekrutiert wurden. Dementsprechend scheint die Antigenverfügbarkeit abhängig von der EBAG9-vermittelten zytolytischen Aktivität zu sein und die Ausbildung eines immunologischen Gedächtnisses zu beeinflussen.

Im Weiteren wurden EBAG9-spezifische micro RNAs (miRNAs) generiert, die zu einer sequenzspezifischen Herunterregulation von EBAG9 führten. Die Unterdrückung der EBAG9-Expression erhöhte spezifisch die Sekretion von Granzym A und die zytolytische Aktivität von primären murinen und humanen T-Zellen. Darüber hinaus konnte nachgewiesen werden, dass auch die *in vitro* und *in vivo* Antitumoraktivität von CAR T-Zellen verbessert wurde. Da eine gesteigerte T-Zell-Funktion in Folge der Herunterregulation von EBAG9 sowohl für BCMA als auch für CD19 CAR T-Zellen beobachtet werden konnte, scheint es sich hierbei um einen universell anwendbaren zellbiologischen Mechanismus zu handeln. Unspezifische Effekte bezüglich Persistenz, Erschöpfung oder Differenzierung der modifizierten T-Zellen wurde mithilfe einer repetitiven *in vitro* Antigenstimulation ausgeschlossen. Die Modulation des sekretorischen Signalweges in T-Zellen mittels einer miRNA-vermittelten Herunterregulation der EBAG9-Expression scheint dementsprechend eine geeignete Strategie zu sein, um die Effizienz der adoptiven T-Zell-Therapie zu erhöhen.

# V Abstract

Adoptive immunotherapy relies on the antigen-specific stimulation, activation, and expansion of autologous T cells *ex vivo* and reinfusion into the patient. Moreover, genetic engineering of cytotoxic T cells (CTLs) prior to reinfusion involves enhancing CTL function by the expression of high-affinity T cell receptors or chimeric antigen receptors (CARs). In addition to endowing CTLs with high avidity, the transfer of long-lived CTLs is important as it ensures for long-term immunological memory and, therefore, protection against tumor relapse. Because EBAG9 is a negative regulator of effector molecule secretion and suggested to interfere with CTL memory formation, targeting the secretory pathway of T cells via EBAG9 may be an alternative strategy to enhance the efficacy of adoptively transferred T cells.

This thesis explored whether the cytolytic strength of $CD8^+$ T cells influences memory differentiation. By employing the strong Tag neoantigen and the minor histocompatibility mismatch antigen HY, increased cytolytic strength at the same effector cell frequencies could be linked to an expanded memory population in EBAG9-deficient mice. Although lineage-determining surface markers were expressed equally, differential recruitment of the transcription factors EOMES, T-bet, ID3 and the IL-12Rβ pathway was consistent with preferential memory formation. Collectively, antigen availability over time appears to be controlled by EBAG9-mediated cytolytic activity and contributes to the formation of a $CD8^+$ T cell memory pool.

To further investigate whether targeting EBAG9 increases the efficacy of adoptively transferred T cells, efficient sequence-specific miRNAs were generated. The miRNA-mediated silencing of EBAG9 specifically increased granzyme A secretion, while the release of effector cytokines remained unaffected. Furthermore, the engineered downregulation of EBAG9 enhanced the cytolytic capacity of mouse and human CTLs. Most importantly, the *in vitro* and *in vivo* antitumor activity of CAR T cells could be further enhanced by EBAG9 knockdown and therefore, effective dose levels were decreased. The cytolytic activity of BCMA and CD19 CAR T cells was increased by the silencing of EBAG9, indicating that this mechanism is a universally applicable principle of cell biology in murine and human CTLs. Adverse effects of the miRNA-mediated silencing of EBAG9 in regard to T cell persistence, exhaustion, or differentiation were excluded by an *in vitro* repetitive antigen stimulation assay. Targeting the secretory pathway of T cells by the engineered downregulation of EBAG9 is, therefore, a suitable strategy to increase the efficiency of adoptive T cell therapy.

# 1. Introduction

## 1.1 The immune system

The immune system is a host defense system comprising a variety of effector cells and molecules that protect against diseases. By discriminating between self and non-self structures, pathogens such as invading parasites, fungi, bacteria, and viruses are recognized and eliminated. Additionally, cell inherent and other environmental factors can lead to harmful genetic transformation in cells. These malignant cells are to some likelihood also removed by the immune system to avoid tumor formation. The immune system can be classified into two subsystems: the innate and adaptive immune responses.

The innate or non-specific immune response represents the phylogenetically oldest component of the immune system. It is an antigen-independent defense mechanism that is used immediately or within hours after pathogen exposure[1,2]. The innate immune system is the earliest line of defense against the invasion of pathogens and comprises many barriers and compartments. The first defense compartment is physical barriers such as the epithelial layer of the skin or the low pH of the stomach. The second line of defense contains cytokines and chemokines to recruit immune cells to the site of infection as well as complement factors to activate the complement cascade. Effector cells of the innate immune system create the third line of defense and can be divided into two groups. The first group contains basophils and mast cells. These cells are able to secrete histamine and other inflammatory mediators to induce inflammation. The second group is composed of natural killer cells (NK cells) and phagocytes namely eosinophils, neutrophils, macrophages and classical dendritic cells (DCs)[3,4]. They recognize non-self structures and infected cells by highly conserved pathogen-associated molecular patterns (PAMPs) such as viral RNA or bacterial lipopolysaccharides (LPS), which are sensed by pattern recognition receptors such as toll-like receptors. Upon activation of these pathways, innate immune cells eliminate or neutralize infected cells and pathogens via phagocytosis or macropinocytosis[5]. Furthermore, cytokine production and antigen presentation by innate immune cells lead to the activation of the adaptive immune system.

The adaptive immune response is highly antigen-specific and involves a lag time between antigen exposure and maximal response. An important hallmark of the adaptive immune response is the development of an immunological memory. Antigen-

presenting cells (APCs) such as DCs act as a bridge between the innate and the adaptive arms of the immune system. After antigen uptake and processing, APCs present various types of antigens on their cell surface to initiate the adaptive immune response[6]. Two cell types are important mediators of the adaptive immunity: B and T lymphocytes. Both recognize specific conserved and non-conserved structures on invading pathogens using antigen-binding receptors on their surfaces. The repertoires of the T and B cell receptors (TCR and BCR, respectively) are highly diverse due to the rearrangement of variable gene segments that are encoded in the germline. The function of B cells, which are the main players of the humoral immune response, is the generation and secretion of antibodies to neutralize antigens. T cells are responsible for cell-mediated immunity and can be further divided into different subpopulations with distinct functions[7].

## 1.2 T cell-mediated immunity

### 1.2.1 T lymphocytes

As a central element of the adaptive immune response, T cells are capable of eliminating infections and transformed tumor cells. They are derived from hematopoietic bone marrow stem cells and further mature within the thymus. Here, somatic recombination occurs, leading to the appearance of T cells expressing TCRs that have passed further quality control selection processes. The TCR is a heterodimer composed of two antigen-binding transmembrane glycoprotein chains ($\alpha$ and $\beta$) that are disulfide-linked and associated with invariant chains of the CD3 complex ($\zeta$, $\delta$, $\varepsilon$ and $\gamma$) involved in intracellular signaling[8]. T cell development in the thymus involves positive and negative selection of immature T cells. During positive selection, interactions with self-peptide-MHC complexes on thymic epithelial cells are crucial for T cell survival. In contrast, potential self-reactive T cells are removed upon negative selection. High-affinity interaction of TCRs on immature T cells with self-antigen on thymic stromal cells results in apoptosis and T cell elimination while T cells with low to moderate affinity migrate to the periphery[9].

Two major surface co-receptors exist that enhance the avidity for major histocompatibility complex (MHC) molecules and define two separate T cell lineages with distinct functions. MHC class I molecules are found on all nucleated cells and present intracellular antigens, whereas MHC class II molecules are only present on macrophages, DCs and B cells, and present extracellular antigens[6]. Self-antigens

presented by MHC class I molecules are recognized by T cells expressing the CD8 co-receptor. These $CD8^+$ T cells can mature into cytotoxic T lymphocytes (CTLs) and are primarily involved in the destruction of infected or transformed cells by releasing cytolytic granules into the immunological synapse[10]. T helper ($T_H$) cells play an important role in establishing and maximizing the immune response. They express the co-receptor CD4 and recognize self-antigens presented by MHC class II molecules. $CD4^+$ T cells can be further divided into different subpopulations based on the production of signature cytokines. $T_H1$ cells secrete mainly IFN-γ, IL-2 and TNF-α to activate macrophages and $CD8^+$ T cells and induce B cells to produce opsonizing and neutralizing antibodies (IgG). $T_H2$ cells produce IL-4, IL-5, IL-6, IL-10 and IL-13 and are important for stimulating IgG, IgA and IgE antibody production by B cells. Furthermore, regulatory $T_H$ cells ($T_{reg}$), follicular T helper cells, and $T_H17$ cells have been identified. $T_{reg}$ cells negatively regulate the immune response and protect against immunopathology while follicular T helper cells are important for mediating humoral immunity through interactions with B cells. $T_H17$ cells are responsible for an effective immune response against extracellular bacteria and fungi but are also involved in the generation of autoimmune diseases[11].

### 1.2.2 Effector and memory $CD8^+$ T cell differentiation

#### 1.2.2.1 The course of a $CD8^+$ T cell response

Following an acute infection, the T cell response has two goals. On the one hand, large numbers of activated effector $CD8^+$ T cells need to be generated to eliminate the current infection. On the other hand, long-term protection against a future encounter with the same antigen needs to be installed by retaining a subset of T cells with enhanced longevity and regenerative capacity. Thus, the T cell response can be divided into different phases. First, the differentiation of $CD8^+$ T cells into effector cells occurs during the clonal expansion of antigen-specific T cells during days 1 to 7 after primary infection. Following the clearance of infection, effector cells undergo a contraction phase, during which most cells die due to apoptosis (days 8 to 21). Approximately 5 to 10% of effector $CD8^+$ T cells survive this selection process and mature into memory cells, which are maintained in an antigen-independent manner through the actions of the cytokines IL-7 and IL-15[12]. Memory cells are characterized as long-lived, self-renewing, multipotent cells that rapidly proliferate and re-acquire effector function upon re-stimulation with the same antigen[13]. Three major classes of extracellular signals modulate the fate of an activated $CD8^+$ T cell: the strength and

duration of antigen exposure, costimulation through costimulatory receptors and their ligands, such as 4-1BB and 4-1BBL, and pro-inflammatory cytokines such as type I interferons, IL-2, and IL-12. All of these mostly environmental signals are linked and impact the number, phenotype, function, and long-term fate of effector $CD8^+$ T cells[12].

#### 1.2.2.2 Memory $CD8^+$ T cell subsets

Phenotypically, memory $CD8^+$ T cells show decreased expression of killer cell lectin-like receptor 1 (KLRG1), whereas the expression of the adhesion molecule CD44 and the IL-7 receptor $\alpha$ chain (CD127) are increased. Furthermore, L-selectin (CD62L) and the CC-chemokine receptor 7 (CCR7) are useful markers for distinguishing between the $CD8^+$ naive, effector and memory subset populations. Naive $CD8^+$ T cells are required to enter the lymph node to find a cognate antigen. While the homing receptor CCR7 recognizes the ligand CCL21 that is immobilized on the high endothelial venules, CD62L expression is necessary to tether to the high endothelial venules. Additionally, CCR7-mediated signaling arrests naive T cells and facilitates migration into the lymph node. After T cell priming and clonal expansion of $CD8^+$ T cells with an effector phenotype, effector T cells are required to leave the lymph node to migrate to the site of infection via downregulation of CD62L and CCR7[14,15]. Sallusto *et al.* identified that memory T cells can be further distinguished by expressing the homing markers CD62L and CCR7 into central memory (TCM) and effector memory (TEM) T cells. Like naive T cells, the expression of CD62L and CCR7 enable TCM to recirculate through the lymph nodes. Upon antigen restimulation, TCM have the potential to differentiate into effector phenotypes. In contrast, TEM lack expression of CD62L and CCR7. They are usually found in non-lymphoid tissues and exhibit effector functions[16].

#### 1.2.2.3 Models of $CD8^+$ T cell diversification

There are different models to explain the generation of effector and memory $CD8^+$ T cells. The separate-precursor model proposes that naive T cells become 'pre-programmed' during thymic development to adopt certain differentiation states following activation. However, this model is supported by little evidence as single-cell tracing experiments using the adoptive transfer of barcoded or congenic marker bearing cells confirmed that a single naive $CD8^+$ T cell is multipotent and can give rise to effector and memory T cells[17,18]. An additional concept suggests that terminal effector cell differentiation is caused by repetitive stimulation with antigens and pro-inflammatory cytokines. This so-called decreasing potential model is a linear

progression model and postulates that naive $CD8^+$ T cells differentiate initially into activated cells with memory potential and subsequently into cytolytic functional effector $CD8^+$ T cells without memory cell properties. Supporting studies showed the occurrence of an accelerated memory formation due to a truncated duration of antigen exposure and decreasing inflammation[19,20]. Another model, the signal-strength model, also enables for the formation of a heterogeneous effector $CD8^+$ T cell population depending on the overall strength of different signals (antigen, costimulation, pro-inflammatory cytokines) during T cell priming. In contrast to the decreasing potential model, T cell differentiation is not linear but more divergent according to the intensities of signals received. In combination, a strong signal drives clonal expansion and is important for selecting T cells that are competent for forming memory $CD8^+$ T cells. If delivered in excess, a strong signal can lead to terminal effector $CD8^+$ T cell differentiation[21]. Lastly, the asymmetric cell fate model assumes that memory and effector $CD8^+$ T cells can originate from the same precursor T cell. Through asymmetric cell division, the proximal daughter cell, which is closer to the antigen-presenting cell, develops an effector cell fate as it receives stronger TCR and costimulatory signals. In contrast, the distal daughter cell is further from the antigen-presenting cell and adopts a memory cell fate[12,22].

#### 1.2.2.4 Transcriptional regulation of $CD8^+$ T cell differentiation

In addition to these different models involving environmental stimuli, effector and memory T cell differentiation is most likely controlled transcriptionally by the graded expression or activity of certain competing sets of transcription factors. For example, $CD8^+$ T cells with higher expression or activity of the T-box transcription factor T-bet or B lymphocyte-induced maturation protein 1 (BLIMP1) acquire a more terminally differentiated phenotype characterized by a reduced proliferative activity and longevity. Counter-regulation of these factors is achieved by the T-box transcription factor Eomesodermin (EOMES) or the B cell lymphoma 6 (BCL-6), respectively. Both transcription factors prevent effector cells from terminal differentiation and maintain memory cell properties[12,23,24].

### 1.2.3 Effector molecules of $CD8^+$ T cells

Following conjugation of CTLs to a target cell, the cytotoxic secretory granules traffic to the immunological synapse and release cytotoxic effector molecules. These include granzymes that induce apoptosis within the target cells, but also cytokines such as IFN-γ, TNF-$\alpha$ and IL-2 with pro-apoptotic and pro-inflammatory functions.

#### 1.2.3.1 Granzymes

Granzymes are a family of cell death-inducing serine proteases within the cytotoxic granules of CTLs and NK cells. In human, five different granzymes have been described, whereas 11 granzymes are known to be expressed in mice[25]. Granzymes are highly homologous, containing the catalytic triad of trypsin family serine proteases (His-57, Asp-102, Ser-195), an N-terminal Ile-Ile-Gly-Gly sequence, three to four disulfide bridges and a conserved motif of eight amino acids[26]. Although granzymes are structurally related, they differ in their substrate specificity. The most prominent and well-studied members of the granzyme family present in human and mice are granzymes A and B. Granzyme expression occurs in activated T cells upon antigen stimulation, require costimulation via cytokines of the common gamma chain ($\gamma_c$) family such as IL-2 and granzymes are expressed concomitantly with perforin[27]. Granzyme mRNA transcripts are translated as pre-pro-proteases. The signal sequence directs the precursor molecules to the endoplasmic reticulum (ER) where it is enzymatically cleaved. A mannose-6-phosphate tag is added in the Golgi apparatus and functions as a sorting signal for lysosomal transport, directing the proenzyme to the cytotoxic granules. For activation of the inactive proenzymes into active proteases, removal of the N-terminal located activation dipeptide is required. This reaction is catalyzed by the proteinases Cathepsin C and H within the cytotoxic granules, a process that also requires low pH[28,29].

As soon as the CTL recognizes and binds its target cell, secretory lysosomes move and cluster around the microtubule organizing center. After membrane fusion, granzymes and perforin are released into the immunological synapse. Via electrostatic interactions, the positively charged granzymes bind to the negatively charged target cell membranes[30,31]. Furthermore, binding to the target cell can be mediated by specific receptors such as the mannose-6-phosphate receptor[32]. Perforin is a pore-forming molecule capable of membrane permeabilization. It is important for the entry of granzymes into the target cell cytosol with studies performed on mice lacking perforin demonstrating an abolished granule-dependent target cell death. Yet, the mechanism of perforin-mediated granzyme entry is not entirely clear[33]. Within the target cell, programmed cell death pathways are initiated by granzymes. Granzyme A induces a caspase-independent apoptosis characterized by the generation of single-stranded DNA nicks. Due to the action of granzyme A, there is a loss of the mitochondrial inner membrane potential, leading to the release of reactive oxygen species (ROS). As a consequence, the ER-associated SET complex translocates to the nucleus. Three members of this complex that are involved in DNA

repair are then cleaved by granzyme A. Furthermore, cleavage of SET leads to the release of the DNase NM23-H1, therefore DNA single-strand nicks are induced[34-36]. On the contrary, in addition to activating a caspase-independent cell death program, granzyme B is able to induce caspase-dependent apoptosis by cleaving and activating the caspases 3, 7, 8 and 10 as well as several of their downstream substrates. As a result, the caspase-activated DNase (CAD) is cleaved and is responsible for granzyme B-mediated DNA damage. Furthermore, granzyme B induces ROS production and the release of cytochrome c from the mitochondria[28,37,38].

There are different mechanisms that exist for protecting CTLs against self-destruction by its own granule enzymes. First, during protein synthesis and storage within the granules, the enzymatic activity of granzymes and perforin is inhibited by the acidic pH within the secretory granules[39]. Second, to protect CTLs from their own enzymes released into the immunological synapse, granzyme-specific inhibitors called serpins (serine protease inhibitors) are endogenously expressed. Serpin B9 inactivates granzyme B and mice lacking serpin B9 expression have a much stronger CTL death during the response to infection[40,41]. Yet, no serpins are known to inactivate granzyme A. In addition, the cytotoxic granule protein cathepsin B, which is capable of proteolytic inactivation of perforin, can be externalized to the CTL plasma membrane during granule fusion[42].

#### 1.2.3.2 Cytokines

The cytokine IFN-γ is the only member of the type II interferons, whereas IFN-$\alpha$, -$\beta$, -$\omega$, -$\tau$ belong to the type I interferons. Both types are distinguishable by their structure and specificity for their receptors. IFN-γ is mainly released by macrophages, NK cells, activated $CD8^+$ T cells as well as $T_H1$ $CD4^+$ T cells[43]. The cellular effects of IFN-γ are mediated by its heterodimeric receptor (IFN-γR) that is expressed ubiquitously on immune and non-immune cells. Therefore, IFN-γ has a large spectrum of effects including macrophage activation, antiviral immunity and regulation of $CD4^+$ T cell polarization towards $T_H1$ $CD4^+$ T cells[44]. Furthermore, it increases T cell-mediated killing through upregulation of MHC class I expression on target cells. Upregulation of MHC class II molecules on B cells and APCs enhances $CD4^+$ T cell activation[45,46]. Reports on IFN-γ action from $CD8^+$ T cells vary. IFN-γ was shown to enhance the ability of CTLs to kill independent of perforin and play an important role in CTL proliferation within murine infection models. In contrast, IFN-γ may also directly

increase T cell apoptosis and reduce proliferation, an important process for T cell contraction. Additionally, within $CD8^+$ T cells, IL-12R expression is induced upon IFN-γR signaling. Although mice lacking IFN-γ and IFN-γR show no defects in the development of the immune system, these mice were more susceptible to infection and tumor formation[47-50].

The tumor necrosis factor α (TNF-α) is produced primarily by activated macrophages, but can also be released by NK cells, neutrophils, eosinophils, mast cells, or $CD4^+$ and $CD8^+$ T cells. Two receptors are able to bind TNF-α and mediate the intracellular signaling. While TNF-αR1 is expressed ubiquitously, TNF-αR2 is usually located in immune cells[51]. Although TNF-α was shown to be part of the cytotoxic effector response of the immune system, putative immune suppressor functions facilitating the biological activity of $T_{reg}$ cells have been recently described[52]. Furthermore, TNF-α triggered melanoma dedifferentiation during adoptive $CD8^+$ T cell therapy of melanoma, therefore, promoting tumor relapse. In addition, through TNF-αR1 signaling, apoptosis of activated $CD8^+$ T cells can be induced[53].

IL-2 belongs to the family of $\gamma_c$ cytokines and is mainly produced by activated $CD4^+$ T cells. Yet, activated $CD8^+$ T cells and NK cells are also able to secrete IL-2. IL-2 signaling is mediated by the IL-2 receptor (Il-2R), a trimeric receptor composed of an α (CD25), β (CD122) and $\gamma_c$ chain[54]. The main function of IL-2 is to promote the differentiation of immature T cells into $T_{reg}$ cells as well as differentiation into effector and memory T cells. Following antigen challenge, IL-2 appears to be responsible for optimal expansion and generation of effector functions. During memory cell generation and the contraction phase where $CD8^+$ T cells die via apoptosis, IL-2 signaling is able to rescue $CD8^+$ T cells from cell death, and therefore increasing memory $CD8^+$ T cell numbers[55].

### 1.2.4 The secretory pathway of $CD8^+$ T cells

#### 1.2.4.1 Secretion of effector molecules

Antigen recognition by CTLs is mediated via interaction between the specific TCR and foreign antigens bound to MHC class I molecules on the target cell surface. Following target antigen recognition and formation of the immunological synapse, effector molecules are released from activated CTLs along the secretory pathway. There are two pathways that principally exist. First, there is the constitutive secretion of newly

synthesized cytokines such as IFN-γ. Second, effector molecules such as granzymes and perforin are released from a storage pool of vesicles in the regulated secretion pathway (Figure 1)[33,56].

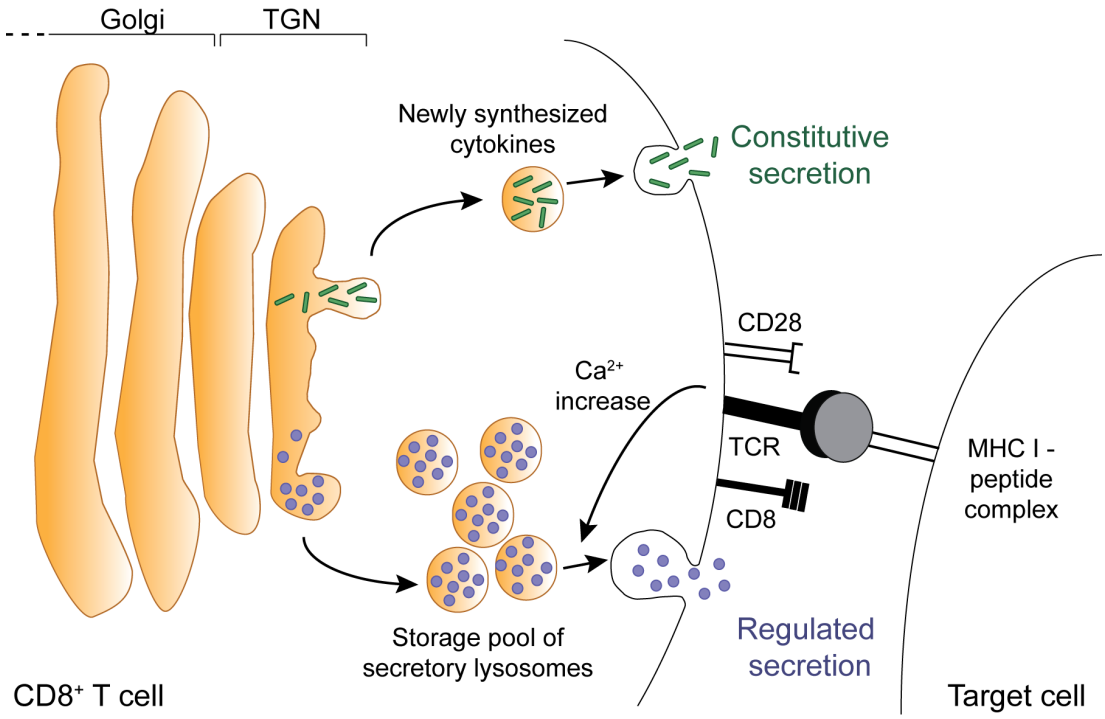


**Figure 1: The secretory pathway in CD8⁺ T cells**
Following CD8⁺ T cell activation via interaction between the TCR and the antigen bound to the MHC class I complex, effector molecules are secreted. Newly synthesized cytokines are released constitutively, whereas the release of granzymes and perforin from a storage pool of secretory lysosomes is regulated, requiring an increase of the intracellular $Ca^{2+}$concentrations [adapted from Rüder, thesis, 2005].

During constitutive secretion, vesicles are transported to the cell membrane and cytokines are released by passive lateral diffusion. The mechanism of constitutive cytokine secretion from $CD8^+$ and $T_H1$ $CD4^+$ T cells has not yet been completely explored. According to Huse *et al.*, two distinct pathways of cytokine secretion in $T_H1$ $CD4^+$ T cells exist. Cytokines such as IL-2 and IFN-γ are released unidirectionally directly into the immunological synapse, while other cytokines such as TNF-α are released multidirectionally from the cell surface. In addition, both pathways use a different set of trafficking molecules[57]. The regulated secretion of effector molecules is characterized by the formation of an immunological synapse at the site of cell-cell contact induced by a target recognition-dependent $Ca^{2+}$ influx. Secretory lysosomes containing perforin and granzymes move along microtubules via interaction between adaptor proteins and kinesin-motors and accumulate at the microtubule-organizing center (MTOC) of CTLs. The polarization of MTOC leads to trafficking of secretory lysosomes towards the presynaptic membrane[58].

Fusion of the vesicles with the membrane can be divided into four steps: tethering, docking, priming and fusion. The soluble N-ethylmaleimide-sensitive fusion factor attachment protein receptor (SNARE) complex regulates the fusion of lysosomes with the plasma membrane of the immunological synapse. This α-helical structure protein complex is necessary to overcome the electrostatic repulsive force between the lysosome and the plasma membrane lipid bilayer. To facilitate this process, vSNAREs such as VAMP7 on the vesicle surface and tSNAREs such as SNAP23 and syntaxin 4 on the target membrane interact with each other[59,60]. Furthermore, Ras-associated small GTPases (Rabs) are important mediators of membrane fusion. Active GTP-bound Rab proteins are attached to the membrane and interact with SNAREs and motor proteins. After fusion of the vesicle and membrane, a hydrolysis of GTP to GDP occurs and GDP-bound Rab proteins diffuse back to the cytosol[61].

To produce mature secretory lysosomes, coordinated transfer of secretory molecules from the endoplasmic reticulum/Golgi apparatus into the vesicles is required. Perforin and granzymes are produced within the ER and transported to the cis-Golgi complex where they are tagged with the mannose-6-phosphate group and accumulate as cargo proteins in the trans-Golgi-network (TGN). The cargo proteins are recognized by sorting proteins such as the mannose 6-phosphate receptor (M6PR) or sortilin. This complex then interacts with heterotetrameric adaptor proteins (APs), Golgi-localizing γ-adaptin ear homology domain Arf-binding protein (GGA), and small GTP-binding proteins of the Arf, Rac1 and/or Rab families to recruit clathrin adaptors. The clathrin-coated vesicles then move along the microtubules to the endosomes. After dissociation of the complex in the endosomes, the effector molecules are targeted to the secretory lysosomes while the sorting receptor is recycled to the TGN[62,63].

#### 1.2.4.2 EBAG9 and its role in the regulated effector molecule secretion

Protein transfer from the TGN to secretory lysosomes is highly regulated. Our group demonstrated the presence of regulatory proteins such as the Estrogen receptor-binding fragment-associated antigen 9 (EBAG9), which is a negative regulator of the $Ca^{2+}$-dependent regulated secretion of effector molecules[64]. Human EBAG9 comprises of 213 amino acids and exhibits a domain structure. Through a C-terminal coiled-coiled structure, human EBAG9 forms homo-oligomers with an N-terminal located transmembrane domain[65]. EBAG9 is an estrogen-inducible protein that is expressed in most tissues. Our group has demonstrated that a loss of EBAG9 enhances the cytolytic activity of CTLs *in vivo* by increasing the release of the secretory lysosome content. Mechanistically, EBAG9 interacts with the γ2-subunit of

AP-1 and inhibits the AP-1 activity clathrin-coated vesicle formation. Furthermore, EBAG9 was also identified as an interaction partner of snapin and BLOS2, which are subunits of the lysosome-related organelles complex-1 (BLOC-1). In the secretory pathway, BLOC-1 regulates protein sorting from the endosome to the secretory lysosomes. Thus, EBAG9 negatively regulates the vesicle transfer from the TGN to the secretory lysosomes[64].

### 1.2.5 T cell exhaustion

Upon chronic viral, bacterial, and parasitic infections as well as during cancer, T cells have been shown to attain a state referred to as exhaustion. Exhaustion is characterized by T cell dysfunction including poor effector functions, inhibitory receptor expression and a transcriptional profile distinct from that of effector and memory T cells[66]. For the development of T cell exhaustion, extrinsic and intrinsic negative regulatory pathways are of importance. During exhaustion, T cells lose their functions in a hierarchical manner. Important properties such as IL-2 production, high proliferative capacity, and *ex vivo* killing are lost during an early phase. Other functions including TNF production, are lost during the intermediate stage of dysfunction, while physical deletion of the antigen-specific T cell represents the final stage of exhaustion[67-69].

Negative regulatory pathways involved in T cell exhaustion include the expression of cell surface inhibitory receptors such as PD-1, CTLA-4, LAG-3, or TIM-3[70,71]. Although PD-1 signaling appears to be a major inhibitory pathway involved in T cell exhaustion, many other inhibitory receptors coregulate T cell exhaustion. It is possible that these individual receptors regulate distinct cellular functions. For example, PD-1 strongly affects the survival and proliferation of exhausted T cells, whereas LAG-3 affects cell cycle progression[70,72-74]. In addition to the intrinsic expression of inhibitory surface receptors, extrinsic immunomodulatory cytokines are also involved in T cell exhaustion. IL-10 and TGF-β have been proven to be associated with an exhausted T cell state[75-77]. Lastly, immunoregulatory cell types such as $T_{reg}$ cells affect exhaustion and dysfunctionalities of antigen-specific T cells[78,79].

Transcriptional analyses demonstrated exhausted T cells to represent a unique state of T cell differentiation as global transcriptional profiles are distinct from those of effector or memory T cells. Although lineage-specific transcription factors have not yet been identified, several transcriptional pathways are involved in T cell exhaustion[80,81]. Amongst these, graded expression of BLIMP1 is known to be

important. Moderate or small amounts of BLIMP1 are associated with T cell memory formation, whereas intermediate amounts promote terminal effector differentiation. In contrast, very high amounts of BLIMP1 are associated with the expression of inhibitory receptors and T cell exhaustion[82].

## 1.3 Cancer immunotherapies

The approach of fighting cancer by manipulating the host immune response for efficient tumor cell killing is termed cancer immunotherapy. This can be accomplished by several means. However, two types of immunotherapy have proven particularly effective in cancer treatment during recent years. First, immune checkpoint inhibitors are used clinically to stimulate the immune system by antibodies that block immune regulatory checkpoints. Second, specific antitumor immune cells are administered by adoptive T cell therapy (ATT).

### 1.3.1 Checkpoint inhibitors

Antitumor responses of T cells are limited due to the release or presentation of negative regulators of immune activation. These regulatory immune checkpoint molecules that inhibit T cell activation can be blocked by specific antibodies. In particular, cytotoxic T lymphocyte-associated protein-4 (CTLA-4) and programmed cell death 1 (PD-1) receptors are clinically relevant targets[83,84]. The inhibitory role of CTLA-4 was demonstrated by the groups of James Allison, who won the Nobel Prize for his work with Tasuku Honjo, and Jeffrey Bluestone[83,85,86]. While CTLA-4 is an intracellular receptor in resting T cells, it translocates to the cell surface upon T cell activation. There, it outcompetes CD28 for binding to costimulatory molecules and mediates inhibitory signaling. Thus, T cell proliferation and activation are blocked. Furthermore, mice lacking CTLA-4 die due to massive lymphocyte infiltration in the majority of organs[86]. The transient blocking of CTLA-4 by monoclonal antibodies led to durable regression of established tumors in a syngeneic mouse model[83,86]. So far, one fully human CTLA-4-blocking monoclonal antibody (ipilimumab) has gained approval from the U.S. Food and Drug Administration (FDA) whereas others are still under clinical trials[87,88]. The inhibitory function of the surface receptor PD-1 is mediated by the tyrosine phosphatase SHP-2 that dephosphorylates downstream TCR signaling molecules. The PD-1 pathway is activated by binding of the ligands PD-L1 or PD-L2. PD-L1 is expressed broadly by many somatic cells upon exposure to pro-inflammatory cytokines, while PD-L2 expression is more restricted to APCs[29]. CTLs with antitumor activity produce inflammatory cytokines such as IFN-$\gamma$ that, in

turn, induces PD-L1 expression in the tumor microenvironment resulting in T cell exhaustion[29,89,90]. Currently, there are five monoclonal antibodies targeting PD-1 or PD-L1 that are approved by the FDA in 11 tumor entities[88].

### 1.3.2 Adoptive T cell therapy (ATT)

Although checkpoint inhibitors can be successfully applied in different solid tumors, a pre-existing immune response is necessary that can be supported. Therefore, another strategy is required to target poorly immunogenic or rapidly progressing cancer types. Transferring naturally-occurring or engineered tumor-specific T cells enables the treatment of such types of cancer. In the case of autologous treatments, the transferred T cells are isolated from a patient, expanded *ex vivo* and/or genetically manipulated, and subsequently reinfused back into the lymphodepleted patient (Figure 2)[91].

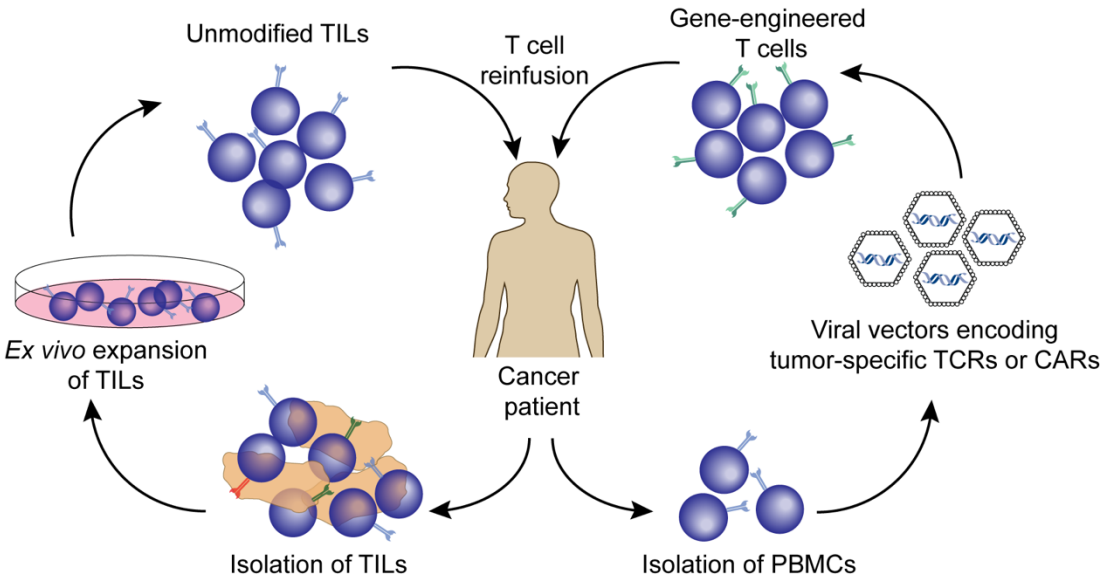


**Figure 2: Principles of adoptive T cell therapy**
The transfer of naturally-occurring or gene-engineered T cells can be used in the treatment of cancer. On the one hand, tumor-infiltrating T cells (TILs) can be isolated from patient material, expanded *ex vivo* and reinfused into the patient (left). On the other hand, peripheral blood mononuclear cells (PBMCs) from the patient can be endowed with tumor-specific TCRs or CARs by retroviral transduction and *ex vivo* expansion prior to reinfusion (right)[adapted from Met *et al.* and Restifo *et al.*[91,92]].

ATT has been shown to be a very successful immunotherapeutic treatment in advanced hematological malignancies[92,93]. Although the ATT-based treatment of solid tumors is more challenging, some promising clinical trial results were reported. Among them, a phase I clinical trial for the treatment of pediatric neuroblastoma

patients with GD2 specific CAR T cells reported a complete remission rate of 27% (3 out of 11 patients)[93-95].

#### 1.3.2.1 Tumor-infiltrating lymphocytes (TILs)

TILs are attracted to the tumor and represent a heterogenous lymphocyte population, mainly comprising of T cells and NK cells. One of the first reports stating the beneficial effect of lymphocyte infiltration was a case report from 1972 where total regression of liver metastasis without prior therapy was observed in a patient with gastric cancer[96]. To date, the efficacy of TIL-based immunotherapy has been well studied and a favorable prognosis due to the presence of TILs in various cancer types has been reported. For example, multiple independent studies between 2005 and 2018 revealed an objective response rate of 40-50% in patients with metastatic melanoma including 10-25% of complete tumor regressions[91,97-100]. TILs express an endogenous and often low-affinity TCR and thus are able to recognize tumor-associated antigens (TAA). The method of large-scale *ex vivo* expansion of TILs was pioneered by the group led by Steven Rosenberg. TILs are isolated from tumor biopsies, rapidly expanded *ex vivo* under high IL-2 supplementation and reinfused into the lymphodepleted patient[101,102]. As this isolated and expanded lymphocyte population compromises an undefined mixture of T cell clones, the individual TIL cultures are selected by determining effector cytokine secretion or cytotoxicity upon TAA stimulation. Advanced selection and expansion protocols employ more clonally restricted TILs[101].

#### 1.3.2.2 TCR-modified T cells

To increase the antitumor function of T cells, a TCR recognizing a specific tumor antigen can be introduced. Therefore, a TCR specific for naturally processed and expressed tumor antigens needs to be isolated and introduced to alter T cell specificity through the expression of a new TCR $\alpha$ and $\beta$ chain. As the T cells will be reinfused into the patient, the tumor-specific TCR is required to match the host MHC allele as a restriction element[91]. Tumor-specific TCRs can be isolated from patient-derived, autologous, highly reactive TILs. Using an allogeneic setting, the repertoire limitations caused by thymic negative selection can be avoided[103]. Furthermore, HLA-transgenic mice exhibiting a full human TCR repertoire can be immunized with the human tumor antigen and used for TCR generation[104]. Following isolation and sequencing, the tumor-specific TCR can be cloned into retroviral or lentiviral vectors. Patient-derived autologous T cells are then isolated from peripheral blood, activated, and genetically modified to express the tumor-specific TCR. ATT using genetically

modified TCRs targeting, for example NY-ESO-1 in melanoma and sarcoma or gp100 in melanoma has been shown to mediate significant tumor regression in cancer patients[105,106].

#### 1.3.2.3 CAR-modified T cells

Chimeric antigen receptors (CARs) consist of a single polypeptide combining an extracellular antigen-binding domain, a spacer, a transmembrane domain, and an intracellular signal domain. With this composition, the specificity and affinity of an antibody are combined with the TCR-mediated cytotoxic potency and activation of a T cell. Antigen recognition by CARs is not restricted to the MHC context. Instead, all surface-expressed molecules are potential targets for CAR-mediated immunotherapy. First-generation CARs contain a single-chain antibody variable fragment, an IgG spacer that determines the distance between the target and T cell, and an intracellular CD3ζ activation domain. As these first-generation CARs failed to induce T cell proliferation and lead to CAR T cell anergy upon repetitive antigen stimulation, further engineering was required[107]. By introducing an additional intracellular costimulatory CD28 or 4-1BB domain, second-generation CARs evolved that demonstrated potent anti-tumor activity in clinical trials[108-111]. Currently, third-generation CARs that contain two costimulatory domains, as well as multi-functional next generation CARs including, for example, an ON- or OFF-switch are under development[112]. Although CARs have been tested within several clinical trials for diverse tumor entities, the success of CAR T cell therapy is, to date, restricted to hematopoietic malignancies. CD19 represents the most prominent and successful target for CAR-mediated T cell therapy and is a B cell lineage antigen expressed on normal and malignant B cells. CD19-specific CAR T cells were shown to be efficient in the treatment of different B cell malignancies such as aggressive B cell lymphoma, chronic lymphocytic leukemia or acute lymphoblastic leukemia[108-110,113,114].

### 1.3.3 RNA interference (RNAi)

Although most of the therapeutic approaches within ATT focus on the gain-of-function by introducing a TCR or a CAR into T cells, cancer therapies have been developed that use RNA molecules and the RNA interference (RNAi) pathway for inhibiting protein functions.

#### 1.3.3.1 The RNA interference pathway

RNAi was first observed in the late 1980s and is a post-transcriptionally mediated gene silencing mechanism that is triggered by double-stranded RNA (dsRNA) to induce sequence-specific translational repression or mRNA degradation[115]. In the

nucleus, the micro RNA (miRNA) genes are transcribed into 500-3000 nucleotide pri-miRNAs by action of the RNA polymerase II. These pri-miRNAs are capped and polyadenylated. In addition, pri-miRNA contain one or multiple stem-loop sequences and are cleaved by the Drosha-DGCR8 complex to 60-100 nucleotide double-stranded pre-miRNA hairpin structures[116-118]. Ran GTPase and Exportin-5 mediate the export of pre-miRNAs from the nucleus into the cytoplasm. There, they are further processed by an RNase III enzyme called Dicer to an imperfect duplex structure of 22 nucleotides[119]. One of the strands resembles the mature miRNA that binds to Argonaut (Ago) proteins and is incorporated in the RNA-induced silencing complex (RISC)[120].

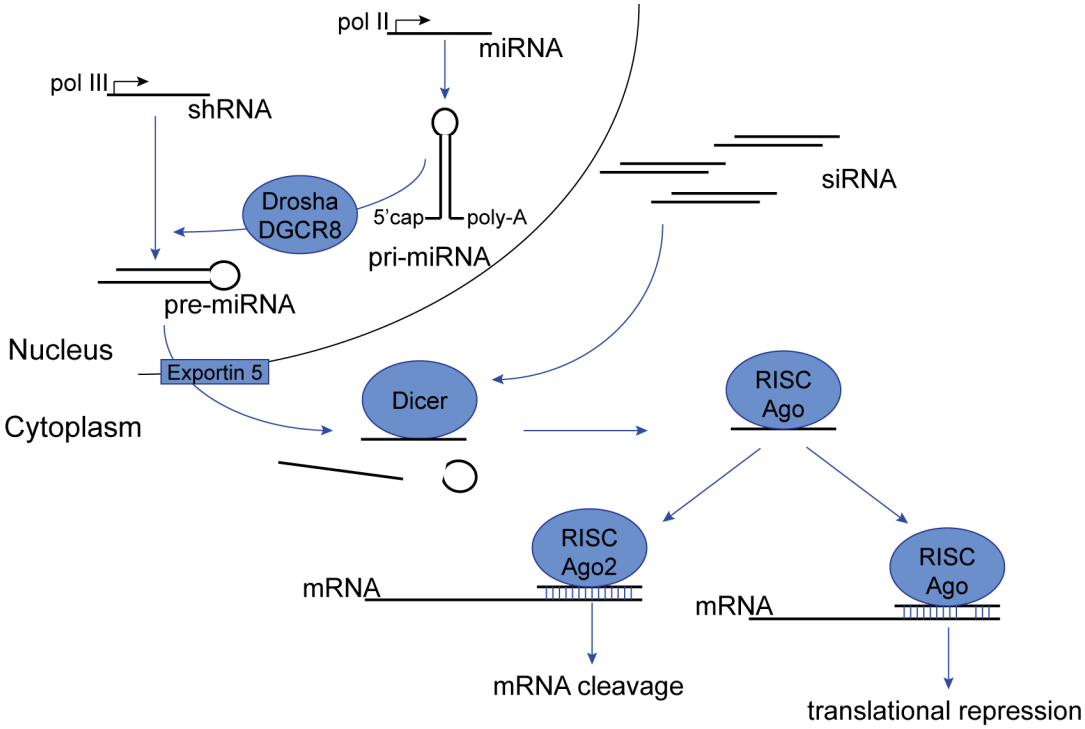


**Figure 3: RNA interference is a post-transcriptional gene silencing mechanism.** Transcription of miRNA genes is controlled by the polymerase II promoter (pol II) and generates pri-miRNA molecules with a characteristic secondary structure. After processing by the Drosha-DGCR8 complex, pre-miRNA molecules leave the nucleus in an exportin 5-dependent manner. A polymerase III promoter (pol III) regulates the transcription of shRNA genes and also generates pre-miRNA molecules that are exported to the cytoplasm. In the cytoplasm, pre-miRNAs and siRNAs are processed by the RNase III enzyme Dicer and 20-25 nucleotide containing single-stranded RNA molecules are loaded to the RNA-induced silencing complex that contains Argonaut (Ago) proteins. Ago2 and complete complementation to the target RNA lead to mRNA cleavage, whereas the other Ago proteins and an imperfect complementation cause translational repression of the target gene [adapted from [121]].

In most cases, the miRNA-RISC complex can recognize and bind to target sequences within the 3' UTR of target mRNA molecules, although some target sequences are also present in the 5' UTR regions. As a consequence of RISC binding, mRNA

degradation or repression of protein translation is induced[120,122]. The fate of the target mRNA molecules depends on the grade of complementarity between the target mRNA molecule and miRNA but is also affected by the incorporated Ago protein. While incorporation of Ago 2 leads to direct cleavage of the target mRNA, the other Ago proteins negatively impact mRNA stability or attenuate translation (Figure 3)[123-125].

For the engineered knockdown of specific targets, several dsRNA molecules can be used that enter the RNAi pathway at different points. Transfection with small interfering RNA (siRNA) molecules leads to transient protein knockdown. siRNAs are duplex RNA molecules consisting of two complementary strands of 22 nucleotides that enter the RNAi pathway in the cytosol[126,127]. To achieve stable protein downregulation, short hairpin RNA (shRNA) or miRNA molecules can be applied. Both enter the RNAi pathway in the nucleus and are then processed to siRNA-like molecules. Transcription of shRNA molecules is mediated by RNA polymerase III and generates a pre-miRNA structure that is transported to the cytosol, further processed by Dicer, and loaded to the RISC. In contrast, the transcription of miRNA molecules is under the control of the RNA polymerase II promoter, produces a transcript that resembles the pre-miRNA structure, and requires processing by the Drosha-DGCR8 complex prior to export of the nucleus[116,128].

#### 1.3.3.2 Applications of the RNAi pathway to T cell engineering

Although various promising cancer immunotherapies exist, limitations often occur as the immune system is restrained by negative feedback mechanisms that originally protect the host against autoimmunity but also prevent antitumor activity. As previously mentioned, monoclonal antibodies for targeting immune checkpoints are available. Yet, using antibodies for targeting multiple checkpoints has been shown to be challenging. Further limitations are caused by immunosuppressive signals originating from the tumor microenvironment and that recruit multiple immune checkpoints. To overcome these challenges, the RNAi pathway can be used by introducing dsRNA molecules to target specific multiple intracellular and extracellular targets in DCs and T cells that restrict their function. Thus, the immune system can be empowered to bypass intrinsic inhibitory pathways and be insensitive to immune suppression mediated by the tumor microenvironment[121].

Mature DCs have an exceptionally strong capacity for presenting antigens and activating T cells but are negatively regulated by feedback mechanisms. The RNAi

pathway can be used to inhibit immunosuppressive pathways within DCs, manipulate $CD4^+$ T cell differentiation towards $T_H1$ $CD4^+$ T cells, or prolong the lifespan of DCs by inhibiting apoptosis. A variety of molecules are expressed in DCs that repress antigen presentation. These include A20 and the suppressor of cytokine signaling 1 (SOCS1). Antigen-loaded DCs silenced for A20 or SOCS1 have been shown to activate larger numbers of effector T cells that correlate with tumor growth inhibition in mice[129-131]. Furthermore, DCs that express the Tyro3/Ax1/Mer family of receptor tyrosine kinases are capable of inducing SOCS1 expression. Mer knockdown in DCs increases the number of antigen-specific T cells *in vivo*[132-134]. In addition to T cell activation, DCs also express the pro-apoptotic surface molecule Fas ligand (FasL). Interaction of FasL with the Fas receptor on T cells induces apoptosis induction within T cells. The effectiveness of an FasL-targeting shRNA to enhance DC function and suppress tumor cell growth has been demonstrated[135]. Furthermore, siRNA-mediated targeting of IL-10 in DCs reduces the level of this immunosuppressive cytokine and, in turn, increases IL-12 production, thereby inducing $T_H1$ $CD4^+$ T cell differentiation instead[136].

Besides antigen presentation by DCs, it is essential that T cells home to, proliferate, and function in the tumor microenvironment to ensure an efficient antitumor response. Therefore, T cells can be manipulated in many different ways using the RNAi pathway to modulate their properties for therapeutic purposes. Tumor regression could be achieved in a mouse model after adoptive transfer of $CD8^+$ T cells with silenced SOCS1 or of $CD4^+$ T cells with silenced STAT3[137,138]. Furthermore, the E3 ubiquitin ligase Cbl-b, which negatively regulates TCR activation, is an attractive target for RNAi-mediated T cell modification. Substantial suppression of tumor growth and increased survival rates of tumor-bearing mice could be observed due to the adoptive transfer of Cbl-b knockdown $CD8^+$ T cells[139]. The adaptor protein SHP-1 negatively regulates T cell activation by diminishing the interaction between T cells and antigen-presenting DCs. Silencing SHP-1 in tumor-specific T cells led to improved therapy of disseminated leukemia cells[140].

Collectively, using the RNAi pathway to avoid inhibitory mechanisms that attenuate the antitumor immune response in T cells is emerging as a promising approach in cancer immunotherapy.

# 2. Aim of the thesis

To overcome the limits of immunotherapy based on the transfer of cytotoxic T cells there is a redirection of the focus from amplifying the cell quantity to improving the quality of individual T cells. In this process, one of the main challenges is to induce a potent antitumor effector cell function without impairing the development of T cell memory response. Previously, our group revealed that EBAG9 negatively regulates the $Ca^{2+}$-dependent effector molecule secretion from $CD8^+$ T cells. Furthermore, mice lacking EBAG9 had a much stronger secondary immune response[64]. Based on these findings, in the present thesis it was investigated whether the secretory pathway of T cells can be manipulated to improve T cell avidity and the efficacy of adoptively transferred T cells.

Firstly, the mechanism of the enhanced secondary immune response in EBAG9-deficient mice should be elucidated in more detail. The question was raised, if the formation of an antigen-specific $CD8^+$ T cell memory pool is altered depending on the increased cytolytic capacity and if so, how the loss of EBAG9 is linked to the transcriptional control of $CD8^+$ T cell fate decision.

The second part of this thesis aimed to strengthen the cytotoxic capacity of effector T cells by miRNA-mediated silencing of EBAG9. Therefore, EBAG9-specific miRNAs should be generated and analyzed for their knockdown efficiency in primary mouse and human T cells. In addition, functional assays should answer the question if a downregulation of EBAG9 can enhance the cytolytic activity of engineered T cells. First, engineered mouse T cells with a loss of EBAG9 were analyzed for their antigen-specific cytotoxic competence in an *in vivo* killing assay. Second, for a robust translational approach, human T cells equipped with a high-affinity CAR and an EBAG9-specific miRNA were investigated in regard to their *in vitro* and *in vivo* antitumor killing capacity. Lastly, it was analyzed if the miRNA-mediated knockdown of EBAG9 impacts on *in vitro* human CAR T cell persistence, exhaustion or differentiation.

# 3. Material

## 3.1 Plasmids and retroviral vectors

The following plasmids and retroviral vectors were used (Table 1).

Table 1: Plasmids and retroviral vectors

| Name | Description |
|---|---|
| pALF-10A1GaV | Eukaryotic expression vector encoding murine leukemia virus *env* gene 10A1 |
| pcDNA3.1gag/pol | Eukaryotic expression vector encoding murine leukemia virus *gag* and *pol* genes |
| MP71_GFP | Retroviral vector MP71 expressing eGFP |
| MP71_140-145_GFP | Retroviral vector MP71 expressing miRNA 140, 141, 142, 143, 144 or 145 and eGFP; mi140 has no endogenous target sequence and serves as a control, mi141-mi145 are sequence-specific EBAG9-targeting miRNAs |
| MP71_H16-H19_GFP | Retroviral vector MP71 expressing human EBAG9-targeting miRNA H16, H17, H18 or H19 and eGFP |
| MP71_BIX | Retroviral vector MP71 expressing the BCMA-targeting CAR (VH-linker-VL-IgG1Δ-CD28-CD3ζ) |
| MP71_H18_BIX | Retroviral vector MP71 expressing the EBAG9-targeting miRNA H18 and the BCMA-targeting CAR (VH-linker-VL-IgG1Δ-CD28-CD3ζ) |
| MP71_CD19 | Retroviral vector MP71 expressing the CD19-targeting CAR (VH-linker-VL-IgG1Δ-CD28-CD3ζ) |
| MP71_H17_CD19 | Retroviral vector MP71 expressing the EBAG9-targeting miRNA H17 and the CD19-targeting CAR (VH-linker-VL-IgG1Δ-CD28-CD3ζ) |
| MP71_SP6 | Retroviral vector MP71 expressing the SP6 CAR (VH-linker-VL-IgG1Δ-CD28-CD3ζ) without any naturally occurring antigen |
| MP71_H17/H18_SP6 | Retroviral vector MP71 expressing the EBAG9-targeting miRNA H17 or H18 and the SP6 CAR (VH-linker-VL-IgG1Δ-CD28-CD3ζ) without any naturally occurring antigen |

## 3.2 Oligonucleotides

The following oligonucleotides were used for qRT-PCR (Table 2).

Table 2: Oligonucleotide primer for qRT-PCR using TaqMan® probes

| Gene | Assay ID |
|---|---|
| *Eomes* | Mm01351985_m1 |
| *Tbx21* | Mm00450960_m1 |
| *Bcl6* | Mm00477633_m1 |
| *Prdm1* | Mm00476128_m1 |
| *Id2* | Mm00711781_m1 |
| *Id3* | Mm0188138_g1 |
| *Il12rb1* | Mm00434189_m1 |
| *Runx3* | Mm00490666_m1 |
| *Tcf7* | Mm00493445_m1 |
| *Bcl2* | Mm00477631_m1 |
| *Il7r* | Mm00434295_m1 |
| *Rora* | Mm01173766_m1 |
| *Foxo1* | Mm00490672_m1 |
| *Ebag9* | Mm00834632_g1 |
| *Gapdh* | Mm99999915_g1 |
| *EBAG9* | Hs00188444_m1 |
| *GAPDH* | Hs02786624_g1 |

## 3.3 Antibodies and MHC multimers

### 3.3.1 Conjugated antibodies specific for mouse surface antigens

The following fluorophore coupled anti-mouse antibodies were used (Table 3). They are conjugated with alexa fluor 647 (AF647), allophycocyanin (APC), brilliant violet (421), fluorescein isothiocyanate (FITC), pacific blue (PB), peridinin chlorophyll protein complex (PerCP) or phycoerythrin (PE).

Table 3: Conjugated anti-mouse antibodies

| Specificity | Conjugate | Clone | Isotype | Host | Source |
|---|---|---|---|---|---|
| CD4 | PE | GK1.5 | IgG2b | Rat | BioLegend |
| CD8a | BV421 | 53-6.7 | IgG2a | Rat | BioLegend |
| CD8a | PB | 53-6.7 | IgG2a | Rat | BioLegend |
| CD19 | PerCP | 6D5 | IgG2a | Rat | BioLegend |
| CD44 | APC | IM7 | IgG2b | Rat | BioLegend |
| CD44 | PE | IM7 | IgG2b | Rat | BioLegend |
| CD45.1 | PB | A20 | IgG2a | Mouse | BioLegend |
| CD45.2 | APC | 104 | IgG2a | Mouse | BioLegend |
| CD62L | FITC | MEL-14 | IgG2a | Rat | BioLegend |
| CD127 | PE | A7R34 | IgG2a | Rat | BioLegend |
| KLRG1 | FITC | 2F1/KLRG1 | IgG | Syrian hamster | BioLegend |
| IFN-γ | FITC | XMG1.2 | IgG1 | Rat | BD |

### 3.3.2 Conjugated antibodies specific for human surface antigens

The following fluorophore coupled anti-human antibodies were used (Table 4).

Table 4: Conjugated anti-human antibodies

| Specificity | Conjugate | Clone | Isotype | Host | Source |
|---|---|---|---|---|---|
| CD3ε | PB | HIT3a | IgG2a | Mouse | BioLegend |
| CD4 | BV421 | RPA-T4 | IgG1 | Mouse | BioLegend |
| CD8a | APC | HIT8a | IgG1 | Mouse | BioLegend |
| CD8a | PE/Cy7 | HIT8a | IgG1 | Mouse | BioLegend |
| CD19 | APC | HIB19 | IgG1 | Mouse | BioLegend |
| CD45RA | PB | HI100 | IgG2b | Mouse | BioLegend |
| CD45RO | PerCP/Cy5.5 | UCHL1 | IgG2a | Mouse | BioLegend |
| CD62L | FITC | DREG-56 | IgG1 | Mouse | BioLegend |
| CD138 | BV421 | MI15 | IgG1 | Mouse | BioLegend |
| CD197 (CCR) | PE | G043H7 | IgG2a | Mouse | BioLegend |
| CD223 (LAG-3) | AF647 | 11C3C65 | IgG1 | Mouse | BioLegend |
| CD269 (BCMA) | APC | 19F2 | IgG2a | Mouse | BioLegend |

| | | | | | |
|---|---|---|---|---|---|
| CD279 (PD-1) | PE | EH12.2H7 | IgG1 | Mouse | BioLegend |
| CD366 (TIM-3) | BV421 | F38-2E2 | IgG1 | Mouse | BioLegend |
| IgG | PE | | Polyclonal | Goat | Southern Biotech |

### 3.3.3 MHC Multimers

The following MHC multimers for staining of antigen-specific T cell were used (Table 5).

Table 5: MHC multimers

| Specificity | Peptide | MHC | Conjugate | Source |
|---|---|---|---|---|
| SV40 large T antigen | VVYDFLKL | H-2Kb | PE | IMMUDEX |
| miHag UTY (ubiquitously transcribed tetratricopeptide repeat gene on the Y chromosome) | WMHHNMDLI | H-2Db | PE | ProImmune |

### 3.3.4 Unconjugated primary antibodies for Western Blot

The following unconjugated primary antibodies were used (Table 6).

Table 6: Uncoupled primary antibodies

| Specificity | Clone | Isotype | Source |
|---|---|---|---|
| Calnexin | Polyclonal | Rabbit | Enzo |
| EBAG9 serum | Polyclonal | Rabbit | Home-made AG Rehm[65] |

### 3.3.5 Secondary antibodies for Western Blot

The following secondary antibodies were used (Table 7).

Table 7: Secondary antibodies

| Specificity | Conjugate | Host | Source |
|---|---|---|---|
| Anti-rabbit | HRP | Goat | Southern Biotech |

## 3.4 Cell lines

The following cell lines were used (Table 8).

Table 8: Cell lines

| Cell line | Description |
|---|---|
| B3Z | Mouse T cell hybridoma, generated by the fusion of an ovalbumin-specific T cell clone with a derivative of the mouse BW5147 thymoma cell line[141] |
| DOHH-2 | Human B-cell non-Hodgkin's lymphoma, specifically follicular centroblastic/centrocytic lymphoma |
| HEK 293T | Human embryonic kidney cell line |
| JeKo-1 | Human B-cell non-Hodgkin's lymphoma, specifically mantle cell lymphoma |
| Jurkat76 | Human TCR-deficient derivative of J.RT3-T3.5 Jurkat cell line |
| MM1.S Luc-eGFP | Human multiple myeloma, stable expression of a firefly luciferase-eGFP construct |
| OPM-2 | Human multiple myeloma cell line |
| PlatE | Ecotropic packaging cell line Platinum-E, derivative of HEK-293T, stable expression of MLV *gag-pol* and *env* genes[142] |

## 3.5 Mice

EBAG9$^{-/-}$ mice (background C57BL/6) were previously generated in our group and described by Rüder *et al*. 2009[64]. Breeding pairs of C57/BL6, the congenic C57BL/6 Ly5.1 strain and the *Rag2*$^{-/-}$ (*recombination activating gene 2*) strain were obtained from Charles River Laboratories. The transgenic MataHari mice that express an MHC class I-restricted HY-specific TCR were kindly provided by Prof. Il-Kang Na (Charité Berlin) and crossed together with the EBAG9$^{+/+}$ and EBAG9$^{-/-}$ mice strain[143]. NOD.Cg-Prkdcscid Il12rg tm1 Wji/SzJ (NSG) mice were purchased form The Jackson Laboratories and subsequently used as breeding pairs. All mice were housed and maintained in a controlled pathogen-free environment at the animal facility of the Max-Delbrück-Centrum for Molecular Medicine (MDC) Berlin. In all experiments, control groups were matched for their age, sex and strain background. All animal studies were conducted in compliance with the institutional guidelines of the MDC and approved by the Berlin State review board at the Landesamt für Gesundheit und

Soziales, Berlin (registered under *Landesamt für Gesundheit und Soziales* TVV G0091/15; G0050/16).

## 3.6 Chemicals and consumables

Abbott: Isoflurane

BD: 7-aminoactinomycin (7-AAD)

C. Roth: 2-propanol, acetone, agar, ammonium persulfate (APS), ampicillin, bovine serum albumin-fraction V, didecyldimethylammoniumchloride, calcium chloride, ethanol, glycerin, glycine, hydrochloric acid, ethylenediaminetetraacetic (EDTA), hydrogen phosphate, yeast extract, methanol, milk powder, peptone, phenylmethysulfonyl fluoride (PMSF), sodium hydroxide, sodium chloride, Rotiphorese Gel 30 (30% acrylamide, 0.8% bisacrylamide), tetramethylethylenediamine (TEMED), TritonX-100, polysorbate 20 (Tween 20)

Gibco: 2-ethansolfonic acid (HEPES), fetal calf serum (FCS), RPMI-1640, DMEM, Penicillin/Streptamycin 100x, glutamine 100x, sodium pyruvate 100x, minimum essential medium non-essential amino acids 100x

Merck: Biocoll, $N^{\alpha}$-Benzyloxycarbonyl-L-lysine Thiobenzyl Ester (BLT)

Miltenyi: human IL-2, human IL-7, human IL-15

PAN: FCS South Africa

Peprotec: mouse IL-2, human IL-2, human IL-7, human IL-15

| | |
|---|---|
| Sigma-Aldrich: | 5,5`-Dithio-*bis*-(2-nitrobenzoic acid) (DNBT), agarose, aprotinin, dimethyl sulfoxide (DMSO), ethidium bromide, tris(hydroxymethyl)aminomethane (TRIS) base, bromophenol blue, sodium dodecyl sulfate, NP-40 |
| Thermo Fisher Scientific: | eBioscience Cell Proliferation Dye eFluor 670, β-mercaptoethanol, blasticidin, puromycin |

## 3.7 Kits

| | |
|---|---|
| Agilent Technologies: | RNA 6000 Pico Kit |
| BD: | BD OptEIA human IFN-γ ELISA Set |
| | BD OptEIA human TNF-α ELISA Set |
| | BD OptEIA human IL-2 ELISA Set |
| Qiagen: | DNA Maxi Kit |
| | RNeasy Micro/Mini Kit |
| | RNase-free DNase Set |
| | QIAquick Gel Extraction Kit |
| Miltenyi Biotec: | $CD8^+$ T Cell Isolation Kit, human |
| | CD138 MicroBeads, human |
| Thermo Fisher Scientific: | SuperScript® III First-Strand Synthesis SuperMix for qRT-PCR |
| | SuperScript® VILO™ cDNA Synthesis Kit |
| STEMCELL Technologies: | EasySep™ PE Positive Selection Kit |
| | EasySep™ Human T Cell Enrichment Kit |
| Stratec: | Invisorb® Spin Plasmid Mini Two |

## 3.8 Software

| | |
|---|---|
| Adobe: | Illustrator® CS6, Photoshop® CS6 |
| BD: | FACS Diva® |
| Caliper LifeScience: | Living Image® 4.5 |
| GraphPad: | Prism® 6 |
| Microsoft: | Office® 2011 |
| TreeStar: | FlowJo® 10 |

# 4. Methods

## 4.1 Molecular biology

Introducing CAR cDNA into miRNA-encoding MP71 constructs

For cloning the BCMA or CD19 CAR cDNA into the human miRNA-encoding MP71-GFP vector, the NotI and EcoRI specific restriction sites were used to replace the GFP cDNA by either the BCMA or CD19 CAR cDNA. For this purpose, fast digest restriction enzymes from Thermo Fisher Scientific were used according to the manufacturer's instructions. In brief, 2 µg to 5 µg plasmid DNA was mixed with 10x restriction enzyme buffer and 1 µl of each restriction enzyme. In order to remove 5' phosphate residues of vector fragments, 1 U of thermosensitive alkaline phosphatase (Fast-AP) was included in the reaction.

After incubating the enzymatic reaction for 30 min at 37°C, DNA fragments were separated by agarose gel electrophoresis (1% agarose in TAE buffer, 0.5 µg/ml ethidium bromide). Corresponding fragments were then manually extracted from the gel and DNA was isolated by the use of the QIAquick Gel Extraction Kit (Qiagen). DNA concentrations were determined spectrophotometrically at an OD of 260 nm and ligation was performed using the T4 DNA Ligase (Thermo Fisher Scientific) according to the manufacturer's instructions. DNA fragments were used in a molar ratio of 3:1 (insert:vector) and incubated with 1 U T4 DNA Ligase for 1 h at RT.

Plasmid DNA was transformed into the chemically competent *Escherichia coli* (*E. coli*) strain XL1-Blue. To this end, 50 µl of competent cells were incubated with 5 µl DNA for 20 min on ice. Following a heat shock at 42°C for 45 s, cells were cooled down on ice for 5 min. Afterwards, bacteria were mixed with 500 µl LB medium and incubated for 1 h at 37°C and 200 rpm. The transformation mix was then plated onto LB-agar plates containing 100 µg/ml ampicillin (Roth) and incubated overnight at 37°C. The next day, plasmid DNA was extracted using either the Invisorb® Spin Plasmid Mini Two (Stratec) for small scale preparations or the DNA Maxi Kit (Qiagen) for large scale preparations according to the manufacturer's instructions. Plasmid sequence was confirmed by Sanger DNA sequencing performed by either Source BioScience or Eurofins Genomics.

TAE buffer (50x): 2 M TRIS, 1 M acetic acid, 50 mM EDTA (pH 8.0)

DNA loading buffer (6x): 30% glycerol, 10 mM EDTA (pH 8.0), 0.25% bromophenol blue, 0.25% xylene cyanol

LB medium: 1% peptone, 1% NaCl, 0,5% yeast extract

LB-agar: 1.5% agar, in LB medium

RNA Isolation, cDNA synthesis and qRT-PCR

Cells were resuspended in 350 µl RLT lysis buffer (Qiagen) supplemented with 3.5 µl β-Mercaptoethanol and either stored at -80°C or immediately used for RNA isolation. RNA was isolated from cell lysates by using the RNeasy Micro or Mini Kit including the RNase-free DNase Set (Qiagen) according to the manufacturer's instructions. RNA concentrations were determined spectrophotometrically at an OD of 230 nm. For the measurement of RNA integrity, the RNA 6000 Pico Kit (Agilent) was used according to the manufacturer's instructions. Samples with a higher RNA integrity number value of 8 were subsequently used.

For transcribing the isolated RNA into complementary DNA (cDNA), either the SuperScript® VILO™ cDNA Synthesis Kit (Thermo Fisher Scientific) or the SuperScript® III First-Strand Synthesis SuperMix for qRT-PCR (Thermo Fisher Scientific) was used according to the manufacturer's instructions.

Quantitative real-time PCR analysis was done by using TaqMan® probes that anneal specifically to a complementary sequence between forward and reverse primer sites. A reporter dye is linked to the 5' end of the probe and a non-fluorescent quencher to the 3' end. Initially, the proximity of the reporter dye to the quencher dye leads to a suppression of the reporter fluorescence. During the polymerase chain reaction (PCR), the 5'-3' exonuclease activity of the Taq polymerase leads to the cleavage of hybridized probes and the separation of the reporter from the quencher dye results in increased fluorescence by the reporter. The reaction was performed in 10 µl by adding 100 ng cDNA, 1x TaqMan® Gene Expression Assay and 1x TaqMan® Gene Expression Master Mix. Reactions were performed in triplicates using the Applied Biosystems StepOnePlus Real-Time PCR system. Results were analyzed by using the StepOne software (v2.3). The expression of a gene of interest (GOI) was calculated relative to the expression of *Gapdh* by using the following formula:

Relative gene expression (GOI to *Gapdh*) = $2^{-[Ct(GOI)-Ct(Gapdh)]}$

(Ct = mean value of in triplicates measured Ct (threshold cycle) value)

## 4.2 Cell culture

Cultivation and cryo-preservation of cell lines

Cells were cultured at 37°C, 5% $CO_2$ and a relative humidity of 95% in a Binder CB 210 incubator (Binder). Adherent cells were passaged depending on their growth rate at a confluency of 90%. For this purpose, medium was removed, cells were washed with PBS and treated with 0.05% trypsin-EDTA in PBS for 5 min. Cells were centrifuged at 400xg for 5 min and the required number of resuspended cells was added into a culture flask with fresh serum-containing medium. Suspension cells were maintained with 20% to 50% medium exchange once or twice a week depending on cell growth. For cryo-preservation, cells were resuspended in 90 % FCS and 10 % DMSO, transferred to cryo-tubes and stored for 48 h at -80°C in cryo-containers (Nalgene). For longtime storage, cells were transferred into liquid nitrogen. Cells were thawed again by incubation at 37°C for 2 min. Thawed cells were taken up into 10 ml cold medium, centrifuged at 400xg for 5 min and seeded in appropriate culture flasks.

Production of viral supernatant

For the production of ecotropic retroviral particles, calcium phosphate transfection of Plat-E cells with the respective MP71 plasmid was used. The 293T-based retroviral packaging cell line Plat-E is already stably transfected with plasmids encoding gag/pol and env genes and is therefore cultivated with blasticidin [10 µg/ml] and puromycin [1 µg/ml][142]. One day prior to transfection, $4x10^6$ Plat-E cells in 10 ml medium (without blasticidin and puromycin) were seeded into tissue culture-treated 10 cm dishes to reach an optimal confluence of 70-80% at the time of transfection. One day later cells were transfected with 10 µg plasmid DNA per dish.

| | | |
|---|---|---|
| Precipitation mixture per well: | 10 µg | DNA |
| | 30 µl | $CaCl_2$ (2.5 M) |
| | ad 300 µl | $ddH_2O$ |

This solution was incubated for 5 min and mixed under agitation with 300 µl transfection buffer (2xHEBS). After 20 min incubation at RT, 300 µl of this mixture were added dropwise onto the cells. Six h later the medium which contained

25 µM chloroquine to improve transfection efficiency was exchanged against chloroquine-free medium. Supernatants containing the retroviral particles were harvested 48 h after transfection, filtered (0,45 µM pore size) and either used directly for transduced or were frozen and stored at -80°C.

For production of amphotropic retroviral supernatants HEK-293T cells were used. $0.8x10^6$ HEK-293T cells per well in 3 ml medium were seeded into tissue-culture 6-well plates. Transfection of HEK-293T cells was performed using an MP71 construct and two plasmids encoding the MLV env (10A1) and gag/pol genes in a 1:1:1 ratio (6 µg each) following the same protocol as described above.

HEBS (2x): 50 mM HEPES, 280 mM NaCl, 1.5 mM $Na_2HPO_4$, pH 7.05 (+/- 0.05)

Culture medium PlatE: DMEM, 10% FCS (Gibco), 1% penicillin- streptomycin, 1% sodium pyruvat, 1% glutamine

Culture medium HEK-293T: DMEM, 10% FCS (Gibco), 1% penicillin-streptomycin, 1% glutamine

Isolation, transduction and culture of primary mouse T cells

Spleens of 10-12 week old mice were isolated and passed through a 40 µM cell strainer to generate single-cell suspensions. After centrifugation at 400xg for 5 min, cells were resuspended in 5 ml hypotonic ACK erythrocyte lysis buffer. By adding mouse T cell culture medium (mTCM) lysis of red blood cells was stopped after 5 min. Cells were washed and seeded for activation onto 6-well plates coated with anti-mouse CD3 [3 µg/ml] and anti-mouse CD28 [2 µg/ml] antibody in 7 ml medium containing 10 IU/ml mouse recombinant IL-2 (Peprotech) per well. Twenty-four h after activation, mouse splenocytes were transduced once. For this purpose, cell density was adjusted to $1x10^6$ cells/ml and 10 µl per $10^6$ cells T-Activator CD3/28 beads (Thermo Fisher Scientific), 10 IU/ml IL-2 and 4 µg/ml polybrene were added. Next, $1x10^6$ cells per well were transferred to a virus-coated 24-well plate. This non-tissue culture plate was incubated overnight at 4°C with 12,5 µg/ml RetroNectin (TaKaRa), blocked for 30 min at 37°C with 2% BSA in PBS and washed with 25 mM HEPES before 500 µl of virus supernatant per well were transferred and centrifuged for 90 min at 3000xg at 4°C. After transferring 1 ml activated splenocytes per well, cells were centrifuged for 20 min at 800xg at 32°C and cultured overnight. One day after

transduction, positively transduced cells were sorted by FACS and injected intravenously (i.v.) into recipient mice.

ACK lysis buffer (10x): 1.67 M $NH_4Cl$, 100 mM $KHCO_3$. 1.26 mM EDTA, pH 7.3

mTCM: RPMI-1640, 10% FCS (PAN), 1% penicillin-streptomycin, 1% glutamine, 1% sodium pyruvate, 1% minimum essential medium non-essential amino acids (MEM NEAA), 50 µM β-mercaptoethanol

Isolation, transduction and culture of primary human T cells and human cell lines

Peripheral blood from healthy voluntary donors was diluted in human T cell culture medium (hTCM). For isolating human peripheral blood mononuclear cells (PBMCs), a density gradient centrifugation with Biocoll (Biochrom) was performed. Enrichment of $CD3^+$ or $CD8^+$ T cells was achieved by magnetic cell separation, using either the "Easy Sep™ Human CD3 Positive Selection Kit" (STEMCELL Technologies), or the "$CD8^+$ T Cell Isolation Kit, human" (Miltenyi), respectively, according to enclosed protocols. After adjusting the cell density to $1x10^6$ cells/ml and adding either 10 IU/ml recombinant human IL-2 and 10 ng/ml recombinant human IL-15, or recombinant human IL-7 and IL-15 (10 ng/ml each, Peprotech or Miltenyi), cells were transferred to a 24-well tissue culture-treated plate which was coated with anti-human CD3 [5 µg/ml] and anti-human CD28 [1 µg/ml] antibodies. Activated human T cells were subjected to two rounds of transduction starting 48 h after T cell activation. For transduction 500 µl retroviral supernatant was transferred to a RetroNectin-coated 24-well non-tissue-treated plate and centrifuged for 90 min at 3000xg and 4°C. Next, 1 ml activated T cells supplemented with the respective cytokines and 4 µg/ml polybrene were transferred to the virus-coated plate. After adding further virus supernatant (1:4 diluted in hTCM), cells were centrifuged at 800xg at 32°C for 20 min and cultured overnight. Next day, transduction procedure was repeated and 4 h after transduction cells were transferred to cell culture flasks. Cell culture medium supplemented with the respective cytokines was added to the cells as required. On day 13 after T cell activation (prior to functional assays 48 h later), medium was exchanged for fresh hTCM containing 10 IU/ml IL-2 and 1 ng/ml IL-15 (for *in vitro* cytotoxicity, granzyme A release and cytokine secretion assay), or IL-7 and IL-15 at a concentration of 10 ng/ml each (for *in vitro* repetitive antigen stimulation).

MACS buffer: 1x PBS, 0.5% BSA, 2mM EDTA

hTCM: RPMI-1640, 10% FCS (PAN), 1% penicillin-streptomycin, 1% glutamine, 1% sodium pyruvate, 1% minimum essential medium non-essential amino acids (MEM NEAA)

human cell lines: RPMI-1640, 10% FCS (Gibco), 1% penicillin-streptomycin, 1% glutamine, 1% sodium pyruvate, 1% minimum essential medium non-essential amino acids (MEM NEAA)

## 4.3 Functional assays

Flow cytometry and fluorescence-activated cell sorting (FACS)

To detect expression of surface antigens, 1-2x$10^6$ cells per sample were transferred to a well of a round-bottom 96-well microtiter plate and stained with specific antibodies in 100 µl FACS buffer for 20 to 30 min on ice in the dark. Cells were washed twice with FACS buffer and centrifuged (1500 rpm for 1 min). Prior to antibody staining, mouse splenocytes were blocked with anti-mouse CD16/32 antibody in FACS buffer for 20 min on ice and washed once. Fc block for human cells was performed by adding 10% human AB serum. To discriminate between living and dead cells, stained samples were incubated with 7-AAD (Biolegend) 5 to 10 min before data acquisition. Samples were acquired on a FACS Canto II flow cytometer (BD Biosciences) and data were analyzed with FlowJo v. 10.0.8 software (Tree Star). All cell-sorting steps were carried out on a “FACS Aria” or a “FACS Aria Fusion” machine (BD Biosciences). Before sorting, cell suspensions were filtered with a 35 µm cell strainer to remove aggregated cells.

FACS buffer: 1x PBS, 0.5% BSA, 0.05% $NaN_3$, pH 7.3

*In vitro* cytotoxicity assay

Antigen-stimulated *in vitro* cytotoxicity was measured by [$^{51}$Cr]-chromium release. Target cells were labeled with 20 µCi [$^{51}$Cr] sodium chromate (PerkinElmer) in hTCM (+15% FCS) for 90 min at 37°C. After washing, target cells were co-cultured with transduced human CAR T cells (day 15 after activation) in different effector to target ratios for 4 h at 37°C. Assay supernatants were transferred to LUMA-scintillation plates, air-dried and counted for [$^{51}$Cr]-chromium release by using a Top γ-Scintillation Count Reader (PerkinElmer). All samples were performed in duplicates. Target cell maximum release was determined by directly counting labeled cells. Spontaneous

release was measured by incubating target cells alone. Calculation of specific lysis was achieved according to the formula:

%lysis = [(experimental lysis-spontaneous lysis)x100]/(maximum lysis-spontaneous lysis)

Granzyme A release assay

To determine the activity of granzyme A, human CAR T cells (day 15 after activation) were resuspended in FCS-free medium containing 1% BSA (Sigma-Aldrich) at a densitiy of $2x10^6$ cells/ml. The granzyme A release was stimulated by transferring 100 µl cells on an anti-mouse CD3 (3 µg/ml) and anti-mouse CD28 (2 µg/ml) antibody-coated 96-well flat-bottom plate. All samples were performed in triplicates. After incubation for 4 h at 37°C, supernatants were frozen at -20°C or analyzed immediately. To determine the total enzymatic activity, cells were lysed by the use of 200 µl medium with 1% Triton X-100 and incubated for 1 h at 4°C. To calculate granzyme A activity, enzymatic reaction of the substrate $N^{\alpha}$-Benzyloxycarbonyl-L-lysine Thiobenzyl Ester (BLT, Merck Millipore) in the presence of 5,5`-Dithio-*bis*-(2-nitrobenzoic acid) (DNBT, Sigma-Aldrich) was analyzed. Thirty µl of supernatant or cell lysate were incubated for 2 to 5 h at 37°C with 100 µl of granzyme A substrate solution. Product concentration was measured at 405 nm and correlates with enzymatic activity. Supernatants of CAR T cells transferred to non-coated plates were used as a control for the basal secretion of granzyme A.

Granzyme A substrate solution: 0.2 mM BLT, 0.2 mM DNBT, 0.2% Triton X-100 in PBS

Cytokine secretion assay

Antigen-stimulated cytokine secretion by human CAR T cells (day 15 after activation) was analyzed by co-culturing $5x10^4$ human T cells with $5x10^4$ antigen-expressing tumor cell lines (100 µl each) in round-bottom 96-well plates for 16 to 24 h. All samples were performed in duplicates. Supernatants were either frozen at -80°C or analyzed immediately. The concentrations of human IFN-γ, TNF-α and IL-2 were determined by enzyme-linked immunoabsorbent assays using flat-bottom 96-well ELISA plates according to manufacturer's instructions (BD Bioscience). Antigen-independent maximal release was achieved by incubation of CAR T cells with 1 µM ionomycin (Calbiochem) and 5 ng/ml phorbol-12-myristate-13-acetate (PMA, Promega). Minimum release represents T cells incubated without target cells.

Assay buffer: 10% FCS in PBS

Repetitive antigen-stimulation assay/stress test

To analyze the effect of *in vitro* repetitive antigen stimulation on CAR T cells, a stress test was performed in a similar manner as described by Künkele *et al.* 2015[144]. CAR T cells were cultured and transduced in the presence of recombinant human IL-7 and IL-15 (10 ng/ml each). On day 10 to 13 of culture, CAR T cells were co-cultivated in 24-well plates with MM.1S tumor cells at a 1:1 ratio ($5x10^5$ cells each), in the presence of 0.1 ng/ml recombinant human IL-7 and IL-15. Supernatants were harvested to quantify the release of IFN-γ 72 h after co-cultivation. To determine the remaining amount of MM.1S tumor cells within the culture, an aliquot of cells was analyzed by flow cytometry using CD138 staining of tumor and CD3 staining of T cells. All cells of the co-culture were treated with CD138 MACS Micro Beads (Miltenyi) to deplete residual $CD138^+$ tumor cells. Enriched CAR T cells were then used for another round of co-culturing with MM.1S tumor cells at a 1:1 ratio. In total, 5 rounds of transfer over 15 days were performed. After each round, T cells were analyzed for cell numbers, viability, and $CD4^+/CD8^+$ subset distribution. In addition, CAR expression, T cell exhaustion and memory marker expression was assessed.

## 4.4 Protein biochemistry

Preparation of cell lysates and SDS gel electrophoresis (SDS-PAGE)

Generation of cell lysates for detection of protein expression was done by resuspension of cells in RIPA lysis buffer freshly supplemented with the protease inhibitors phenylmethysulfonyl fluoride (PMSF) and aprotinin at a concentration of 1 mM and 5 µg/ml, respectively. After 30 min of incubation at 4°C, lysates were centrifuged (13000 rpm, 10 min, 4°C) to remove cellular debris. The supernatant was either stored at -20°C or analyzed immediately by SDS-PAGE. For the latter, protein samples were mixed with SDS sample buffer and heated at 95°C for 5 min. For protein separation, a 12.5% running gel with 4% stacking gel was used. As a standard for the molecular weight, the “PageRuler prestained protein ladder 10-170 kDa” (Thermo Fisher Scientific) was applied. The electrophoresis was performed in Laemmli running buffer at a constant current of 20 mA per gel.

RIPA: 50 mM TRIS/HCl (pH 7.5), 50mM NaCl, 0.5 mM EDTA, 0.5% NP-40, 0.25% sodium deoxycholate

Lower TRIS buffer (4x): 1.5 M TRIS, 0.4% SDS, pH 8.8

Upper TRIS buffer (4x): 1.5 M TRIS, 0.4% SDS, pH 6.8

SDS sample buffer (2x): 125 mM TRIS/HCl (pH 6.8), 8% SDS, 20% glycerin, 10% β-mercaptoethanol, 0.002% bromophenol blue

Laemmli running buffer (10x): 250 mM TRIS, 2.5 M glycine, 1% SDS, pH 6.8

Protein transfer and immunological protein detection

Separated proteins on the SDS gel were transferred via electroblotting (Mini-PROTEAN® Tetra Cell system, Bio-Rad) onto a nitrocellulose membrane ("Protean BA85 Nitrocellulose Membrane", Whatman) at 150 mA per gel for 90 min in transfer buffer. Alternatively, the transfer was performed at 20 mA per gel overnight. After transfer, the non-specific protein binding sites were blocked by incubation of the membrane in PBS-T supplemented with 5% milk powder for 60 min under agitation at RT. For antibody staining, the membrane was incubated in PBS-T supplemented with 1% milk powder and an uncoupled protein specific primary antibody for 2 h under agitation at RT. The membrane was then washed three times for 5 min with PBS-T and incubated with PBS-T supplemented with 1% milk powder and an HRP-coupled secondary antibodies for 1 h under agitation at RT. This secondary antibody specifically detects and binds to the primary antibody species. The membrane was then washed for three times and protein detection was performed by treating the membrane with the "Pierce ECL western blotting substrate" (Thermo Fisher Scientific) according to the manufacturer's instructions. HRP activity resulted in chemiluminescence signals that were detected using the ChemiDoc (Bio-Rad Laboratories).

Transfer buffer: 25 mM TRIS, 192 mM glycine, 20% methanol

PBS-T: 0.05% Tween 20 in PBS (1x)

## 4.5 *In vivo* experiments

Immunization of EBAG9$^{+/+}$ and EBAG9$^{-/-}$ mice

For the analysis of memory formation, EBAG9$^{+/+}$ and EBAG9$^{-/-}$ mice were immunized once intraperitoneally (i.p.) with 1x10$^6$ Co16.113 cells. On day 6 or between days 55

to 65, mice were sacrificed, and spleens were removed. Splenocytes were isolated by gently disrupting the spleen and application on a 70 µm cell strainer to obtain single cell suspensions. Following lysis of erythrocytes with hypotonic ACK lysis buffer for 5 min at RT, cells were subsequently processed for flow cytometry.

Adoptive transfer of MataHari cells

For the analysis of memory formation upon minor histocompatibility antigen stimulation, splenocytes from female CD45.2$^{+}$ MataHari mice that were EBAG9$^{+/+}$ or EBAG9$^{-/-}$ were isolated and sorted by FACS for CD8$^{+}$ CD62L$^{+}$ naive cells. Afterwards, 4-5x10$^{4}$ sorted cells were transferred into female CD45.1$^{+}$ EBAG9$^{+/+}$ or EBAG9$^{-/-}$ recipient mice by intravenous injection (i.v.). One day later, recipient mice were immunized i.p. with 5x10$^{6}$ male HY$^{+}$ splenocytes. On day 7 or between days 50 to 56, mice were sacrificed, splenocytes isolated and subsequently analyzed by flow cytometry.

*In vivo* killing assay

Donor C57Bl/6 mice were immunized twice i.p. with the SV40 large T-antigen expressing cell line Co16.113 prior to isolation and retroviral transduction of splenocytes. Twenty-four h after transduction, GFP-expressing transduced cells were sorted by FACS and transferred i.v. into RAG2$^{-/-}$ recipient mice. RAG2$^{-/-}$ mice were immunized i.p. on days 1 and 14 after T cell transfer with Co16.113 cells. *In vivo* killing assay was performed on day 19 after transfer. Splenocytes from untreated C57Bl/6 mice were isolated and resuspended in PBS at a density of 1x10$^{7}$ cells/ml. Peptide labeling was achieved by incubation of splenocytes with 4 µg/ml Tag peptide IV for 30 min at 37°C. Half of the cells was left without peptide. Cells were washed and labeled with different amounts of eFluor670 for 10 min at 37°C. The peptide-loaded population was stained with 1 µM eFluor670, while the non-loaded population was stained with 0,1 µM eFluor670. Afterwards, cells were washed once in mTCM and twice in PBS. 2x10$^{7}$ stained target cells were injected i.v. into recipient RAG$^{-/-}$ mice at a ratio of 1:1 of peptide-loaded and non-loaded cells. Recipients were sacrificed 16 h after transfer. Splenocytes were isolated and analyzed by flow cytometry. To calculate the specific lysis, the following formula was applied:

%specific lysis = [1-(control ratio/experimental ratio)]x100

Ratio = % low eFluor670 peak/% high eFluor670 peak

(Low = w/o peptide, high = peptide-pulsed)

Multiple myeloma xenograft model

The human multiple myeloma cell line MM.1S ($0{,}8x10^7$ to $1x10^7$ cells) was injected i.v. into 6-10 week old NSG mice (NOD.Cg-Prkdc$^{scid}$Il2rg$^{tm1\ Wji}$/ SzJ, Jackson Laboratories). The MM.1S cell line is transduced with a lentivirus encoding firefly luciferase in tandem with eGFP[145]. Using luciferin (Biosynth) i.p. application and 10 min later IVIS spectrum imaging (Caliper Life Sciences), the tumor growth was monitored. On day 7 after tumor injection, i.v. CAR T cells were administered ($1x10^6$ CAR positive T cells per mouse). Tumor progression was monitored on day 7 and 13 after T cell injection by measurement of bioluminescence signals. Mice were imaged for several exposure times, ranging between 1 and 150 s. Binning and exposure were adjusted to achieve maximum sensitivity without leading to image saturation. To analyze the bioluminescence signal flux for each mouse as photons/s per $cm^2$ per steradian, the Living Image software version 4.5 (Caliper Life Sciences) was used. On day 15 to 16, animals were sacrificed. Tumor cells and remaining human CAR T cells were detected and analyzed in bone marrow, blood and spleen. To analyze bone marrow cells, femora were dissected and flushed with PBS. The cell suspension was applied to a 70 µm cell strainer, centrifuged (400xg, 5 min, 4°C) and lysed with hypotonic ACK erythrocyte lysis buffer for 5 min at RT. PBMCs from blood were retrieved from heart puncture. The blood was immediately mixed with 50 µl 0.5 M EDTA and lysed twice with hypotonic ACK erythrocyte lysis buffer. Subsequently, cells derived from bone marrow, blood and spleen were analyzed by flow cytometry.

## 4.6 Statistics

For data analysis and determination of statistical significance between groups, the Prism software version 6.0 (GraphPad) was used. Results are expressed as arithmetic means ± standard error of the mean (SEM). Normally distributed data were analyzed by using the Student's unpaired or paired two-tailed t-test or a one sample t-test. The unpaired Mann-Whitney U test was used to analyze non-normally distributed data. Non-normalized values were evaluated using the Wilcoxon signed rank test. Values of $p<0.05$ were considered as statistically significant and were illustrated by one asterisk, values of $p<0.01$ were marked with two asterisks, and values of $p<0.001$ with three asterisks.

# 5. Results

## 5.1 EBAG9 regulates CD8$^+$ T cell memory differentiation

Rüder *et al.* reported that genetically engineered mice with an EBAG9 deletion showed a higher killing capacity of CTLs. The release of granzyme A-containing secretory lysosomes from CD8$^+$ T cells is facilitated in these mice. In addition, a stronger secondary immune response against target cells expressing the SV40 large T-antigen (Tag) was observed[64]. It is currently unclear how the cytolytic capacity of CD8$^+$ T cells is linked to the memory commitment of these cells. Therefore, the first part of this project focused on analyzing the relationship between enhanced cytolytic efficacy and memory formation upon loss of EBAG9. By using a low dose of the strong Tag neoantigen and the minor histocompatibility antigen (mHag) HY, the role of cytolytic strength on T cell fate decision under non-inflammatory conditions was explored.

### 5.1.1 Loss of EBAG9 leads to an enhanced antigen-specific memory CD8$^+$ T cell development after immunization with the strong Tag neoantigen

To date, loss of EBAG9 was shown to increase the secondary immune response in animals rechallenged on day 30 with the viral SV40 large T antigen-expressing cell line Co16.113. To examine whether there were differences in the frequency of antigen-specific CD8$^+$ T cells due to EBAG9 deficiency, EBAG9$^{+/+}$ and EBAG9$^{-/-}$ mice were immunized i.p. with a low dose of 1x10$^6$ Tag-expressing Co16.113 tumor cells. Memory formation was analyzed by flow cytometry after 55 to 65 days. To detect antigen-specific T cells, tetramers were used. These multimers are oligomeric forms of MHC molecules bioengineered to present the Tag-derived immunodominant peptide IV (TetIV). Co-staining of CD8$^+$ T cells with TetIV and CD44 revealed 1.5-fold higher frequencies of CD8$^+$ TetIV$^+$ CD44$^{high}$ T cells among all splenocytes of mice lacking EBAG9. While 0.06% of antigen-specific memory CD8$^+$ T cells could be detected in EBAG9$^{+/+}$ mice, 0.09% were present in EBAG9$^{-/-}$ mice. Total cellularity in the spleen of EBAG$^{+/+}$ and EBAG9$^{-/-}$ mice was previously shown to be similar[64]. Naive non-immunized mice served as a negative control for the presence of antigen-specific memory T cells (Figure 4).

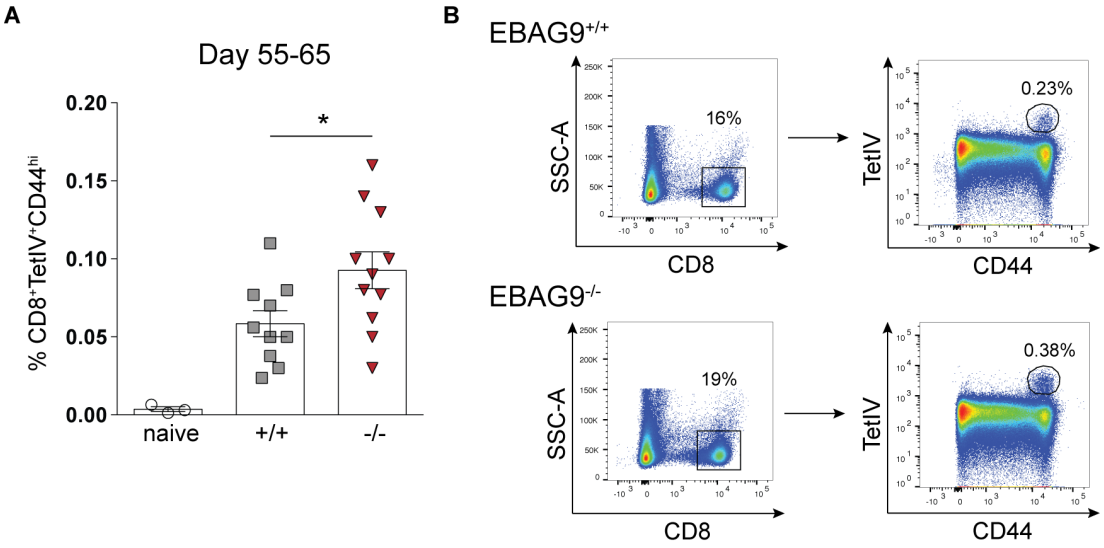


**Figure 4: Loss of EBAG9 leads to an increased CD8⁺ T cell memory formation upon immunization with the Tag neoantigen.**
**(A)** EBAG9$^{+/+}$ and EBAG9$^{-/-}$ mice were immunized i.p. with 1x10$^6$ Tag-expressing Co16.113 tumor cells. On days 55-65, splenocytes were isolated, stained for CD19, CD8, TetIV, and CD44 and subsequently analyzed by flow cytometry. CD19 staining was used to exclude B cells. Frequencies of CD19$^-$ CD8$^+$ TetIV$^+$ CD44$^{high}$ T cells among all splenocytes are depicted. Bars represent mean values ± SEM of n=3 experiments with n=10-11 mice per genotype. *p<0.05, **p<0.01, *p<0.001; ns, not significant. An unpaired t-test was applied. **(B)** Dot plots show one representative gating example for each genotype. Frequencies of CD8$^+$ TetIV$^+$ CD44$^{high}$ T cells are indicated as percentages on the gate.

Effector and memory T cells can be phenotypically distinguished by the expression of distinct surface markers. While increased expression of the killer-cell lectin-like receptor G1 (KLRG1) is associated with differentiation into short-lived effector T cells, expression of the IL-7 receptor α subunit CD127 defines early memory or memory precursor T cells, respectively[146-148]. To examine whether there were differences in precursor frequencies, EBAG9$^{+/+}$ and EBAG9$^{-/-}$ mice were immunized with 1x10$^6$ Co16.113 cells i.p. and analyzed by flow cytometry in the expansion phase on day 6 after immunization in collaboration with Dr. Dana Hoser (Charité Berlin). No differences in antigen-specific CD8$^+$ T cell frequencies were observed at this early stage (Figure 5A). Additionally, in comparison to EBAG9$^{+/+}$ controls, EBAG9-deficient mice exhibited similar frequencies of activated T cells that were characterized by CD44 expression (Figure 5D). Co-staining of antigen-specific CD8$^+$ TetIV$^+$ T cells with KLRG1 and CD127 revealed identical proportions of terminal effector and memory precursor T cells in EBAG9$^{+/+}$ and EBAG9$^{-/-}$ mice (Figure 5B-C). Therefore, in regard to a surface marker-defined distinction into effector and precursor memory CD8$^+$ T cells, the differentiation processes associated with EBAG9 deletion could not be resolved.

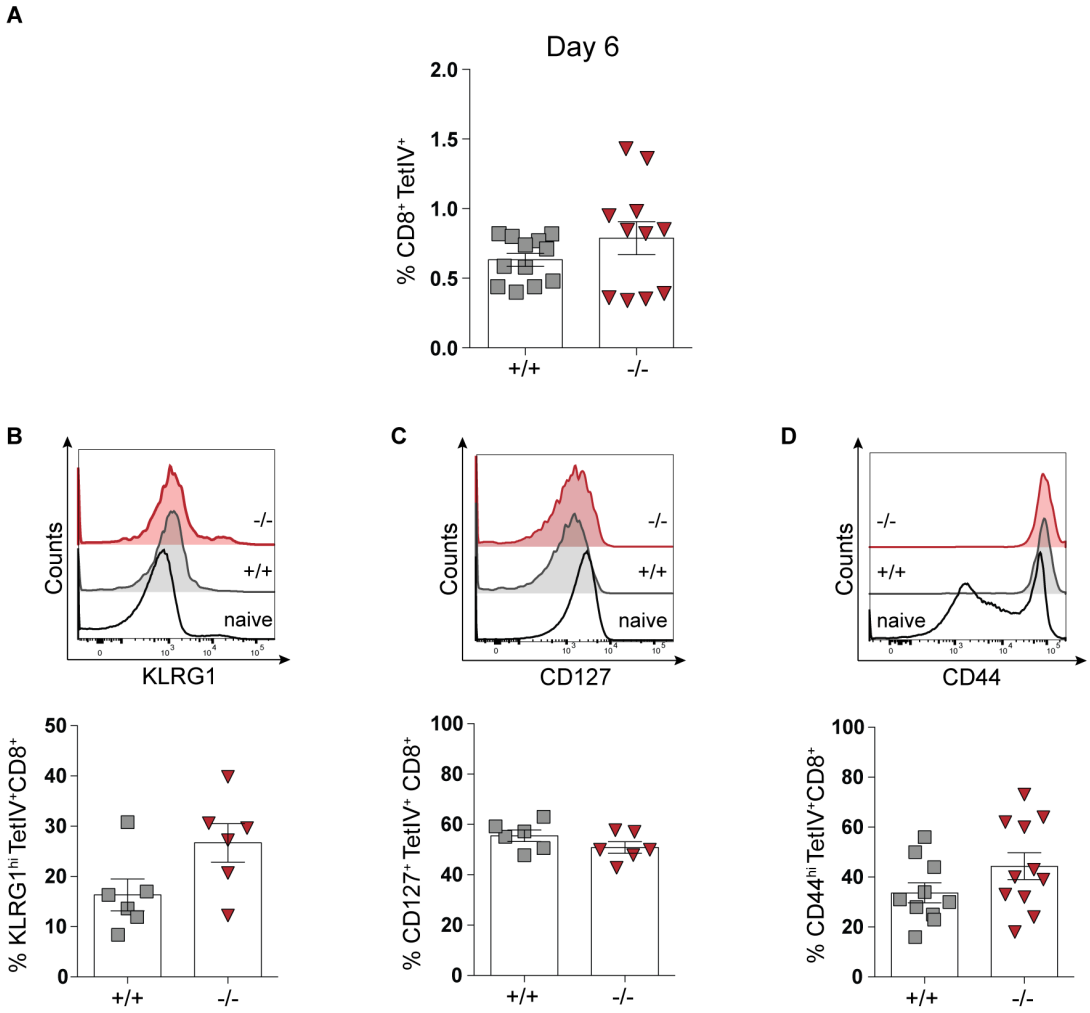


**Figure 5: Similar expression of classical effector and memory surface markers by EBAG$^{+/+}$ and EBAG9$^{-/-}$ mice on day 6 after Tag-immunization.**
**(A)** EBAG9$^{+/+}$ and EBAG9$^{-/-}$ mice were immunized with 1x10$^6$ Tag-expressing Co16.113 tumor cells i.p. and analyzed on day 6 by flow cytometry for frequencies of antigen-specific CD8$^+$ TetIV$^+$ T cells. Bars represent mean values ± SEM of n=3 experiments with n=11-13 mice per genotype. *p<0.05, **p<0.01, *p<0.001. A Mann Whitney U test was applied. **(B-D)** Expression of surface markers for effector and memory T cells on day 6 after immunization by co-staining of CD19$^-$ CD8$^+$ TetIV$^+$ cells with KLRG1, CD127 or CD44. Histograms show one representative example per genotype. For KLRG1 and CD127, gates were set for CD8$^+$ TetIV$^+$ KLRG1$^+$ or CD8$^+$ TetIV$^+$ CD127$^+$ cells, respectively, while the CD44 histogram represents expression of CD44 in the CD8$^+$ TetIV$^+$ gate. Bars represent mean values ± SEM of n=3 experiments with n=6-11 animals per genotype. Significances were calculated by an unpaired t-test; all comparisons are non-significant.

Several transcription factors have been shown to coordinate and regulate the balance between long-lived memory and terminally differentiated CD8$^+$ T cells. These transcription factors often function in pairs and form counter-regulatory axes. For example, Eomesodermin (EOMES) and T-bet are T box transcription factors with crucial roles in the formation and function of effector and memory T cells. Although EOMES and T-bet cooperate in many aspects for sustaining CTL identity in early activated CD8$^+$ T cells, their expression is of a reciprocal nature. The ratio of EOMES to T-bet is highest at memory cell stages and lowest at effector cell stages[23]. Another

interesting pair of antagonistic transcription factors is BCL-6 and BLIMP1. While BLIMP1 is a transcriptional repressor that is expressed by effector T cells, BCL-6 expression is inversely correlated with the expression of BLIMP1. Therefore, BCL-6 is crucial for the memory T cell formation[12].

To gain a better understanding of transcription factors that are important during the early stages of activation in Tag-specific $CD8^+$ T cells, qRT-PCR analysis was performed. $EBAG9^{+/+}$ and $EBAG9^{-/-}$ mice were immunized with $1x10^6$ Tag-expressing Co16.113 cells followed by the fluorescence-activated cell sorting (FACS) of antigen-specific $CD8^+$ $TetIV^+$ T cells on day 6 after immunization. Gene expression analysis revealed that *Eomes* expression was upregulated 4-fold in EBAG9-deficient mice compared to EBAG9-proficient mice. There were no significant differences in the expression of *Tbx21* (encodes for T-bet), *Bcl6*, or *Prdm1* (encodes for BLIMP1) detected (Figure 6).

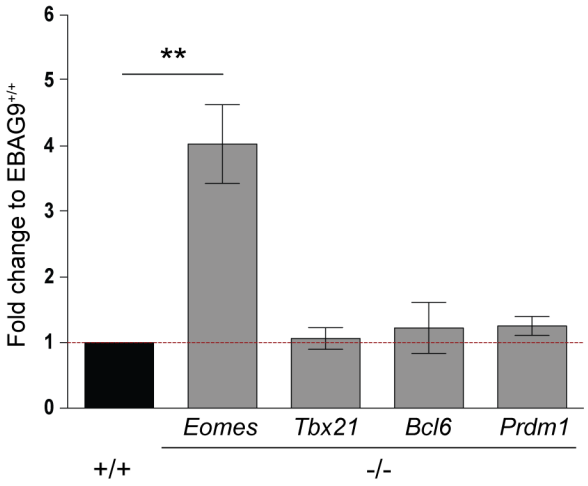


**Figure 6: Loss of EBAG9 leads to the increased expression of the memory formation promoting transcription factor EOMES.**
On day 6 after immunization of $EBAG9^{+/+}$ and $EBAG9^{-/-}$ with $1x10^6$ Co16.113 i.p., antigen-specific $CD19^-$ $CD8^+$ $TetIV^+$ T cells were sorted by FACS followed by RNA isolation. Gene expression analysis was performed by qRT-PCR. Gene expression in the $EBAG9^{+/+}$ samples was set arbitrarily at 1. Bars represent mean values ± SEM of n=3 experiments with n=3 samples pooled from 2-3 animals per genotype. *p<0.05, **p<0.01, *p<0.001; ns, not significant. An unpaired t-test was applied.

### 5.1.2 Deletion of EBAG9 confers mice with a selective advantage for the development of a larger HY-specific $CD8^+$ memory pool

The previous results were obtained under non-inflammatory conditions by employing an immunization protocol whereby a low dose of a strong neoantigen was administered. These immunizations recruit a polyclonal T cell repertoire. To avoid

potential alterations in the TCR repertoire, affinities, or precursor frequencies that might exist in EBAG9$^{-/-}$ mice, these mice were crossed to transgenic monoclonal MataHari mice expressing an MHC class I-restricted HY-specific TCR[143]. HY is a D$^{b}$-restricted weaker immunogenic mHag encoded by genes on the Y chromosome.

To mimic low physiological precursor frequencies, an adoptive transfer approach was used. Accordingly, 4-5x10$^{4}$ naive (CD8$^{+}$ CD62L$^{high}$) EBAG9$^{+/+}$ and EBAG9$^{-/-}$ MataHari CD8$^{+}$ CD45.2$^{+}$ T cells from female donors were sorted by FACS and transferred i.v. into CD45.1$^{+}$ female recipient mice. The congenic markers CD45.1 and CD45.2 were used to further distinguish recipient-derived and transferred T cells. On days 50-56 following immunization with 5x10$^{6}$ HY$^{+}$ male splenocytes i.p., memory formation in the donor-derived CD45.2$^{+}$ population was analyzed by flow cytometry. Co-staining of CD8$^{+}$ CD45.2$^{+}$ T cells with CD44 revealed 1.5-fold higher frequencies of EBAG9$^{-/-}$-derived MataHari memory T cells (CD8$^{+}$ CD45.2$^{+}$ CD44$^{high}$) in all splenocytes (Figure 7A). In addition, there was a significantly higher ratio of CD44$^{high}$ memory cells amongst the CD8$^{+}$ CD45.2$^{+}$ population. Sixty percent of the CD44$^{high}$ T cells were derived from EBAG9$^{+/+}$ mice whereas 75% of the CD44$^{high}$ T cells were from EBAG9-deficient mice. Therefore, in accordance with the results obtained in the polyclonal immune response, loss of EBAG9 also resulted in the development of a larger antigen-specific CD8$^{+}$ memory pool in a monoclonal TCR population (Figure **7**B).

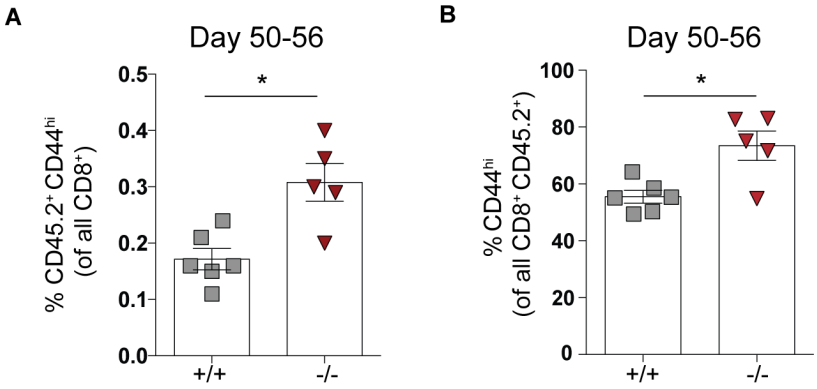


**Figure 7: Higher frequencies of HY-specific CD8$^{+}$ memory T cells within EBAG9-deficient mice.**
**(A-B)** Naive EBAG9$^{+/+}$ or EBAG9$^{-/-}$ CD45.2$^{+}$ MataHari T cells (CD8$^{+}$ CD62L$^{high}$) from female donors (4-5x10$^{4}$) were transferred i.v. into female CD45.1$^{+}$ recipient mice followed by immunization i.p. with 5x10$^{6}$ male HY$^{+}$ splenocytes. On days 50-56, memory formation of the transferred T cells was analyzed by flow cytometry and staining for CD8$^{+}$ CD45.2$^{+}$ CD44$^{high}$ T cells. Bars represent mean values ± SEM of n=2 experiments with n=5-6 mice per genotype. *p<0.05, **p<0.01, *p<0.001; ns, not significant. An unpaired t-test was applied.

To determine whether EBAG9$^{-/-}$-derived memory cells were still functional, the ability of these cells to release the effector cytokine IFN-γ was analyzed. FACS-sorted MataHari memory T cells (CD8$^{+}$ CD45.2$^{+}$ CD44$^{high}$) derived from EBAG9$^{+/+}$ or EBAG9$^{-/-}$ mice were restimulated *in vitro* by co-culture with HY peptide-pulsed dendritic cells (DCs). Flow cytometric analysis revealed, the capability of EBAG9$^{-/-}$-derived memory cells to produce identical rates of IFN-γ (Figure 8).

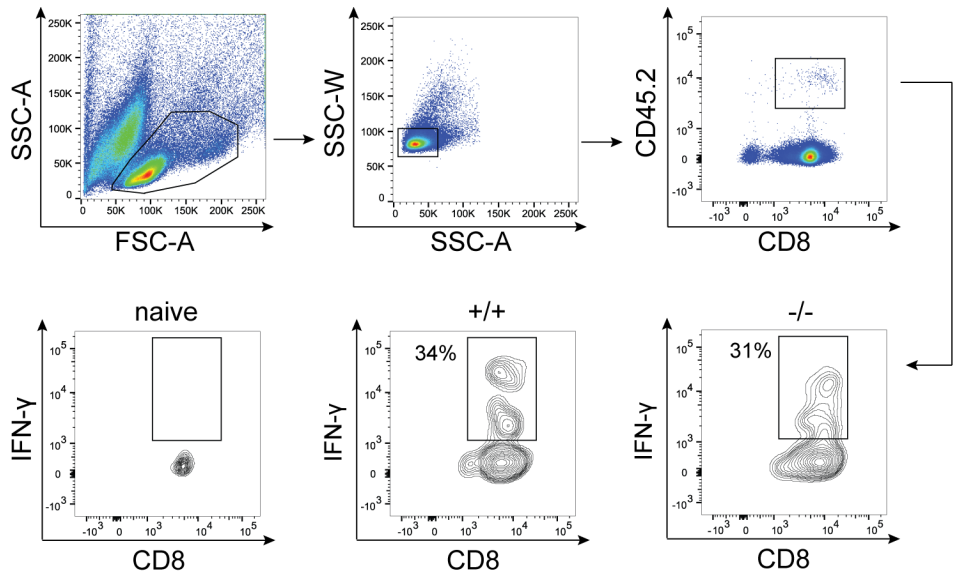


**Figure 8: Functionality of EBAG9-deficient MataHari memory T cells.**
MataHari memory T cells (CD8$^{+}$ CD45.2$^{+}$ CD44$^{high}$) were sorted by FACS and restimulated *in vitro* by co-culture with HY peptide-pulsed dendritic cells. Effector cytokine release was measured by intracellular staining of IFN-γ. Frequencies of CD45.2$^{+}$ CD8$^{+}$ IFN-γ$^{+}$ positive populations are indicated as percentages on the gate.

To explore whether lineage commitment after transfer of low numbers of monoclonal MataHari T cells resembles the observations on the polyclonal Tag-specific precursor activation, surface markers for effector and memory differentiation were analyzed. After transferring 4-5x10$^{4}$ naive EBAG9$^{+/+}$ or EBAG9$^{-/-}$ MataHari T cells (CD8$^{+}$ CD45.2$^{+}$ CD62L$^{high}$) from female donors into female CD45.1 recipient mice i.v., mice were immunized i.p. with HY$^{+}$ male splenocytes. On day 7 after immunization, identical amounts of CD8$^{+}$ CD45.2$^{+}$ T cells among all splenocytes were found for EBAG9$^{+/+}$ and EBAG9$^{-/-}$-derived MataHari T cells. Comparable total cell numbers of these antigen-specific T cells in the spleen were observed. This result indicates a similar expansion of both populations (Figure 9A-B). In accordance with the data obtained when animals were immunized with the strong Tag neoantigen, EBAG9-deficient MataHari T cells revealed similar frequencies of terminal effector (CD8$^{+}$ KLRG1$^{+}$) and memory precursor (CD8$^{+}$ CD127$^{+}$) T cells as EBAG9$^{+/+}$ controls. Furthermore, a similar activation level was observed as the frequency of

$CD44^{high}$ $CD8^+$ $CD45.2^+$ T cells for both genotypes were similar. Altogether, HY-specific $CD8^+$ T cell populations form EBAG9-proficient or EBAG9-deficient mice did not reveal phenotypical differences regarding activation (CD44), effector (KLRG1), or memory (CD127) differentiation in this early expansion phase (Figure 9C-E).

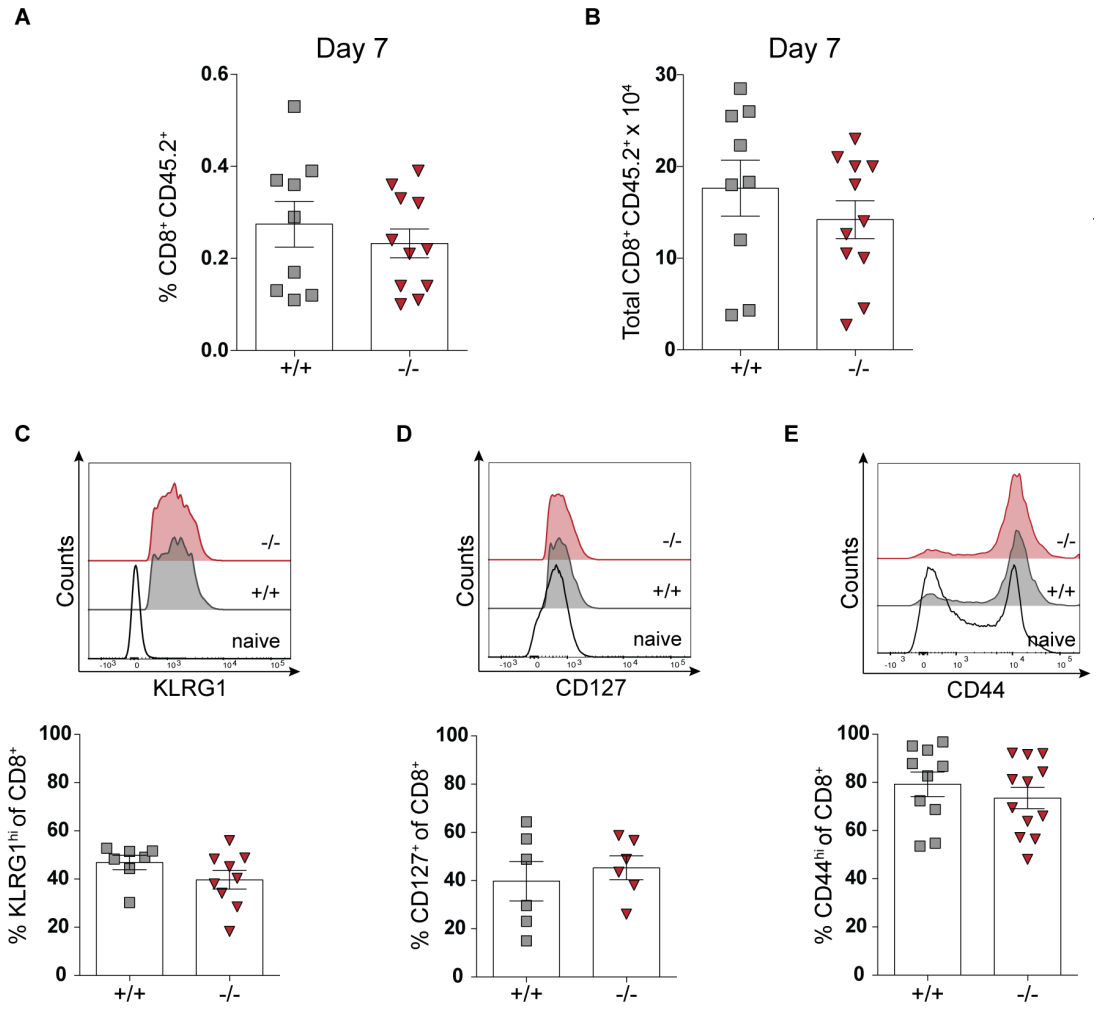


**Figure 9: No differences in the expression of lineage determining T cell surface markers in EBAG9-deficient mice on day 7 after immunization with male splenocytes**
**(A-B)** Naive $EBAG9^{+/+}$ or $EBAG9^{-/-}$ $CD45.2^+$ MataHari T cells from female donors (4-5x$10^4$ cells) were transferred i.v. into female $CD45.1^+$ recipient mice followed by immunization i.p. with 5x$10^6$ male $HY^+$ splenocytes and analysis on day 7 by flow cytometry. **(A)** Frequencies of $CD8^+$ $CD45.2^+$ T cells among all splenocytes and **(B)** total cell numbers are depicted. Bars represent mean values ± SEM of n=3 experiments with n=9-11 mice per genotype. **(C-E)** Expression of surface markers for effector and memory T cells on day 7 after immunization by co-staining of $CD8^+$ $CD45.2^+$ cells with KLRG1, CD127 or CD44. Histograms show one representative example per genotype. For KLRG1 and CD127, gates were set for $CD8^+$ $CD45.2^+$ $KLRG1^+$ or $CD8^+$ $CD45.2^+$ $CD127^+$ cells, respectively, while the CD44 histogram represents expression of CD44 within the $CD8^+$ $CD45.2^+$ gate. Bars represent mean values ± SEM of n=3 experiments with n=6-12 mice per genotype. Significances were calculated by an unpaired t-test; all comparisons are non-significant.

To examine the transcriptional profile of HY-specific T cells that may lead to memory differentiation, female $EBAG9^{+/+}$ and EBAG9-deficient mice were immunized twice i.p.

with $HY^+$ male splenocytes. Our group previously demonstrated the effective elimination of $HY^+$ male target cells in female mice 11 days after immunization with $HY^+$ male splenocytes via *in vivo* killing assays (unpublished data). Therefore, this time point was selected for the sorting of $HY^+$-specific T cells ($CD19^-$ $CD8^+$ $Pentamer^+$). These antigen-specific T cells were further analyzed for gene expression of well-known transcription factors involved in establishing and maintaining a memory T cell pool. In addition to the aforementioned counter-regulatory pairs of the transcription factors EOMES/T-bet and BCL-6/BLIMP1, inhibitor of DNA binding 2 (ID2) and 3 (ID3) were analyzed. Id2 and Id3 are expressed by effector $CD8^+$ T cells. Whereas ID2 supports the survival of effector T cells upon naive to effector cell transition, ID3 regulates their survival at a later stage during effector to memory transition[149]. Furthermore, the IL-12 receptor (IL-12R), the IL-7 receptor (IL-7R), the transcription factor 7 (TCF7), the apoptosis regulatory B-cell lymphoma 2 protein (BCL-2), and the forkhead box protein O1 (FOXO1) are factors rather associated with memory precursor cell differentiation. In contrast, the nuclear receptor RORα and the Runt-related transcription factor 3 (RUNX3) are important for the development of an effector cell population[150].

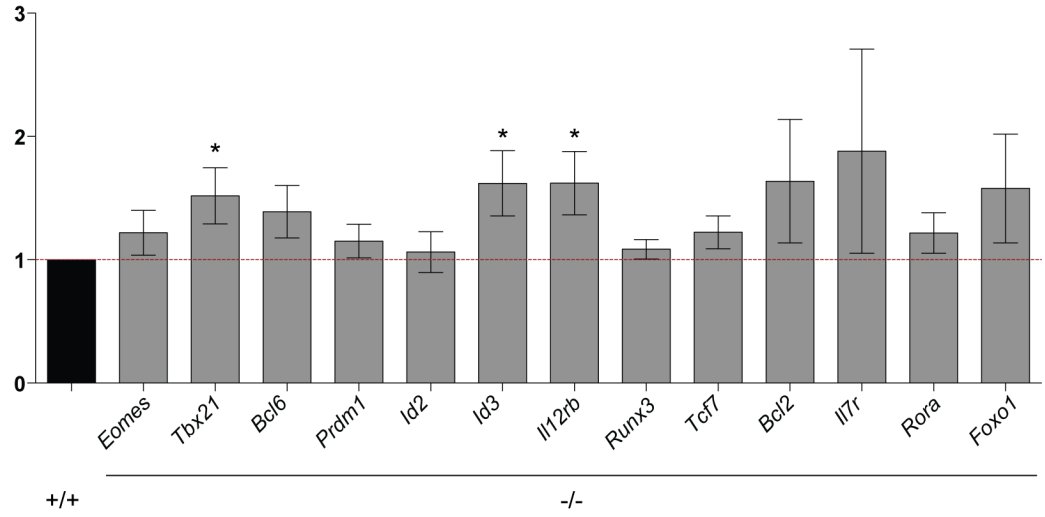


**Figure 10: Differential transcription factor gene expression in $CD8^+$ T cells derived from EBAG9-deficient mice.**
On day 11 after immunization of female $EBAG9^{+/+}$ and $EBAG9^{-/-}$ mice with $5x10^6$ $HY^+$ male splenocytes, antigen-specific T cells ($CD19^-$ $CD8^+$ $Pentamer^+$) were sorted by FACS followed by RNA isolation. Gene expression was determined by qRT-PCR. Gene expression within $EBAG9^{+/+}$ samples was set arbitrarily at 1. Bars represent mean values ± SEM of n=5-6 experiments with n=5-6 samples pooled from 2-3 animals per genotype. *p<0.05, **p<0.01, *p<0.001; ns, not significant. An unpaired t-test was applied.

Of all tested transcription factors, the T box transcription factor *Tbx21* (encodes for T-bet), *Id3*, and *Il12rb* (encodes for the β-subunit of the IL-12 receptor) were

significantly ($p<0.05$) up-regulated by at least 1.5-fold in EBAG9$^{-/-}$ CD8$^+$ T cells compared to EBAG9$^{+/+}$ CD8$^+$ T cells. Although a difference in the gene expression of the *Id3* counterpart *Id2* was not detected, the ratio of *Id2* and *Id3* was clearly shifted towards *Id3* in EBAG9-deficient mice (Figure 10).

Altogether, loss of EBAG9 increased the formation of an CD8$^+$ T cell memory pool within a polyclonal and monoclonal T cell repertoire under non-inflammatory conditions. The increase of the memory population was associated with the differential expression of several transcription factors involved in memory differentiation. Hence, EBAG9 links the cytolytic activity, the duration of antigen accessibility over time, and the commitment to the CD8$^+$ memory lineage. Therefore, EBAG9 defines a regulatory checkpoint for T cell cytotoxicity and memory formation.

## 5.2 Target site validation for EBAG9 knockdown

Most efforts to strengthen ATT are devoted to CTL maturation, high-affinity TCR, or CAR selection. Besides identifying a suitable strategy for inducing potent effector cell function, ensuring the development of a T cell memory response is also important because it is required for long-term immune surveillance[151]. The secretory pathway of T cells appears as an attractive alternative target for improving ATT. We previously showed that EBAG9 negatively impacts the ability of CTLs in recognizing and killing of transformed cells[64]. Furthermore, in the first part of this project, loss of EBAG9 was shown to link the T cell cytolytic strength to an increased formation of an antigen-specific memory pool. Therefore, EBAG9 could be a suitable gene function to connect both aspects of T cell biology, which could play a role in successful T cell tumor immunotherapy. These experiments were performed in genetically deleted animals generated by conventional knockout technology in embryonic stem cells. In order to translate these observations into ATT applicable to patients, it is necessary to generate and analyze *ex vivo* engineered mature CTLs with a stable EBAG9 knockdown. In the next part of this project, different EBAG9-targeting miRNAs were designed and analyzed for knockdown efficiency in the mouse T cell hybridoma cell line B3Z.

For silencing of EBAG9, five different miRNAs (mi141-mi145) targeting different regions within the open reading frame of the mouse *Ebag9* gene and a control miRNA without any target sequence in the genome (mi140) were generated in cooperation with Dr. Mario Bunse (Max-Delbrück-Center Berlin). Four different target site

prediction programs were used for the miRNA design reflecting the requirements of the endogenous RNAi machinery to identify suitable target sites. The miRNA secondary structure is important for recognition and processing by the RNAi machinery. Characteristic features of the miRNA structure are the rather unstructured backbone and the highly base-paired hairpin that encodes the antisense sequence.

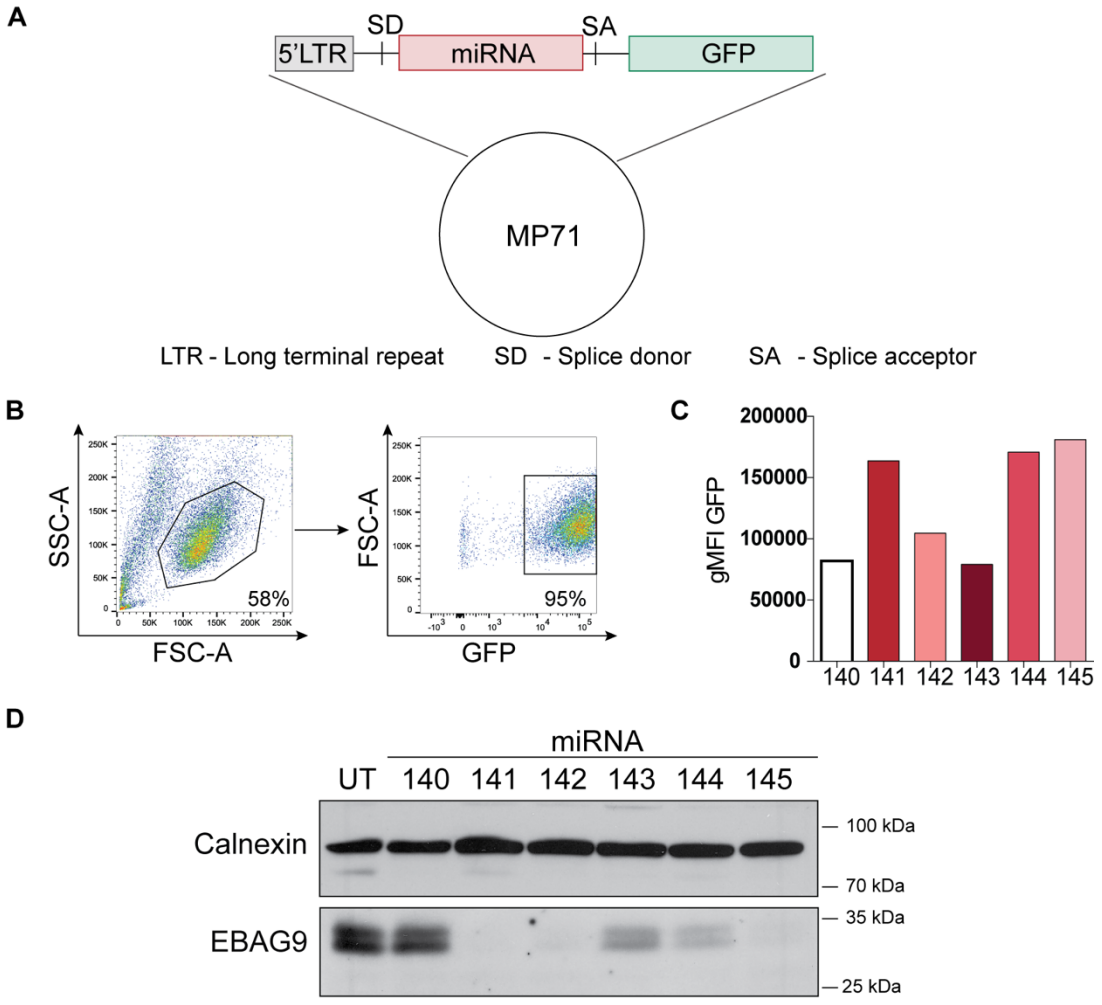


**Figure 11: Effective EBAG9 knockdown after transduction with miRNAs targeting different sites within the murine EBAG9 transcript.**
**(A)** The MP71 vector was used for the simultaneous expression of intronically located EBAG9-targeting miRNA and GFP. **(B-C)** The mouse T cell hybridoma cell line B3Z was transduced with vectors expressing GFP and miRNAs targeting different regions of the *Ebag9* transcript (141-145). miRNA 140 is a negative control without any endogenous target site. GFP expressing positively transduced cells were analyzed by flow cytometry. One representative dot plot for mi142 is shown. The gMFI of GFP is depicted in C. **(D)** Western blot analysis revealed a reduced EBAG9 protein levels due to transduction with sequence-specific miRNAs. Calnexin was used as a loading control. Lysates of $1x10^6$ B3Z cells per group were analyzed.

To generate *Ebag9*-targeting miRNAs, the endogenous miRNA-155 was used. Exchanging the 21 nucleotide containing targeting sequence led to *Ebag9* knockdown. The backbone sequence of miRNA-155 was used, however, in comparison to the native variant, there was a central mismatch of two base pairs and

the GU at the 5' end of the antisense sequence was missing. The resulting miRNA-coding sequences were introduced into a GFP-encoding retroviral MP71 vector at an intronic position. The MP71 vector is known for high transduction efficiency and stable transgene expression in primary T cells[152]. As miRNA transcription is regulated by the polymerase II promoter, the highly active 5' LTR of MP71 can be used to drive miRNA and transgene expression (Figure 11A).

To examine the knockdown efficiency of the different miRNAs, the mouse T cell hybridoma cell line B3Z was transduced. The B3Z cell line is a fusion cell line of myeloma tumor cells and murine primary T cells. GFP expression of transduced cells was analyzed by flow cytometry and revealed a high transduction rate (<90%) for all miRNAs (Figure 11B). Analysis of the mean fluorescence intensity (MFI) of GFP showed that GFP expression is reduced after introducing mi140, mi142, and mi143 in comparison to the miRNAs 142, 144, and 145 (Figure 11C). Western blot analysis revealed that all five sequence-specific miRNAs strongly decreased EBAG9 protein expression. Knockdown efficiencies of mi141, mi142, and mi145 exceeded 90%, whereas the silencing effect of mi143 and mi144 was less effective. The non-targeting mi140 did not alter the EBAG9 protein levels. The ER-located chaperone Calnexin served as a loading control and its expression remained unaffected by retroviral transduction (Figure 11D).

## 5.3 Analysis of RNAi-modified mouse T cells

In the previous section, three highly efficient miRNAs for the silencing of EBAG9 were identified. Vectors encoding for these miRNAs were able to efficiently express RNA molecules that enter the RNAi pathway. Next, two of these three miRNA constructs were selected and a strategy for the efficient transduction of primary mouse T cells was designed. The next part of this project focused on the functionality of RNAi-modified mouse T cells and the question of whether EBAG9 knockdown increases the cytolytic activity of modified T cells *in vivo*. For this purpose, *in vivo* killing assays were performed.

### 5.3.1 Efficient RNAi-mediated EBAG9 downregulation in primary mouse T cells

As mi141 and mi142 were identified as suitable tools for RNAi-mediated EBAG9 silencing in B3Z cells, these miRNAs were also used for further characterization in primary mouse T cells. Activated mouse T cells were retrovirally transduced with the MP71-vector encoding GFP and either one of the sequence-specific EBAG9-targeting

miRNAs or the non-targeting mi140. GFP expression of transduced cells was analyzed by flow cytometry and compared to the unmodified parental MP71-GFP vector on day 4 after transduction. Although high transductions rates of around 50% for GFP$^+$ cells of all T cells were achieved, the transduction efficiency was reduced in comparison to the unmodified vector (Figure 12A-B). Furthermore, GFP intensity was decreased upon miRNA introduction to around 35% to 50% of the parental MP71-GFP vector (Figure 12C-D).

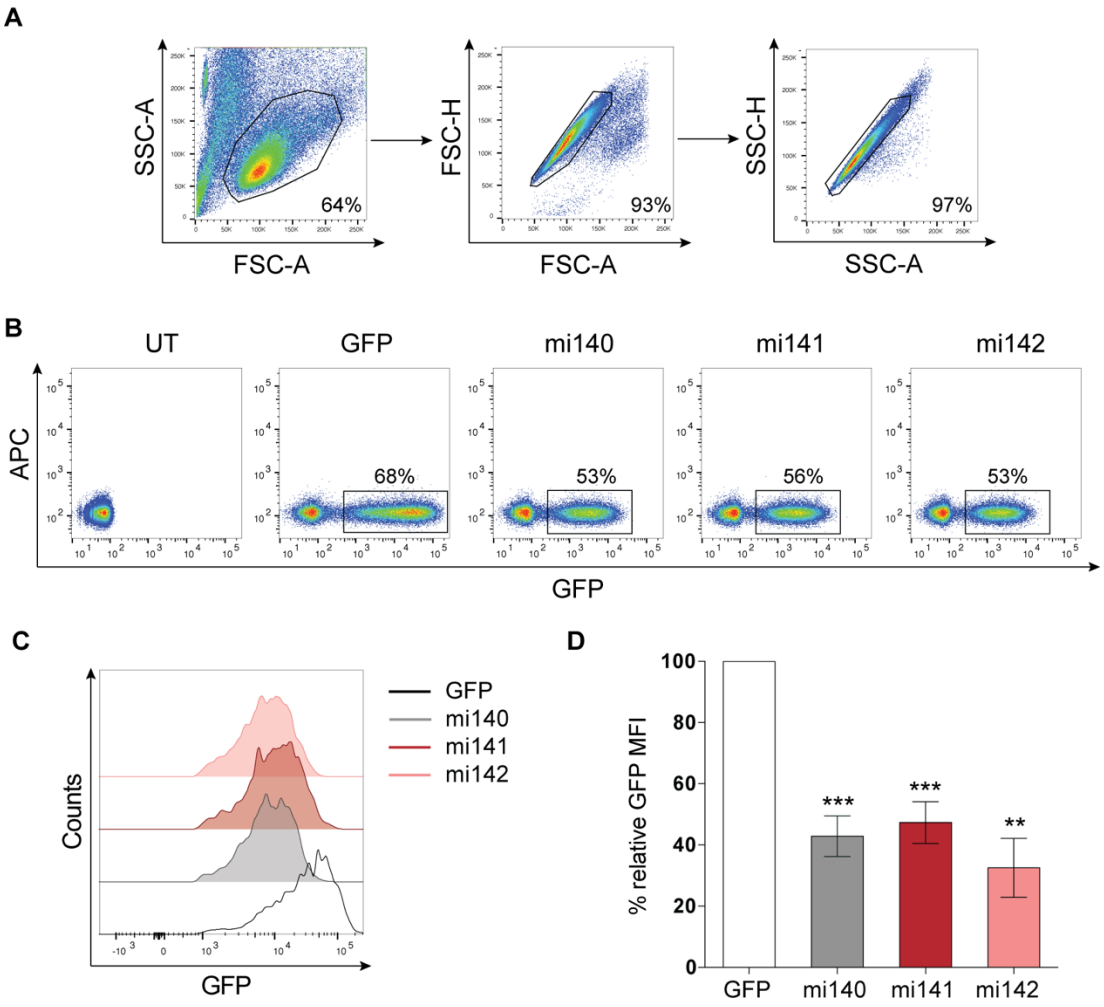


**Figure 12: Efficient transduction of primary mouse T cells with reduced transgene expression.**
**(A-B)** Retrovirally transduced mouse T cells were analyzed by flow cytometry. The gating strategy for lymphocytes and single cells is shown. Positively transduced cells expressed GFP. Transduction rates are indicated by numbers on the gates. **(C-D)** Transduction with vectors carrying GFP and the miRNA led to reduced GFP expression levels. MFI is depicted compared to GFP alone. The histogram shows one representative example for each group. Bars represent mean values ± SEM of n=7 experiments with n=4-8 samples. *p<0.05, **p<0.01, *p<0.001; ns, not significant. A one sample t-test was applied.

To confirm the sequence-specific knockdown of EBAG9 in primary mouse T cells, EBAG9 mRNA and protein levels were examined. RT-PCR and Western blot analysis

were performed after FACS of GFP-expressing transduced T cells. Compared to untransduced mouse T cells, *Ebag9* mRNA levels were reduced by around 80% when the mi141 was employed, whereas the mi142 led to a decrease of about 70%. Transduction with the non-targeting mi140 had no effect on the *Ebag9* gene expression (Figure 13A). On the protein level, an RNAi-mediated EBAG9 knockdown of >90% could be observed for both miRNAs. Transduction with the parental MP71-GFP or the non-targeting mi140 did not alter EBAG9 protein expression (Figure 13B). For subsequent experiments, the mi141 was selected because it had the most efficient silencing effect on EBAG9 gene and protein expression.

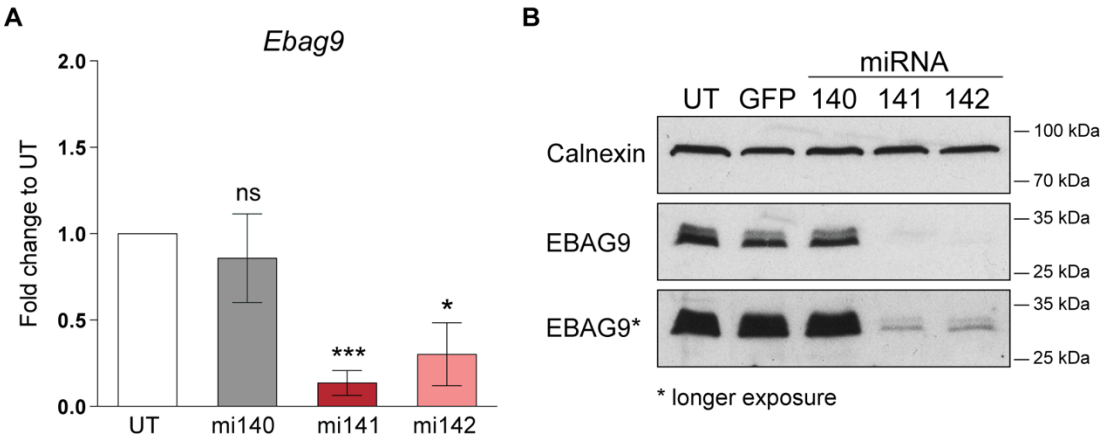


**Figure 13: Validation of an effective EBAG9 downregulation in primary mouse T cells.** **(A)** Following transduction, stable knockdown of EBAG9 mRNA and protein was achieved. Prior to analysis, positively transduced GFP$^+$ lymphocytes were sorted by FACS followed by RNA isolation. mRNA expression was analyzed by qRT-PCR and compared to untransduced control cells. Bars represent mean values ± SEM of n=3 experiments. *p<0.05, **p<0.01, *p<0.001; ns, not significant. A one sample t-test was performed. **(B)** A representative Western blot out of two experiments is depicted. Calnexin was used as a loading control. Lysates of 1x10$^6$ T cells were analyzed.

### 5.3.2 The engineered knockdown of EBAG9 amplifies antigen-specific killing by cytotoxic mouse T cells *in vivo*

To prove the functionality of RNAi-modified cytotoxic T cells *in vivo*, a mouse model was established. C57BL/6 mice were immunized twice with the Tag-expressing cell line Co16.113. Three weeks later, splenocytes were isolated and transduced. Positively transduced GFP-expressing T cells were enriched by FACS and transferred i.v. into immunodeficient RAG2$^{-/-}$ mice. These mice are immunodeficient and lack mature T and B cells[153]. Hence, they are particularly capable of supporting homeostatic and antigen-induced lymphocyte expansion. On days 1 and 14, RAG2$^{-/-}$ mice were immunized twice i.p. with Co16.113 cells. On day 19 after T cell transfer, an *in vivo* killing assay was performed (Figure 14A).

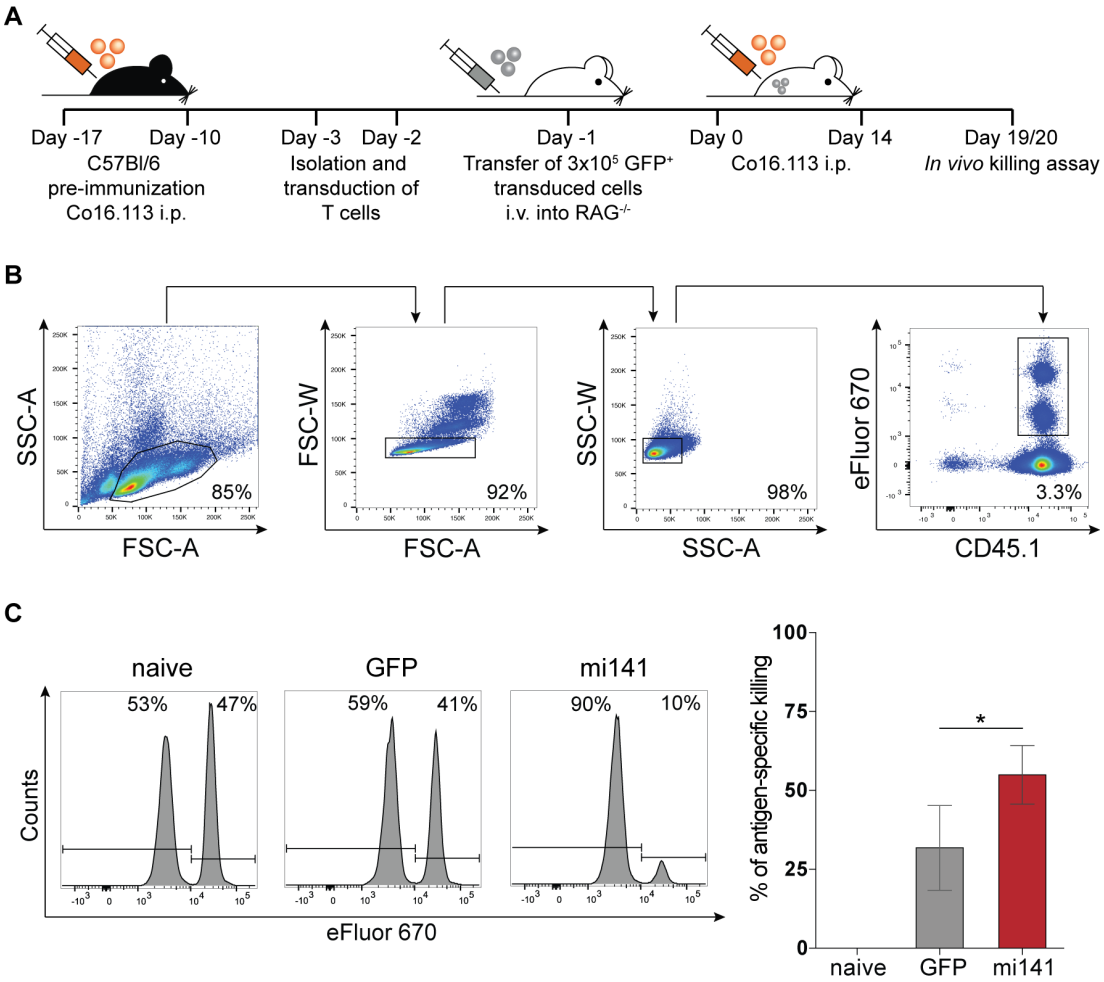


**Figure 14: The *in vivo* killing capacity of engineered mouse CTLs can be doubled by RNAi-mediated silencing of EBAG9.**
**(A)** Schematic representation of the experimental procedure. T cells of pre-immunized mice were transduced and transferred i.v. into RAG2$^{-/-}$ mice. *In vivo* killing assay was performed on day 19 following T cell transfer by challenging RAG2$^{-/-}$ mice with an equal mixture of non-loaded and peptide-loaded splenocytes labelled with different amounts of eFluor 670. The ratio between both populations was determined by flow cytometry after 16 h. **(B)** Gating strategy for leukocytes and single cells is shown. In addition, transferred CD45.1 positive and eFluor 670 stained target cells were analyzed. Frequencies are indicated as percentages on the gate. **(C)** Histograms show one representative example for each group. Percentages of non-loaded and peptide-loaded fractions are indicated. Mean values ± SEM of n=5 experiments are shown with n=5-15 mice per group. *p<0.05, **p<0.01, *p<0.001; ns, not significant. A Mann-Whitney U test was applied.

The killing capacity of transferred T cells was tested by challenging RAG2$^{-/-}$ mice with peptide IV-loaded and non-loaded splenocytes stained with different amounts of eFluor 670. The ratio between both populations was determined by flow cytometry on the following day (Figure 14B). Naive control mice that did not receive T cells and were not immunized failed to recognize and kill transferred peptide-loaded target cells. Mice treated with T cells isolated from immunized mice and transduced with an MP71-GFP retrovirus showed a mean antigen-specific killing rate of 31%. This

antigen-specific killing rate in mice that had received the EBAG9-specific mi141 was 2-fold higher compared to the GFP control group (Figure 14C).

Analysis of T cells revealed no differences in the engraftment or expansion of GFP-transduced or RNAi-modified T cells. For both cell populations, around 10% of transduced T cells among all splenocytes were detectable within RAG2$^{-/-}$ mice on day 20 following transfer (Figure 15B). Collectively, the enhanced killing capacity of T cells equipped with EBAG9 silencing miRNAs was not caused by different effector cell numbers.

Furthermore, transduced cells were co-stained for CD4 and CD8 expression prior to and 20 days after transfer. On the day of injection, GFP- and mi141-transduced T cells exhibited a similar ratio of CD4$^+$ and CD8$^+$ T cells. An average composition of 26% CD4$^+$ and 35% CD8$^+$ T cells could be detected (Figure 15A). In contrast, on day 20 after transfer, there was a significant difference in the T cell subset composition between GFP-transduced and RNAi-modified T cells. While GFP-transduced T cells exhibited a composition of 88% CD4$^+$ and 10% CD8$^+$ T cells, 75% CD4$^+$ and 23% CD8$^+$ T cells were detected after transfer of mi141-transduced T cells (Figure **15**C). These data indicate that RNAi-modification may either lead to a preferential proliferation of CD8$^+$ T cells or to a disturbed CD4$^+$ T cell development. Therefore, CD4$^+$ to CD8$^+$ T cell ratios could be influenced by introducing a miRNA encoding sequence.

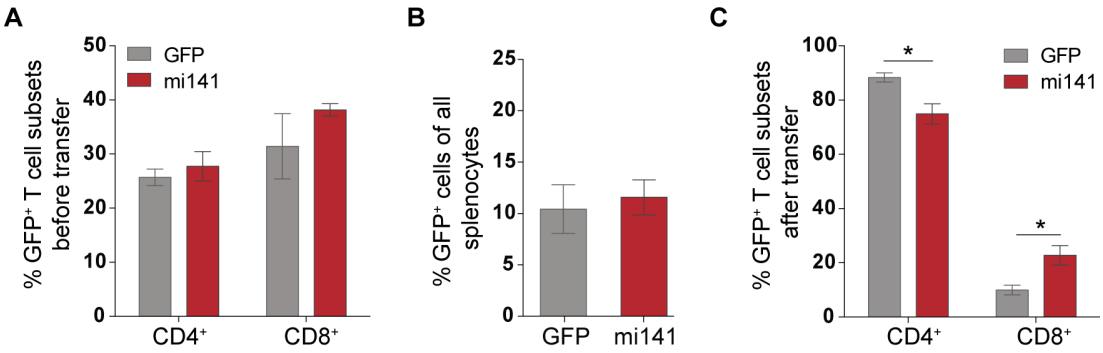


**Figure 15: T cell subset composition differs after RNAi-mediated knockdown of EBAG9.** **(A)** Prior to transfer into RAG2$^{-/-}$ mice, positively transduced mouse T cells (GFP$^+$) were analyzed by flow cytometry. GFP$^+$ cells were co-stained with CD4$^+$ and CD8$^+$. Bars represent mean values ± SEM of n=3 experiments with n=3 samples per group. **(B)** On day 20 after T cell transfer, mice were sacrificed followed by lymphocyte analysis. GFP$^+$ transferred cells were detected by flow cytometry. Bars represent mean values ± SEM of n=5 experiments with 10-15 mice per group. **(C)** Twenty days after T cell transfer, mice were sacrificed, and T cells were analyzed again. GFP$^+$ transferred T cells were detected by flow cytometry and co-stained with CD4$^+$ and CD8$^+$. Bars represent mean values ± SEM of n=5 experiments with 10-15 mice per group. *p<0.05, **p<0.01, *p<0.001; ns, not significant. An unpaired t-test was applied.

## 5.4 RNAi-mediated silencing of EBAG9 in human T cells

As a proof-of-concept, the mouse model has shown that the engineered downregulation of EBAG9 is a suitable strategy to enhance the cytolytic competence of adoptively transferred CTLs. In the next part of this project, a robust translational approach was developed to transfer the RNAi-mediated EBAG9 silencing into a human cell system. Therefore, humanized miRNAs were designed and tested for the ability to silence EBAG9. Furthermore, EBAG9-targeting miRNAs were combined with antigen-specific CARs. Human CAR T cells harboring an engineered knockdown of EBAG9 were then functionally analyzed in regard to their effector molecule secretion and cytotoxic capacity *in vitro*. To exclude adverse effects associated with a loss of EBAG9 and its involvement in secretory pathway regulation, *in vitro* repetitive antigen stimulation was performed. This so-called stress-test provides information on T cell functionality as well as on the differentiation capacity of T cells.

### 5.4.1 Development of a γ-retroviral vector for RNAi-mediated EBAG9 knockdown and the expression of an antigen-specific CAR

In cooperation with Dr. Mario Bunse (MDC Berlin), four humanized miRNAs (H16-H19) were designed and cloned into the MP71-GFP vector. H16, H17, and H18 target the same region within the open reading frame of the *EBAG9* gene as mi141 for murine *Ebag9*, whereas H19 represents a new target site.

Retroviral transduction efficiency and EBAG9 downregulation on the mRNA and protein level were tested in the human acute T cell leukemia cell line Jurkat J76. Compared to the MP71-GFP control vector without miRNA, all humanized miRNAs led to a 1.5-2.5-fold decrease of transduction efficiency (Figure 16A). Yet, an EBAG9 knockdown efficiency of around 80% could be detected for H16, H17, and H18 on an mRNA and protein level compared to untransduced T cells (UT). In contrast, H19 did not effectuate EBAG9 gene or protein downregulation (Figure 16B-C). The most efficient miRNAs H17 and H18 were selected for further analysis in primary human T cells.

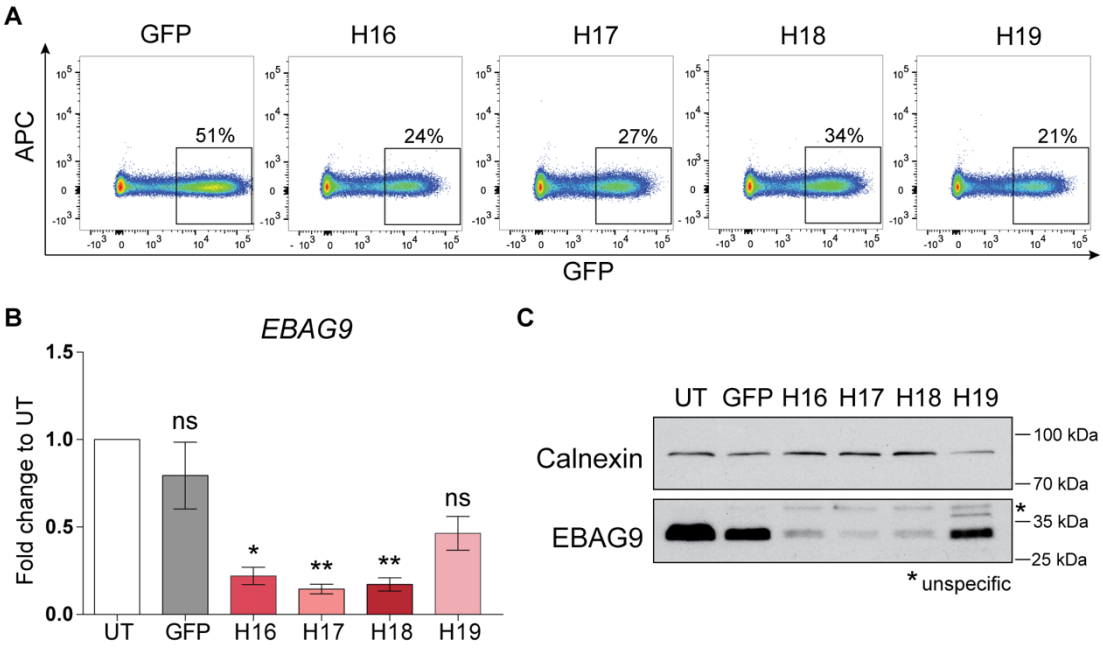


**Figure 16: Decreased human EBAG9 expression in Jurkat cells after transduction with γ-retroviral vectors encoding for different EBAG9-targeting miRNAs.**
**(A)** Retroviral transduction of human Jurkat cells with different GFP-encoding vectors expressing different miRNAs directed against human EBAG9. To determine the transduction rate, GFP expression was measured by flow cytometry. Transduction rates are indicated by numbers on the gates. **(B-C)** Transduction of Jurkat cells with sequence-specific miRNAs leads to a reduction of EBGA9 mRNA and protein. Prior to analysis positively transduced $GFP^+$ cells were enriched by FACS. **(B)** Bars represent mean values ± SEM of n=2 experiments with n=3 samples per group. *p<0.05, **p<0.01, *p<0.001; ns, not significant. A one-sample t-test was applied. **(C)** One representative Western blot out of three experiments performed is shown. Calnexin was used as a loading control. Lysates of $1x10^6$ Jurkat cells were analyzed.

In a next step, the retroviral MP71 vector containing the miRNA H18 was modified to further accommodate a chimeric antigen receptor (CAR) targeted at BCMA as previously generated in our group (Figure 17). This second generation CAR is able to specifically target $BCMA^{high}$-expressing human multiple myeloma (MM) and $BCMA^{low}$-expressing non-Hodgkin's B-cell lymphoma (B-NHL) cells. As a consequence of antigen recognition, BCMA CAR T cells are endowed with effector functions[154].

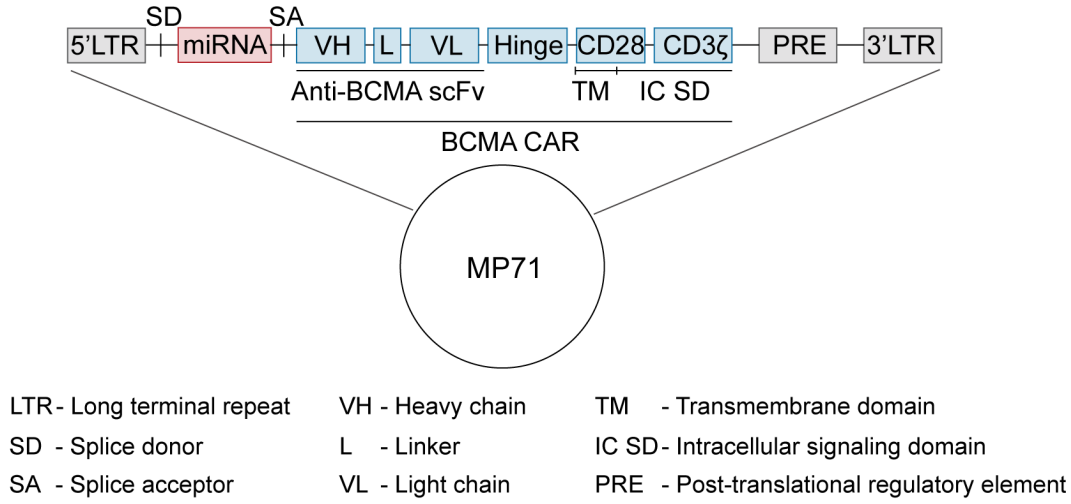


**Figure 17: The MP71 vector is suitable for a simultaneous expression of an EBAG9-targeting miRNA and the BCMA CAR.**
The BCMA CAR was introduced into a miRNA-containing MP71 vector at the indicated position. Schematic representation of the second generation CAR construct containing a high-affinity anti-BCMA scFv, a Whitlow linker, an IgG1 hinge region, a CD28 transmembrane and intracellular signaling domain as well as an intracellular activation domain of CD3ζ.

As a negative control for functional assays, the SP6 CAR without any naturally occurring ligand was combined with the EBAG9-targeting miRNA H18. Retroviral transduction of primary human T cells with the MP71 vector expressing only the BCMA CAR decreased EBAG9 mRNA and protein expression by an average rate of 40% compared to UT. However, RNAi-mediated EBAG9 knockdown in combination with the SP6 or BCMA CAR was efficient and led to EBAG9 downregulation of around 70% to 80% (Figure 18A-B). Comparing transgene expression between T cells transduced with the MP71 vector encoding the BCMA CAR alone with the vector combining the H18 miRNA with the BCMA CAR, revealed a 50% reduction of CAR surface density in the latter (Figure 18C-D).

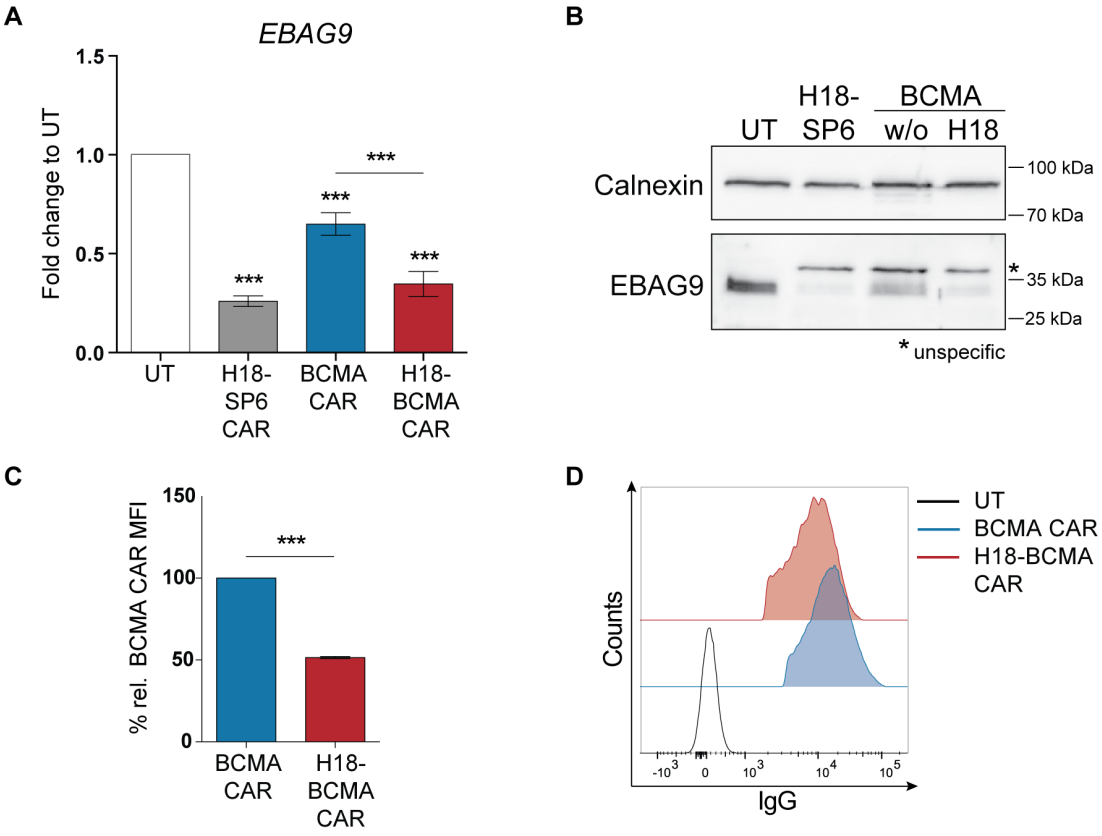


**Figure 18**: **EBAG9 knockdown and BCMA CAR expression in transduced primary human T cells.**
**(A-B)** Transduction of human T cells with vectors encoding either an SP6 or BCMA CAR in conjunction with the miRNA H18 led to a reduction of EBGA9 mRNA- and protein levels. Before analysis, positively transduced cells were sorted by FACS ($CD8^+$ and $IgG^+$). Gene expression was determined by qRT-PCR. UT was set arbitrarily at 1. Bars represent mean values ± SEM of n=2-5 experiments n=4-10 samples per group. *p<0.05, **p<0.01, *p<0.001; ns, not significant. A one-sample t-test was applied. One representative Western blot out of two experiments performed is shown. **(C-D)** Reduced BCMA CAR surface expression of transduced T cells was observed after introducing the miRNA H18 into the vector. BCMA CAR surface density (gMFI) was set arbitrarily at 100%. Bars represent mean values ± SEM of n=2 experiments with n=4 samples. *p<0.05, **p<0.01, *p<0.001; ns, not significant. A one-sample t-test was applied. The histogram shows one representative sample for each group.

### 5.4.2 Downregulation of EBAG9 increases granzyme A release whereas cytokine secretion is not affected

As previously described, EBAG9 negatively influences the regulated secretion of granzyme A from a storage pool of vesicles inside the cell. On the other hand, the constitutive release of newly synthesized cytokines such as IFN-γ is not affected[64]. To prove that EBAG9 silencing specifically increases the release of granzyme A from activated T cells, an *in vitro* release assay was performed. $CD8^+$ T cells from healthy donors were isolated, transduced twice, and cultivated under IL-2 supplementation for 13 days. Prior to functional *in vitro* assays on day 15, IL-2 supplementation was lowered for 48 h (Figure 19A). Retroviral transduction efficiency of human primary

CD8$^+$ enriched T cells was determined by staining of the IgG hinge region and resulted in variable transduction rates between miRNA-transduced and control groups. Therefore, for all further *in vitro* characterizations, transduction rates were adjusted to 20%-30% by adding UT cells. On day 15 of culture, T cells were antigen-independently activated by re-stimulation with anti-human CD3/CD28 antibodies for 4 h. The granzyme A amount released from BCMA CAR-transduced T cells was similar to those of UT (mean of 38%). In contrast, T cells transduced with the H18-BCMA CAR construct released 2-fold higher amounts of granzyme A (mean of 50%). Likewise, the H18 miRNA also endowed SP6 CAR T cells with enhanced cytolytic effector molecule secretion (Figure 19B).

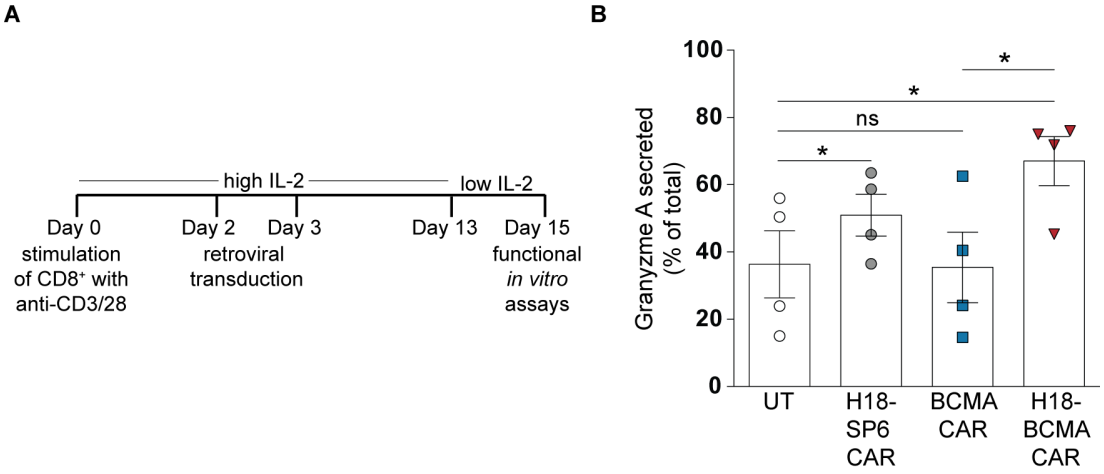


**Figure 19: EBAG9 downregulation facilitates the antigen-independent release of granyzme A from activated human CD8$^+$ T cells.**
**(A)** Experimental timeline for retroviral transduction of human primary T cells prior to functionally *in vitro* assays. **(B)** Human CD8$^+$ T cells were transduced with vectors encoding an SP6 or BCMA CAR in conjunction with the EBAG9-targeting miRNA H18 or the BCMA CAR alone. Enzymatic activities in supernatants were measured on day 15 after CD8$^+$ T cell activation. Granzyme A release was induced by re-stimulation of T cells with anti-human CD3/CD28 antibody for 4 h. Values show the release in percentages relative to the total content. Bars represent mean values ± SEM of n=3 experiments with n=4 independent donors per group. *p<0.05, **p<0.01, *p<0.001; ns, not significant. A paired t-test was performed.

To examine antigen-specific effector cytokine secretion, transduced CD8$^+$ T cells on day 15 of culture were co-cultured with BCMA$^{high}$-expressing MM (OPM-2) and BCMA$^{low}$-expressing B-NHL (DOHH-2, JeKo-1) cell lines at a 1:1 ratio for 24 h. As a negative control, Jurkat cells, which do not express BCMA on the surface, were used (Figure 20A). Experimental controls included minimal cytokine release (MIN) represented by a CAR T cell-only culture, and maximum release achieved by T cell stimulation with PMA/Ionomycin (MAX).

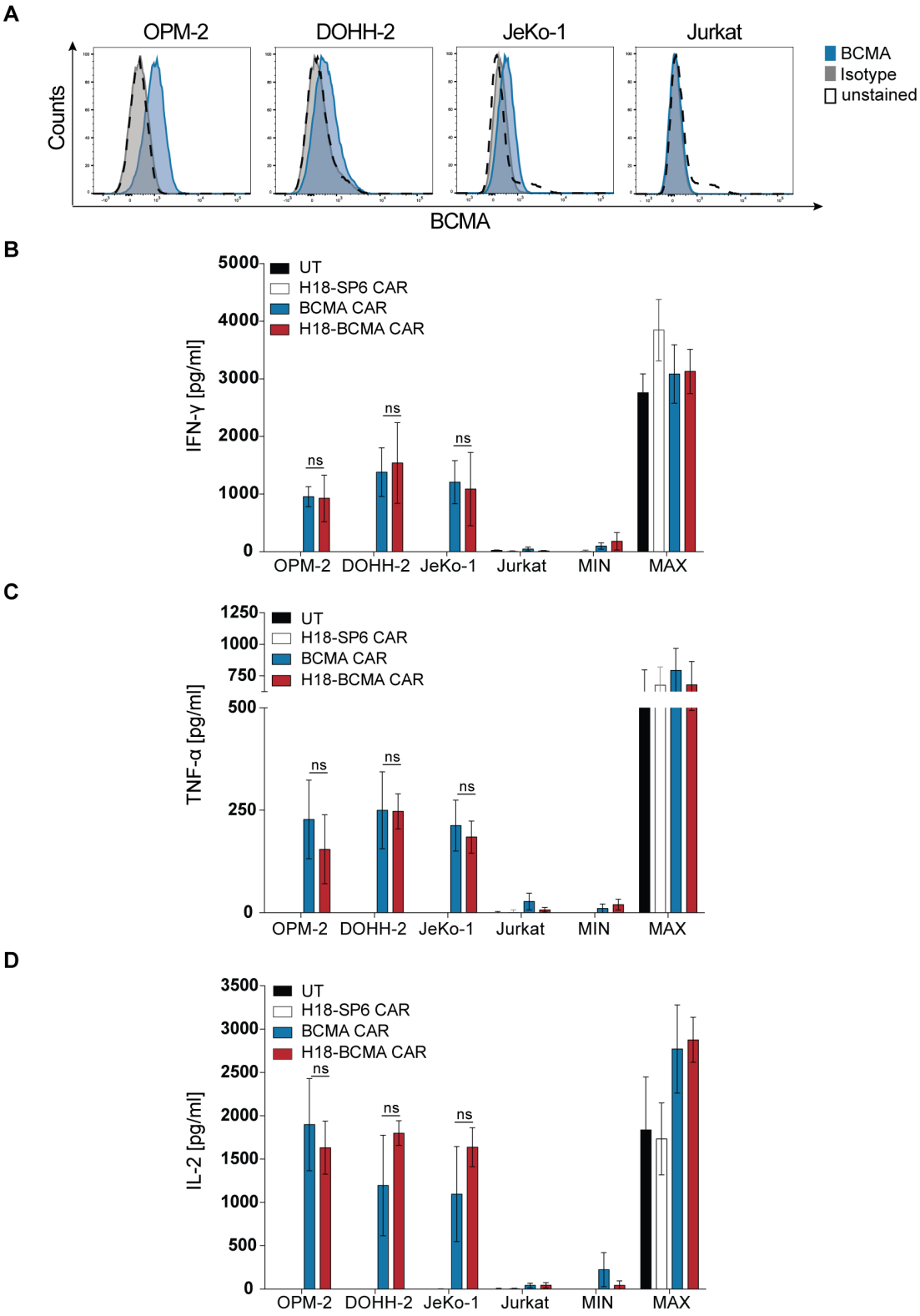


**Figure 20: Antigen-stimulated cytokine secretion from activated human T cells is not influenced by silencing of EBAG9.**
**(A)** BCMA expression on different cell lines was confirmed by flow cytometric analysis. **(B-D)** $CD8^+$ T cells (transduction rates adjusted to 20%-30% by addition of UT) were co-cultured with target cell lines on day 15 after T cell activation at a 1:1 ratio for 24 h. Cell-free supernatants were harvested to measure IFN-γ **(B)**, TNF-α **(C)** and IL-2 **(D)** secretion by ELISA. Bars represent mean values ± SEM error bars, n=2-3 experiments with n=3-6 independent donors per group performed in duplicates. *p<0,05, **p<0,01, ***p<0,00.1; ns, not significant. A Mann-Whitney U test was employed.

All BCMA-expressing cell lines led to activation of BCMA CAR T cells as demonstrated by the secretion of typical T cell effector cytokines IFN-γ, TNF-α, and IL-2. Importantly, there were no significant differences in the cytokine release as a result of EBAG9 downregulation. H18-SP6 CAR T cells were not activated, demonstrating that EBAG9 downregulation did not confer non-specific T cell activation (Figure 20B-D).

### 5.4.3 Downregulation of EBAG9 confers CAR T cells with enhanced cytolytic activity

To investigate the effect of EBAG9 downregulation on the antigen-specific cytolytic capacity of CAR T cells, *in vitro* cytotoxicity assays were performed.

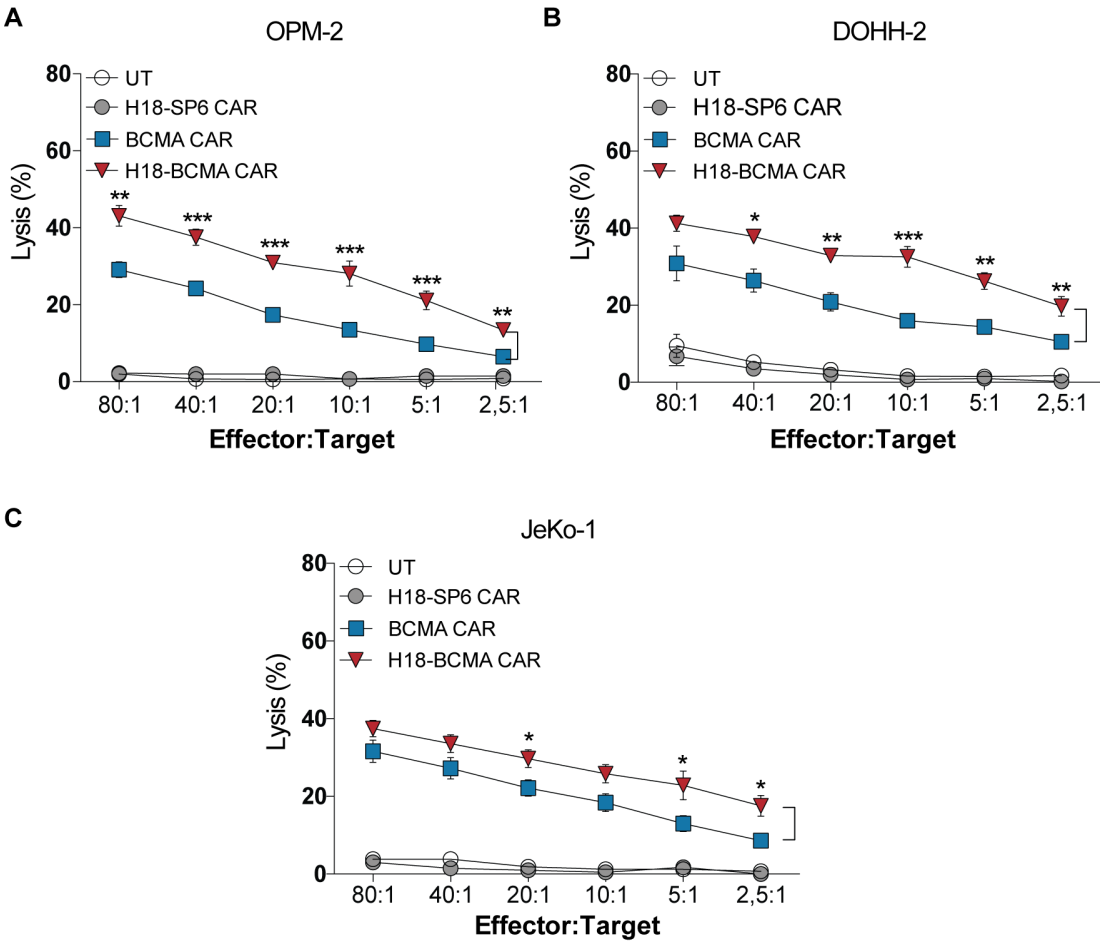


**Figure 21: Antigen-specific cytolytic activity of CAR T cells can be increased by the downregulation of EBAG9.**
**(A-C)** *In vitro* cytotoxicity assays were performed on day 15 of CAR T cell culture. Transduction rates were adjusted to 20%-30% by addition of UT. [$^{51}$Cr] chromium-labeled MM **(A)** and B-NHL **(B-C)** cell lines were co-cultured with transduced human T cells at different effector to target ratios for 4 h. Data represent mean ± SEM error bars, n=5 experiments performed in duplicates with 4-8 different donors per group. *p<0,05, **p<0,01, ***p<0,00.1; ns, not significant. A Mann-Whitney U test was employed.

The BCMA$^{high}$-expressing MM cell line OPM-2, as well as the BCMA$^{low}$-expressing B-NHL cell lines DOHH-2 and JeKo-1, were used as target cells. In contrast to the aforementioned cytokine release assays, *in vitro* cytolytic activity reports on the release of granzymes and perforin. This secretion process is controlled by EBAG9[64]. Prior to co-cultivation with CAR T cells on day 15 of culture, target cells were incubated with [$^{51}$Cr] chromium. After 4 h of co-cultivation with different effector to target ratios, cytolytic activity was observed in BCMA CAR-transduced CD8$^+$ T cells, whereas no or little activity could be detected in UT or SP6 CAR T cells. Therefore, in accordance with the cytokine release assays, no non-specific T cell activation occurred upon EBAG9 downregulation. At the highest effector to target ratio of 80:1, target cell lysis of BCMA CAR T cells was around 30%. The combination of the BCMA CAR with EBAG9 silencing in H18-BCMA CAR T cells led to a significant increase in CAR T cell-mediated cytolytic efficiency in all cell lines tested. For example, in the MM cell line OPM-2, H18-BCMA CAR T cells had a lysis rate approximately 1.5-fold higher than the BCMA CAR only. In a different calculation, the maximal killing rate of BCMA CAR-transduced T cells (E:T 80:1) could be achieved with only one-quarter to one-eighth of EBAG9 knockdown BCMA CAR T cells. Thus, effective dose levels were substantially decreased (Figure 21A-C).

To confirm the RNAi-mediated increase in CAR T cell cytotoxic activity, another miRNA sequence, H17, was used in the context of a CD19 CAR. The CD19 CAR plasmid was kindly provided by the group of Prof. Hinrich Abken (Uniklinik Köln)[155]. As shown for the H18 miRNA, the SP6 CAR was combined with the EBAG9 sequence-specific miRNA H17. Retroviral transduction with the miRNA-containing MP71 vector led to a reduction of the EBAG9 mRNA and protein expression by up to a mean of 50% relative to UT. In contrast, transduction with the CD19 CAR alone did not alter the expression of EBAG9 (Figure 22A-B). As for the BCMA CAR, *in vitro* cytotoxicity assays were performed. Transduction rates of retrovirally transduced CD8$^+$ T cells were adjusted to around 15% using UT. The CD19$^{high}$-expressing B-NHL cell lines JeKo-1 and Raji were used as target cells in a chromium release assay (Figure 22C). After 4 h of co-cultivation, almost no lysis activity could be detected for UT and the control H17-SP6 CAR T cells. In Jeko-1 cells, CD19 CAR-transduced T cells effectuated a specific target cell lysis of about 20% (E:T 80:1). Consistent with the previous results, EBAG9 silencing endowed CAR T cells with a substantial gain in killing activity. For both cell lines, RNAi-mediated T cell engineering resulted in a cytotoxicity increase of 2-fold. Furthermore, to achieve maximal lysis of JeKo-1 or Raji

cells by CD19 CAR T cells, only one-fifth to one-eighth of the H17-CD19 CAR T cells were required (Figure 22D-E).

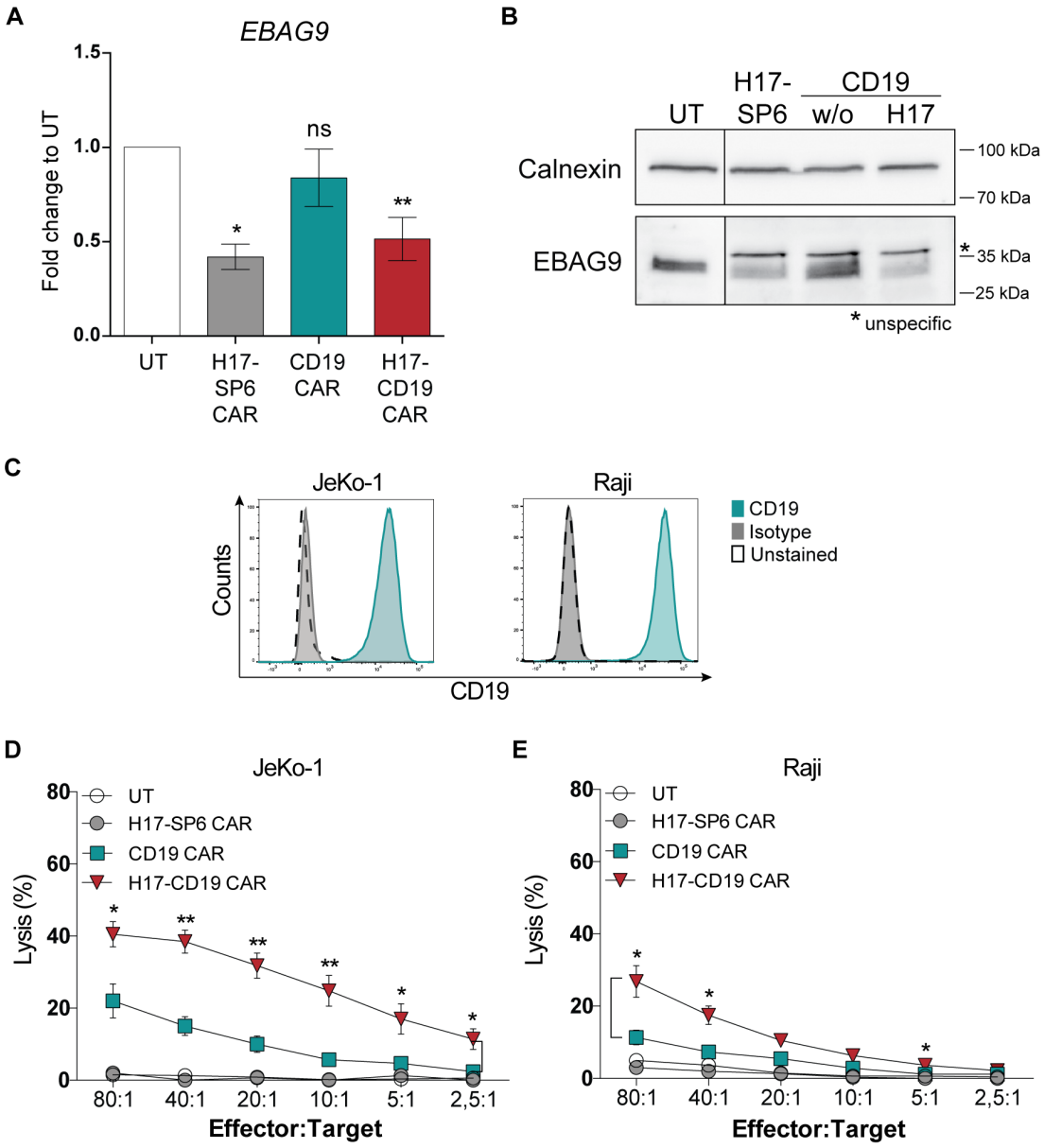


**Figure 22**: **Increasing cytolytic activity of CAR T cells by silencing EBAG9 is a universally applicable cell biological mechanism.**
**(A-B)** Transduction of human CD8$^+$ T cells with vectors encoding either an SP6 or CD19 CAR in conjunction with the EBAG9-targeting miRNA H17 lead to a reduction of EBGA9 mRNA- and protein expression. Prior to analysis, positively transduced cells were staining for CD8$^+$ IgG$^+$ cells sorted by FACS. Bars represent mean values ± SEM of n=2-4 experiments with n=3-9 independent donors per group. *p<0.05, **p<0.01, *p<0.001; ns, not significant. A one-sample t-test was performed. One representative Western blot out of two experiments performed is shown. **(C)** CD19 expression of B-NHL cell lines was confirmed by flow cytometric analysis. **(D-E)** *In vitro* cytotoxicity assays were performed on day 15 of CAR T cell culture. Transduction rates were adjusted to 15% by the addition of UT. [$^{51}$Cr] chromium-labeled Jeko-1 **(D)** and Raji **(E)** cell lines were co-cultured with transduced human T cells at different effector to target ratios for 4 h. Data represent mean ± SEM error bars n=3 experiments performed in duplicates with 3-6 different donors per group. *p<0,05, **p<0,01, ***p<0,00.1; ns, not significant. A Mann-Whitney U test was employed.

Therefore, targeting EBAG9 to increase the cytolytic capacity of CAR T cells is not restricted to the BCMA CAR but appears to be rather a universally applicable cell biological mechanism.

### 5.4.4 No link between enhanced cytolytic activity and exhaustion of RNAi-modified CAR T cells upon repetitive antigen stimulation

The results presented so far proved that EBAG9 knockdown in human supports the increased granzyme A secretion and thus, enhanced target cell lysis by CAR T cells *in vitro*. To exclude that this higher cytotoxic activity causes rapid T cell exhaustion or accelerated activation-induced cell death, an *in vitro* serial transfer was performed to simulate repetitive antigen stimulation[144,154]. Therefore, CAR T cells and RNAi-modified CAR T cells were co-cultured with the BCMA- and CD138-expressing multiple myeloma cell line MM.1S at a ratio of 1:1. CAR T cells (mixed $CD4^+$ and $CD8^+$) were used on days 10 to 13 after activation and culturing under IL-7/IL-15 supplementation. After co-culturing for 72 h, remaining tumor cells were counted and removed using CD138 MACS beads, whereas CAR T cells were transferred to fresh MM1.S target cells. In total, five rounds of transfers were performed, and different T cell functionality and exhaustion parameters were analyzed.

After each round of co-cultivation, remaining tumor cells were stained for CD138 and quantified by flow cytometry. The capacity of BCMA CAR-transduced and RNAi-edited BCMA CAR T cells to eliminate tumor cells to subtotal levels remained high throughout the repetitive antigen stimulation. Only a minor amount of MM.1S tumor cells of around 0.5%-2% were still present in the culture. In contrast, H18-SP6 CAR T cells were unable to kill $CD138^+$ tumor cells as shown exemplarily for day 3. Therefore, consistent with the previous results, no antigen-independent CAR T cell activation could be observed when EBAG9 was downregulated (Figure 23A-B). Accordingly, cell-free co-culture supernatant from H18-SP6 CAR T cells did not contain IFN-$\gamma$. In contrast, IFN-$\gamma$ secretion was found for co-cultures of BCMA CAR and H18-BCMA CAR-transduced T cells. IFN-$\gamma$ secretion decreased slowly upon serial transfer and comprised in round five one-third of the amount after the first round (Figure 23C). In accordance, the proliferation capacity of CAR T cells remained at least 2-fold between each transfer cycle starting from the second round of transfer (Figure 23D). Altogether, no differences between EBAG9 proficient and knockdown CAR T cells were observed.

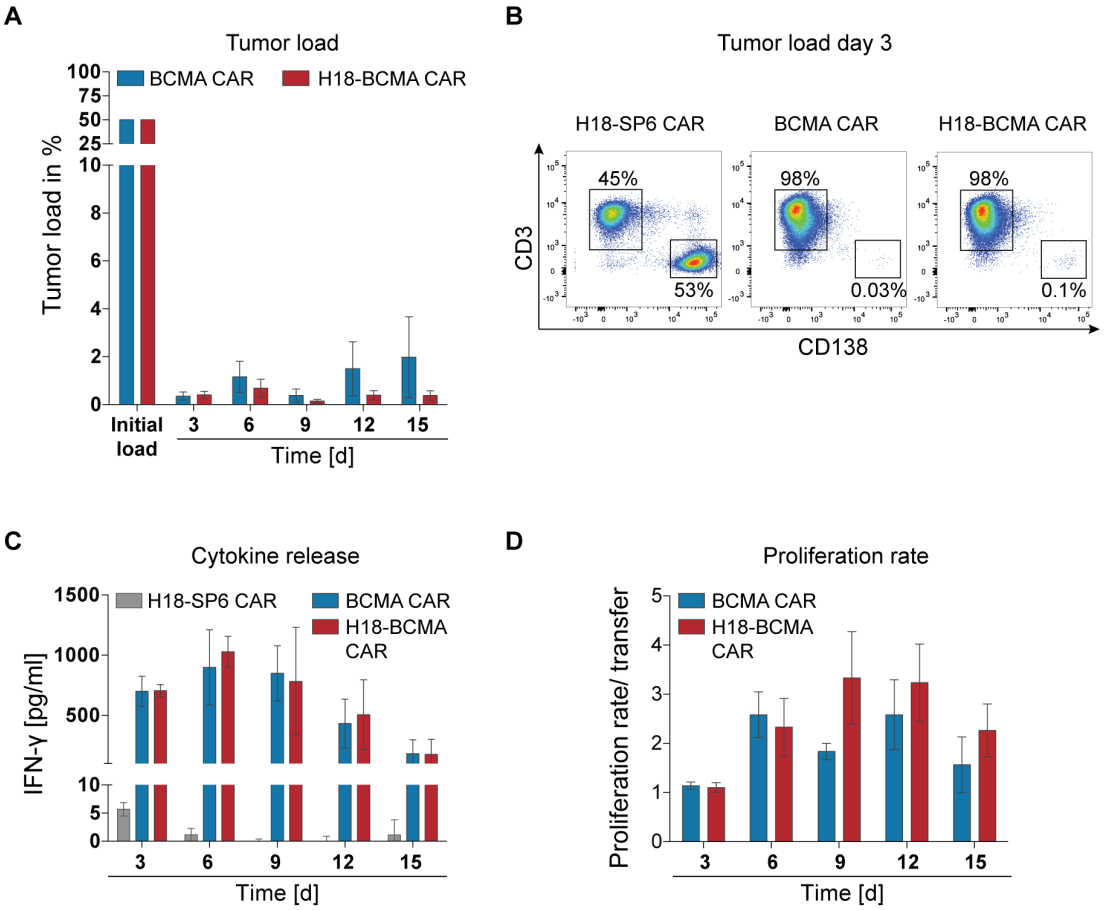


**Figure 23: RNAi-modified CAR T cells maintain their effector functions and proliferation capacity upon recursive antigen exposure *in vitro*.**
**(A-B)** CAR T cells were co-cultured on days 10-13 after activation with MM.1S target cells at a ratio of 1:1. After 72 h, CAR T cells were transferred to fresh target cells for a total of five transfer rounds. Remaining viable tumor cells were quantified after each round by staining for $CD138^+$ $CD3^-$ $7AAD^-$ cells and analysis by flow cytometry. Dot plots show one representative example for each group. Frequencies of $CD138^+$ $CD3^-$ $7AAD^-$ tumor cells and $CD138^-$ $CD3^+$ $7AAD^-$ T cells are indicated as percentages on the gate. **(C)** To measure IFN-γ secretion, cell-free supernatants were analyzed by ELISA. **(D)** The proliferation rate was assessed by manually counting of viable T cells after removing $CD138^+$ MM.1S cells by MACS. The ratio of T cells after each round versus the number of input T cells was calculated. Bars represent mean values ± SEM of n=2 experiments with 3 independent donors.

To characterize CAR T cell differentiation in more detail, cells were analyzed by flow cytometry after each round of transfer (Figure 24A). T cells were stained with 7-AAD, indicating that more than 90% viable T cells were present throughout all transfer rounds. This observation, in the context of consistent proliferation, argued against an activation-induced cell death (Figure 24B). CAR T cell frequency was analyzed by staining of the IgG hinge region. Starting with a transduction rate of 38% $7\text{-}AAD^-$ $CAR^+$ cells, an enrichment of the $CAR^+$ T cell population was observed. After three rounds of repetitive antigen stimulation, 90% of T cells were positive for CAR expression independent of the RNAi modification. Altogether, despite an enhanced cytolytic activity antigen-dependent proliferative activity remained unaffected (Figure 24C).

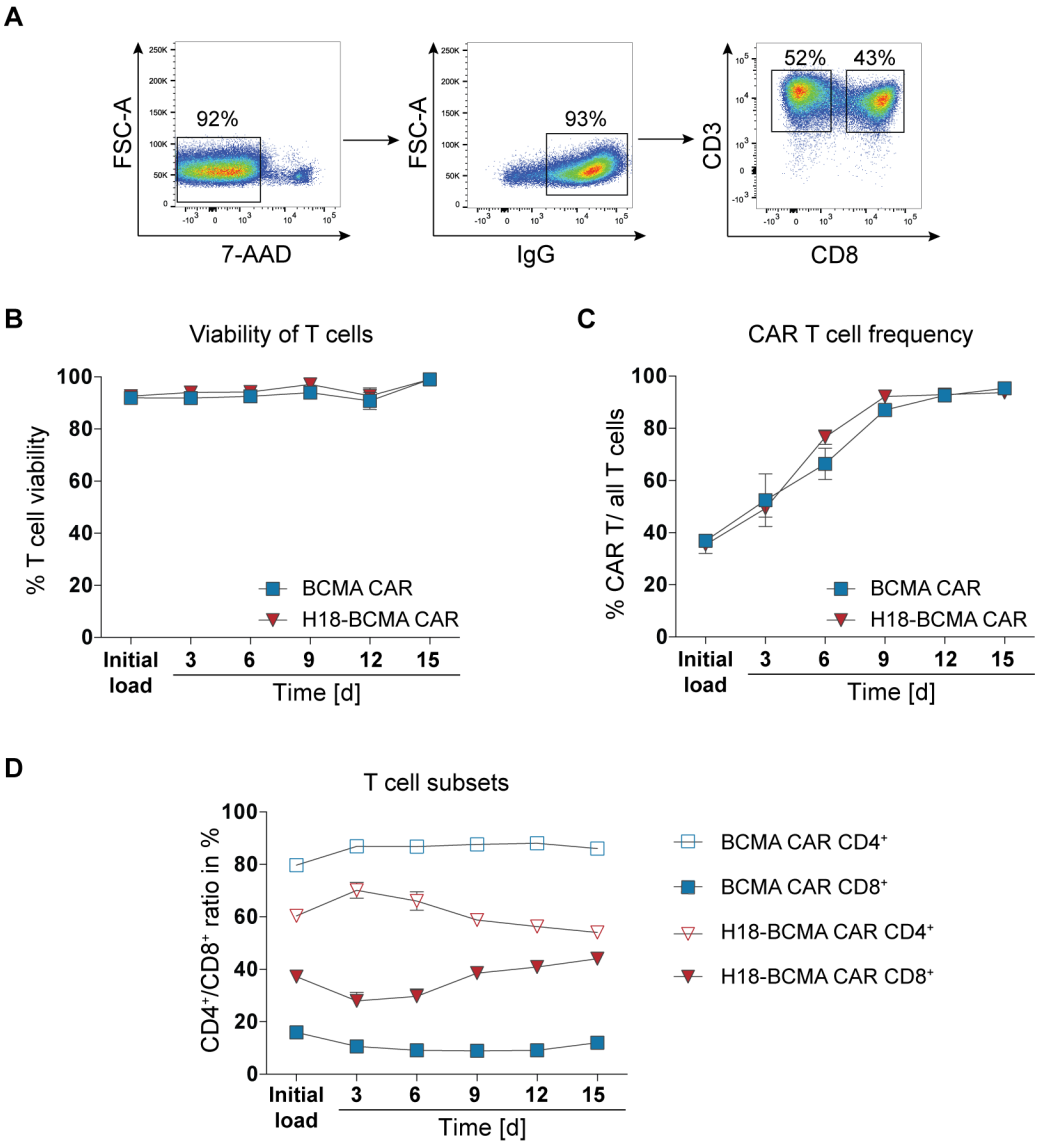


**Figure 24: Repetitive tumor cell exposure enriches antigen-specific CAR T cells and leads to different T cell subset composition depending on RNAi modification.**
**(A)** T cells from co-cultures were analyzed every 72 h by flow cytometry. The gating strategy is shown. Frequencies are indicated as percentages on the gate. **(B)** T cell viability was determined by 7-AAD staining. Mean values ± SEM are plotted. **(C)** Frequencies of transduced CAR$^+$ cells were determined by anti-IgG staining. Mean values ± SEM are plotted of n=1 experiment with 2 independent donors. **(D)** T cell subset composition was analyzed by staining of CD3 and CD8. CD3$^+$CD8$^+$ double positive cells were defined as CD8$^+$ T cells while CD3$^+$CD8$^-$ cells were considered as CD4$^+$ T cells. Mean values ± SEM are plotted of n=2 experiments with three independent donors.

Additionally, T cell subset composition of CAR$^+$ T cells was explored by staining for CD3$^+$ and CD8$^+$. The CD3$^+$ CD8$^+$ population defined cytotoxic T cells, whereas CD3$^+$ CD8$^-$ T cells defined CD4$^+$ T helper cells. Already at the beginning of the co-culture T cell subset composition differed between BCMA CAR and H18-BCMA CAR-transduced T cells. Transduction with the BCMA CAR revealed a predominant occurrence of CD4$^+$ T cells. Starting at a rate of 80%, CD4$^+$ T cells were further enriched to 90% of the co-culture after five rounds of repetitive transfer. Conversely,

only 20% of CD8$^+$ T cells were present at the beginning and declined to 10% after five rounds of repetitive stimulation. For the RNAi-modified H18-BCMA CAR T cells, the initial CD4$^+$ to CD8$^*$ ratio was 60% to 40%. Upon repetitive antigen stimulation, this ratio changed over time and attained a 50% to 50% distribution (Figure 24D).

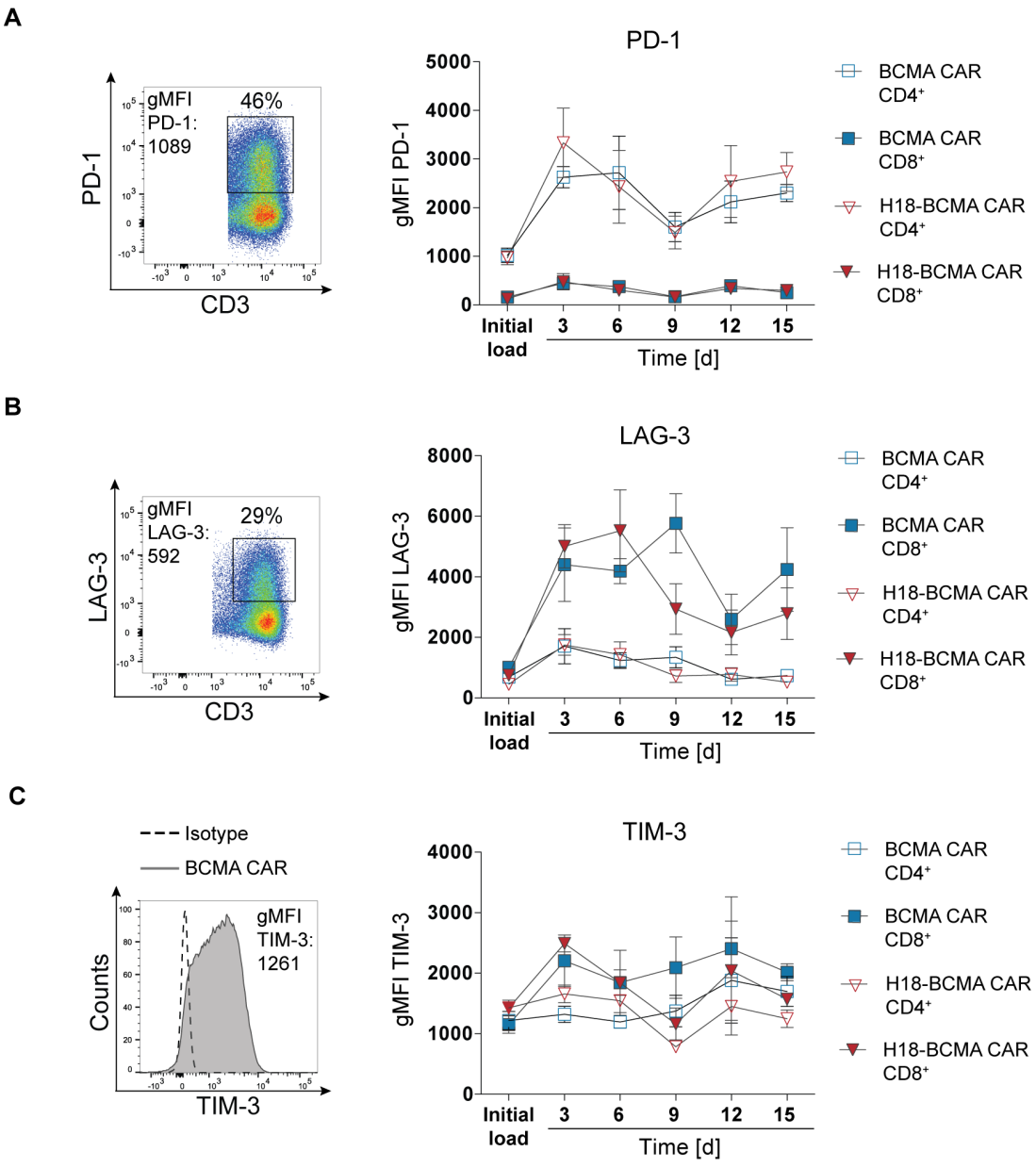


**Figure 25: Enhanced cytotoxic activity of CAR T cells due to silencing of EBAG9 does not alter the expression of T cell exhaustion markers.**
**(A-C)** Expression of T cell exhaustion markers PD-1 **(A)**, LAG-3 **(B)** and TIM-3 **(C)** was analyzed in every round of co-cultivation by co-staining of 7-AAD$^-$ CD3$^+$ CD8$^-$ CAR$^+$ T cells (CD4$^+$ CAR T cells) or 7-AAD$^-$ CD3$^+$ CD8$^+$ CAR$^+$ T cells (CD8$^+$ CAR T cells) and flow cytometry in two independent experiments with n=3 independent donors. Mean fluorescence intensities (MFI) ± SEM for each marker over time are shown. Values for isotype intensities were always subtracted. Dot plots and histograms show one representative example for each marker on day 0 of co-culture (initial load). Cells were pre-gated on 7-AAD$^-$ CD3$^+$ CAR$^+$. Frequencies and gMFIs are indicated as numbers on the gate.

Next, the expression of the activation and exhaustion markers PD-1, LAG-3, and TIM-3 was assessed over the co-cultivation period. Consistent with the activation process, the expression of all three markers increased within the first round of co-cultivation. For $CD8^+$ T cells transduced with the BCMA CAR or H18-BCMA CAR, expression of PD-1 and TIM-3 was unaltered during repetitive antigen stimulation (Figure 25A, C). In contrast, after the third round of transfer (day 9) LAG-3 expression in BCMA CAR-transduced T cells was moderately increased, while for RNAi-modified BCMA CAR T cells a decrease of LAG-3 expression could be observed. At round four, LAG-3 expression for both CAR T cell populations was, again, similar (Figure 25B). For $CD4^+$ T cells transduced with BCMA CAR or H18-BCMA CAR, expression of LAG-3 and TIM-3 remained very stable upon serial transfer (Figure 25B-C). PD-1 expression of all transduced T cells reached a peak after one round of co-cultivation (day 3), declined to around 50% of the MFI until the third round and slightly increased again (Figure 25A). While transduced $CD4^+$ T cells revealed a higher expression of PD-1, LAG-3 expression was stronger in $CD8^+$ T cells. Collectively, RNAi-mediated silencing of EBAG9 did not favor a condition where T cells undergo faster exhaustion.

### 5.4.5 T cell differentiation upon repetitive antigen stimulation is not altered due to the loss of EBAG9

Another aspect of CAR T cell functionality when challenged by recursive antigen stimulation is the development of a memory status. To distinguish between effector and memory T cells, the surface markers CD45RA and CD45RO were analyzed (Figure 26A). The protein tyrosine phosphatase CD45 is expressed on all hematopoietic cells, but several isoforms can occur by alternative splicing. CD45RA expression is characteristic for naive, effector and stem cell-like memory T cells. In contrast, CD45RO is a prototypical marker for central and effector memory T cells[156,157]. At the starting point of co-cultivation with MM.1S tumor cells (day 0), around 55% to 60% of transduced BCMA CAR T cells and H18-BCMA CAR T cells showed a memory phenotype. Upon repetitive antigen stimulation, the predominance of CD45RO-expressing memory T cells increased and after five rounds of transfer, no CD45 RA-expressing effector T cells were present. No differences due to RNAi-modification of BCMA CAR T cells could be detected (Figure 26B). Memory T cells can be further divided into effector (TEM) and central memory T cells (TCM) depending on the presence of the lymph node homing receptors CD62L and CCR7 (Figure 26A)[16,158,159].

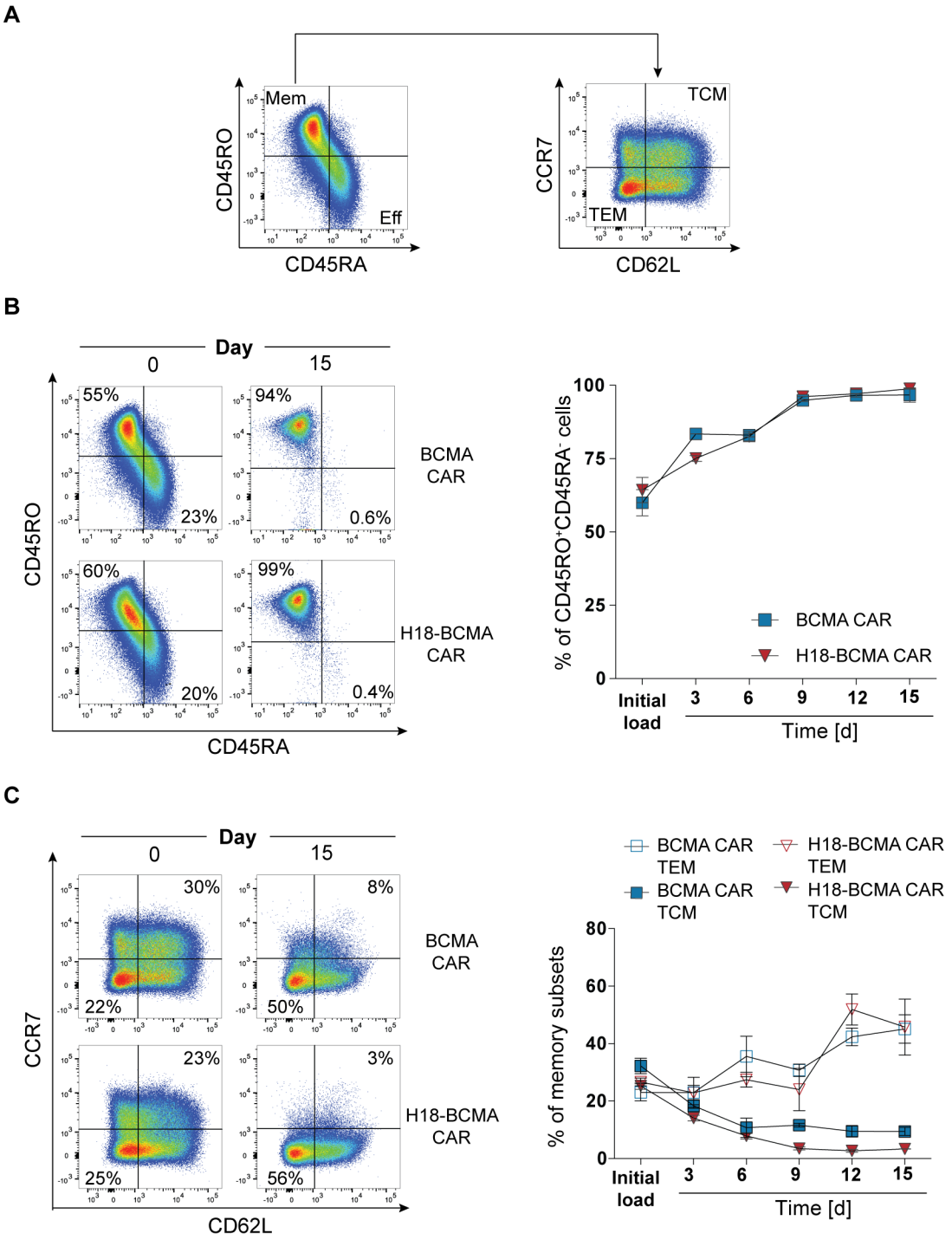


**Figure 26: Differentiation of transduced human T cells towards effector memory T cells is not affected by the loss of EBAG9.**
**(A)** In every round of co-cultivation, memory T cell subset composition was analyzed by flow cytometry. Gating strategy for the definition of memory subtypes is shown (TEM: $CD45RO^+$ $CD45RA^-$, $CD62L^-$ $CCR7^-$; TCM: $CD45RO^+$ $CD45RA^-$, $CD62L^+$ $CCR7^+$). **(B)** Percentages of memory T cells were determined by analysis of $CD45RO^+$ $CD45RA^-$ cells in one experiment with n=2 independent donors. Mean values ± SEM are plotted. Representative dot plots are shown on the left. Frequencies are indicated as percentages on the gate. **(C)** Co-staining of $CD45RO^+$ $CD45RA^-$ cells with CD62L and CCR7 was used to distinguish between central and effector memory T cells in one experiment with n=2 independent donors. Mean values ± SEM are plotted. Representative dot plots are shown on the left. Frequencies are indicated as percentages on the gate.

Approximately 23%-30% of T cells at the starting point of co-cultivation were characterized as TCM ($CD45RA^-$ $CD45RO^+$ $CD62L^+$ $CCR7^+$). TEM ($CD45RA^-$ $CD45RO^+$ $CD62L^-$ $CCR7^-$) were present at the same frequencies. Upon serial transfer, BCMA CAR T cells differentiated towards TEM, and only a minor fraction of TCM was still present. Again, RNAi-mediated EBAG9 silencing did not alter T cell differentiation compared with BCMA CAR T cells alone (Figure 26C).

## 5.5 EBAG9 silencing amplifies the cytolytic activity of CAR T cells at low effector frequencies in a multiple myeloma xenograft model

*In vitro* characterization of EBAG9 knockdown CAR T cells revealed an increased released of granzyme A, whereas effector cytokine secretion remained unaltered. Accordingly, cytolytic activity of CAR T cells was improved and a gain in cytotoxic efficiency was obtained *in vitro*. To translate these findings into an *in vivo* model, a multiple myeloma xenograft model was established.

A suitable animal model for the xenotransplantation of human multiple myeloma cell lines and primary human CAR T cells is the immunodeficient NOD scid gamma-chain deficient (NSG) mouse strain. Due to the *scid* mutation in the DNA repair complex *Prkdc*, which is important during recombination, these mice do not have mature T or B cells. In addition, they lack the common $\gamma$-chain for IL-2 receptor expression, therefore, NK cell differentiation is blocked[160,161]. NSG mice were inoculated with the BCMA-expressing multiple myeloma cell line MM.1S. Tumor progression was monitored by bioluminescence imaging of the MM.1S cell line stably expressing a firefly luciferase-eGFP construct (Figure 27B). Tumor cell engraftment was detected by IVIS imaging six days after transfer. A single dose of $1x10^6$ $CAR^+$ T cells on days 10-13 of culture under IL-7/IL-15 supplementation was injected i.v. one day later. Tumor development was followed by serial IVIS imaging until day 14 after transfer. Mice were sacrificed on days 15-16. Bone marrow was analyzed by flow cytometry for the number of remaining tumor cells and CAR T cells (Figure 27A). Before transfer, $CAR^+$ T cells were stained for CD3 and CD8 and revealed divergent T cell subset composition. BCMA CAR-transduced T cells showed a predominance of $CD4^+$ T cells (72%), whereas a smaller amount of $CD8^+$ T cells (23%) was present. In contrast, H18-BCMA CAR T cells contained 40% of $CD8^+$ T cells, compared to 58% of $CD4^+$ T cells, respectively (Figure 27C).

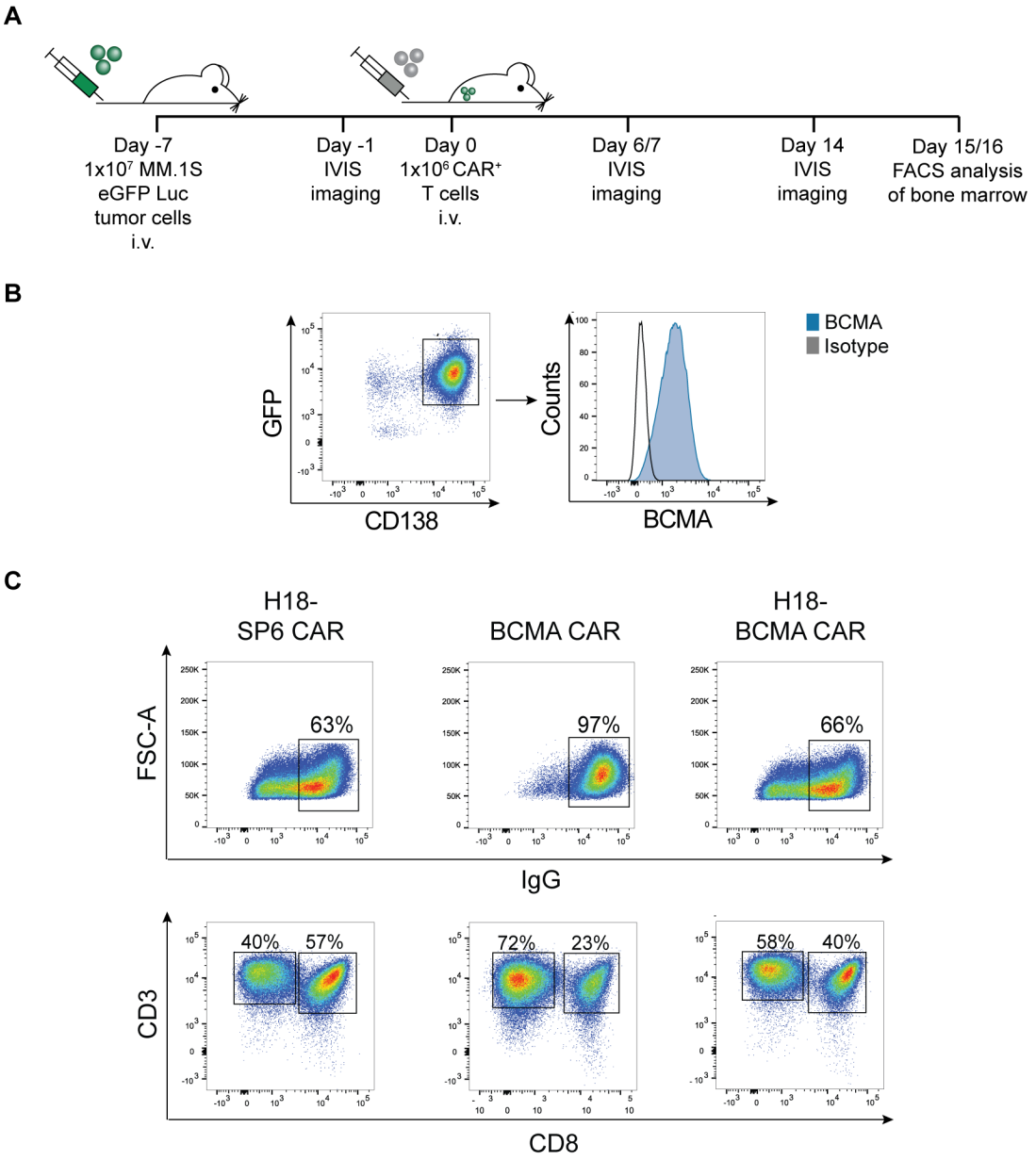


**Figure 27: Targeting of BCMA⁺ MM.1S cells with engineered CAR T cells.**
**(A)** The experimental procedure is depicted. On day 8 after tumor cell injection, CAR T cells were transferred, and tumor development was monitored over 2 weeks. **(B)** MM.1S tumor cell line expressing GFP and the surface markers CD138 and BCMA. **(C)** Transferred CAR T cells were enriched for positively transduced T cells. T cell subset composition was determined by CD3 and CD8 staining. $CD3^+CD8^+$ double positive cells were defined as $CD8^+$ T cells, whereas $CD3^+CD8^-$ cells were considered as $CD4^+$ T helper cells. Transduction rates after enrichment and percentages of T cell subsets are indicated by numbers on the gate.

Serial IVIS imaging revealed rapid tumor growth between days 6 and 14. The highest specific luciferase signal, which correlates with tumor activity, could be localized to the bone marrow. Treatment with the non-targeting H18-SP6 CAR T cells was unable to control tumor growth. The highest tumor burden was observed in mice from this group. Hence, there was no antigen-independent T cell activation due to EBAG9 silencing and subsequently increased ability of effector molecule release. Mice

treated with BCMA CAR T cells showed less tumor progression. However, clinical efficacy at this low number of effector CAR T cells was modest. In contrast, mice that received H18-BCMA CAR T cells showed almost no tumor signal (Figure 28A).

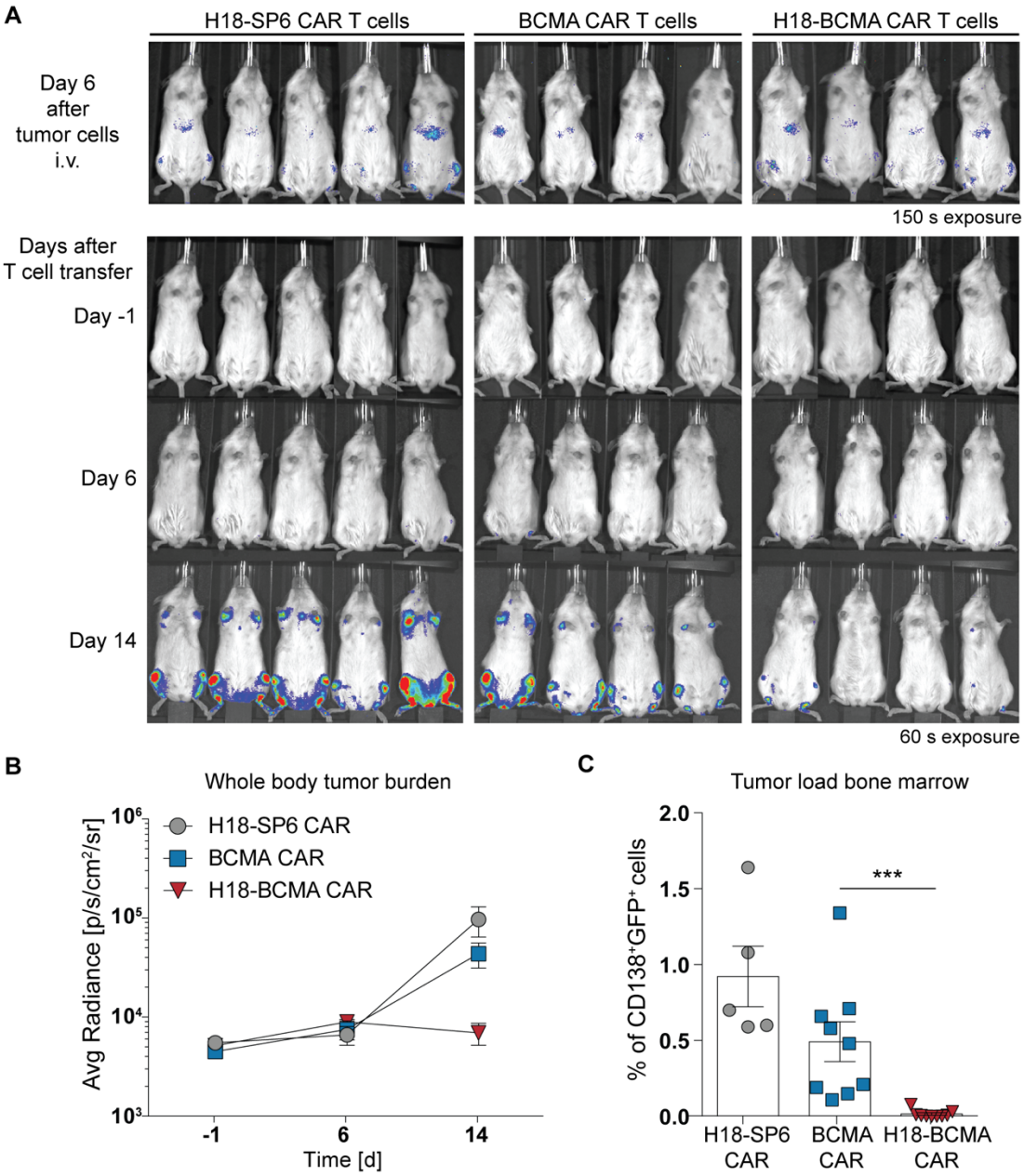


**Figure 28: *In vivo* engineered CAR T cells with silenced EBAG9 eradicate multiple myeloma cells more efficiently.**
**(A)** NSG mice were engrafted with 1x10$^7$ MM.1S cells stably expressing GFP and a firefly luciferase. On day 6, tumor inoculation was visualized by IVIS with 150 s exposure. One day later, 1x10$^6$ CAR$^+$ cells were transferred and treatment efficiency was observed by IVIS at 60 s exposure. **(B)** Mean values ± SEM of bioluminescence signal intensities obtained from regions of interest covering the entire body were plotted for each group and timepoint in one experiment. **(C)** On days 15 and 16, animals were sacrificed and CD138$^+$ GFP$^+$ tumor cells in the bone marrow were quantified by flow cytometry. Mean values ± SEM of n=2 experiments are plotted. *p<0,05, **p<0,01, ***p<0,00.1; ns, not significant. A Mann-Whitney U test was employed.

Accordingly, mean values of bioluminescence signal intensities obtained from regions of interest covering the entire body of each mouse essentially showed no tumor growth within the H18-BCMA CAR-treated mice (Figure 28B). Paradoxically, the IVIS imaging results were only partially reflected when analyzing tumor cell numbers ($GFP^+$ $CD138^+$) in bone marrow, the prime niche for myeloma cell homing. Although only modest differences in bioluminescence intensity between the H18-SP6 CAR and the BCMA CAR groups were detected, tumor cell quantitation revealed 2-fold higher numbers in the control group. Notably, almost no tumor cells were present in mice treated with RNAi-mediated EBAG9 silencing in BCMA CAR T cells (Figure 28C). Altogether, RNAi-mediated downregulation of EBAG9 led to a strongly increased antitumor efficiency even at low effector cell numbers.

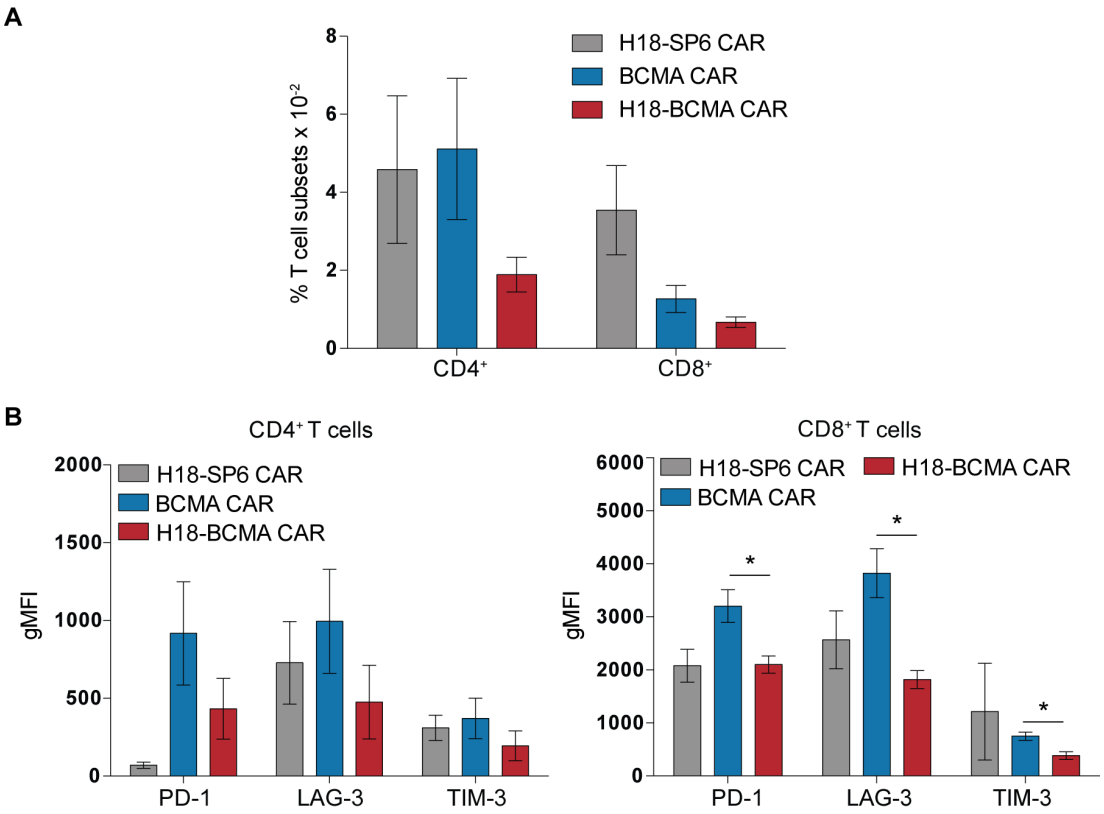


**Figure 29: CAR T cell exhaustion marker expression *in vivo* are not increased due to an enhanced cytolytic efficiency.**
**(A)** NSG mice were sacrificed on days 15 and 16 after T cell transfer and CAR T cell subset composition was analyzed by staining of CD3 and CD8 and flow cytometry analysis. $CD3^+CD8^+$ double positive cells were defined as $CD8^+$ T cells, whereas $CD3^+CD8^-$ cells were considered as $CD4^+$ T cells. Data are given as the percentage of T cells among total bone marrow cells. Bars represent mean values ± SEM of n=2 experiments with 5-9 animals per group. **(B)** Anti-PD-1, LAG-3 and TIM-3 co-staining for the detection of $CD4^+$ and $CD8^+$ T cell exhaustion. Quantitation was performed by determining fluorescence intensities (gMFI). Bars represent mean values ± SEM of n=2 experiments with 2-9 animals per group. *p<0,05, **p<0,01, ***p<0,00.1. A Mann-Whitney U test was employed.

In addition, human T cells were isolated from the bone marrow and analyzed by flow cytometry. Although H18-BCMA CAR T cells showed the highest cytotoxic activity, only a small number of $CD3^+$ $CD8^+$ T cells could be detected on days 15 and 16 following transfer. In contrast, about 2 to 3 times more H18-SP6 CAR and BCMA CAR T cells remained detectable. For all groups, $CD4^+$ T cells were the predominant fraction (Figure 29A). Co-staining of $CD4^+$ CAR T cells with the exhaustion markers PD-1, LAG-3 and TIM-3 revealed no significant differences between all groups. Conversely, expression of all tested exhaustion markers was lower in $CD8^+$ RNAi-modified BCMA CAR T cells compared to BCMA CAR T cells, however, the values were in the range of the H18-SP6 CAR control group. Therefore, in accordance with previous *in vitro* results, increasing the cytotoxic activity *in vivo* by silencing EBAG9 was not linked to overt T cell exhaustion (Figure 29B).

# 6. Discussion

Cancer immunotherapy is a promising curative approach to treat patients with advanced hematological and solid malignancies. The adoptive transfer of either naturally-occurring or gene-engineered T cells can mediate tumor regression in patients with metastatic cancer. In contrast to naturally-occurring T cells that require an already existing tumor-reactive T cell population, manipulating T cells by introducing TCRs or CARs can endow them with potent cytotoxic activity against many desired specificities[92,162]. $CD8^+$ T cells play a prominent role in tumor clearance due to their ability to destroy tumor cells by secreting effector molecules[10,163]. Yet, tumor-specific T cells can also fail to mediate tumor regression due to the negative regulatory milieu of the tumor microenvironment or T cell-intrinsic inhibitors[164-166]. Furthermore, long *ex vivo* culturing times of T cells that are necessary for manipulating and generating therapeutic quantities may reduce T cell functions[167]. Therefore, enhancing the functional avidity of these effector T cells is necessary. One approach used is to genetically manipulate the intrinsic properties of T cells[168,169]. In addition, focus should be placed on T cell memory formation because this process is thought to confer long-term immune surveillance. Within the scope of this thesis, an analysis was performed on whether targeting the secretory pathway of T cells by miRNA-mediated downregulation of EBAG9 can fulfill these criteria.

## 6.1 EBAG9 links cytolytic strength to $CD8^+$ memory formation

### 6.1.1 Loss of EBAG9 allows for the preferential formation of $CD8^+$ memory T cells

After the effector phase, most CTLs undergo activation-induced cell death, whereas only a few cells remain and form the memory T cell pool. The mechanisms that underlie T cell memory development are not yet fully understood. The impact of the cytotoxic strength of a T cell has been, in particular, poorly investigated. Most knowledge about the role of effector molecules for $CD8^+$ memory differentiation was obtained from effector molecule-deficient animals[170]. In contrast to this loss-of-function study, EBAG9-deficient mice enable us to study memory formation from a completely different perspective, namely the loss of EBAG9 that enhances the cytolytic efficacy of $CD8^+$ T cells.

Our group previously reported that mice with a genetically engineered loss of EBAG9 showed a higher secondary immune response when rechallenged at day 30 with the strong Tag neoantigen[64]. To address the question of how this increased secondary immune response is achieved, frequencies of antigen-specific $CD8^+$ memory T cells were analyzed after Tag antigen challenge, with substantially higher frequencies of antigen-specific $CD8^+$ T cells observed in EBAG9-deficient mice. However, $CD8^+$ T cell expansion and differentiation in the effector phase were indistinguishable between $EBAG9^{+/+}$ and $EBAG9^{-/-}$ mice as determined by the expression of lineage-specific surface markers. Challenge with the strong immunogenic Tag neoantigen leads to the development of a heterogenic effector $CD8^+$ T cell pool regulated through inflammatory cytokines such as IL-12 or interferons[171,172]. To avoid the confounding effect of the polyclonal TCR repertoire on the memory T cell pool formation, the monoclonal MataHari HY mHag system was used. This system allows for the analysis of T cell fate in the absence of an inflammatory stimulus. Yet, HY-specific alloresponses are of clinical relevance as they can mediate graft-versus-host as well as graft-versus-leukemia effects[173-175]. When naive T cells from MataHari donor mice were adoptively transferred and recipient mice were challenged with the HY antigen, activation and memory differentiation processes similar to those in the Tag antigen model were recapitulated. This suggests that the EBAG9-mediated effects on $CD8^+$ T cell lineage decision were not restricted to the polyclonal or monoclonal TCR model. Furthermore, it provides formal evidence that these fate decisions are independent of TCR strength, affinity, or precursor frequency.

Little is known about the consequences of altered cytolytic strength on $CD8^+$ T cell memory formation. To date, investigations concerning such consequences have focused on effector-function-deficient T cells. Opferman *et al.* suggested that T cells that differentiate into memory T cells are somehow able to escape from activation-induced cell death as mediated by the same effector molecules that clear infections. They adoptively transferred T cells with an inhibitor-induced selective block of the perforin/granzyme-mediated cytotoxicity and could observe that memory formation occurred only under conditions of low cytolytic activity. This led to the conclusion that effector $CD8^+$ T cells with low killing rates were also less likely to undergo activation-induced cell death and, therefore, are more likely to differentiate into memory T cells. Hence, maximal cytolytic activity involving a high frequency of antigen-specific T cells prevented the formation of a memory T cell pool[170]. This hypothesis appears to contradict to the results obtained with EBAG9-deficient mice. Loss of EBAG9 released the break on effector molecule secretion from $CD8^+$ T cells, thereby, increasing T cell

cytotoxicity on a single cell basis. Yet, higher numbers of memory $CD8^+$ T cells were also detected in these mice. Based on these observations, for the removal of identical amounts of antigen, EBAG9-deficient effector $CD8^+$ T cells were more efficient, with a reduction of the duration of antigen availability over time, and thus, favoring memory differentiation. Specifically, maximal cytolytic activity was not required for the removal of a given amount of antigen, because individual T cells have a higher cytolytic capacity. This hypothesis is supported by the decreasing potential model of memory formation and by studies that showed an enhanced memory pool upon the truncated duration of antigen exposure[19,20,146,176]. Accordingly, Blair *et al.* reported that memory differentiation of T cells is influenced by the duration of antigen availability. By using MHC peptide-specific blocking antibodies, the authors were able to modulate antigen access to $CD8^+$ T cells and observed an impact on memory development. Yet, there was no correlation between memory generation and the magnitude of the primary response and therefore, the requirements for continued T cell expansion and memory differentiation are different[177].

Another interpretation of the increased $CD8^+$ memory T cell pool upon enhanced cytolytic activity in EBAG9-deficient mice is in accordance with Opferman *et al*[170]. The authors also hypothesized about memory development based on antigen access over time. Effector $CD8^+$ T cells that arrive early at the site of infection would be confronted with high antigen levels, perform cytolysis, and undergo apoptosis. Effector $CD8^+$ T cells arriving at a later stage would encounter a lowered antigen amount. Therefore, they would be less cytolytically active, but are, in turn, capable of differentiating into memory T cells[170]. Applying this hypothesis to the results from EBAG9-deficient mice, it appears plausible that the increased cytolytic activity of EBAG9-deficient $CD8^+$ T cells would lead to activation-induced cell death. Because only a few cells would be necessary to clear an infection or an antigenic challenge, more antigen-specific T cells remain and eventually form the $CD8^+$ T cell memory pool.

To further substantiate the consequences of an increased cytolytic activity on memory differentiation, the fate of individual $CD8^+$ T cells needs to be followed. This approach might help to solve the question of whether individual $CD8^+$ T cells with higher cytotoxic activity differentiate preferentially into a memory T cell, or if a more efficient antigen clearance enables additional cells to form a memory T cell pool.

### 6.1.2 Transcriptional regulation of memory formation depends on the antigenic challenge

Many cell-intrinsic factors regulate the generation of terminally differentiated effector versus memory $CD8^+$ T cells. On the molecular level, the graded expression of opposing pairs of transcription factors facilitates either effector or memory $CD8^+$ T cell lineage decision in the primary immune response[12]. Stimulation with the strong Tag neoantigen induced substantial upregulation of *Eomes* and a graded effect in regard to T-bet-encoding *Tbx21* expression. Both effects are consistent with the preferential formation of Tag-specific memory $CD8^+$ T cells in EBAG9-deficient mice. EOMES and T-bet are among the best-studied pairs of counterregulatory transcription factors. They are highly homologous and appear to be master regulators of $CD8^+$ T cell differentiation and function. Both have cooperative and partially redundant functions in the early stages of $CD8^+$ T cell activation as they promote cytotoxic T cell generation by inducing the expression of effector molecules like perforin and granzyme B[178,179]. In the context of memory $CD8^+$ T cell formation, EOMES and T-bet cooperate to sustain a memory phenotype. This is achieved by stabilizing the expression of IL-2Rβ (CD25) and promoting IL-15 signaling, as well as the continued proliferation of memory $CD8^+$ T cells[23]. However, EOMES and T-bet also have unique functions in regard to $CD8^+$ T cell differentiation. The early stages of effector $CD8^+$ T cells are known to be characterized by high levels of T-bet expression, while a graded decline of this expression can be observed as cells differentiate towards memory T cells. EOMES is also upregulated in early effector $CD8^+$ T cells but its expression increases with the progression from effector to memory $CD8^+$ T cells[176,180]. In mice lacking either EOMES, T-bet, or both, high T-bet expression was shown to drive terminal effector differentiation, whereas EOMES is important for long-term memory formation and homeostatic renewal[176,181,182]. Yet, upon LCMV infection, T-bet deficiency leads to an impaired formation of effector T cells, and, surprisingly, also of memory T cells[183].

In contrast to the results obtained with the Tag neoantigen, increased expression of T-bet-encoding *Tbx21* could be observed in the polyclonal anti-HY primary response, whereas *Eomes* expression was similar to the wild-type. This result is in accordance with the aforementioned importance of T-bet in sustaining memory T cell generation. In addition, the *Id3* to *Id2* ratio was 1.6-fold higher and *Il12rb* gene expression was upregulated by 1.6-fold in EBAG9-deficient $CD8^+$ T cells. ID2 and ID3 partly act by inhibiting the DNA-binding activity of transcription factors belonging to the E-protein

family; however, they function in a non-redundant manner. While ID2 mediates the expression of apoptosis-regulating genes like BCL-2, ID3 induces the expression of genes involved in DNA replication and genome stability such as FOXO1[184,185]. ID2 and ID3 are expressed by effector $CD8^+$ T cells but their activity appears to be temporally separated. On the one hand, ID2 promotes the survival of effector $CD8^+$ T cells during the naive to effector transition[185]. On the other hand, ID3 is important at a later stage for the survival during effector to memory transition[184]. Thus, ID2 is essential for the formation of $KLRG1^{high}$ $CD127^{low}$ effector $CD8^+$ T cells; a loss of ID2 impairs the survival of these acute effector cells. Overexpression of ID3 sustains the survival of $CD8^+$ effector cells that would normally undergo apoptosis during the contraction phase[149]. Therefore, ID3 mediates the formation of long-lived memory $CD8^+$ T cells. In contrast, the role of signaling through the IL-12 receptor in $CD8^+$ T cell fate is less clear. There is evidence that IL-12 favors the generation of short-lived, terminally differentiated, effector $CD8^+$ T cells mediated by a repressive effect on EOMES expression, while T-bet expression is stimulated simultaneously[186]. However, in support of a memory-promoting function, Xiao *et al.* demonstrated that IL-12 receptor deficiency in $CD8^+$ T cells impairs the formation of a memory $CD8^+$ T cell pool upon *Listeria monocytogenes* infection[187]. Moreover, Garcia *et al.* reported that loss of the IL-12 receptor led to reduced CD127 and increased KLRG1 expression. As a consequence, memory expansion was virtually undetectable[188]. Mechanistically, IL-12 appears to mediate STAT4 phosphorylation upon antigen stimulation that, in turn, prolongs the survival of effector $CD8^+$ T cells through activation of anti-apoptotic BCL-2/BCL-3-regulated gene expression[188,189]. Notably, IL-12-conditioned $CD8^+$ T cells have been shown to exhibit increased sensitivity to IL-7/IL-15 signals that are important for homeostatic self-renewal and memory maintenance[189].

Interestingly, the transcriptional profile mediating enhanced memory formation in EBAG9-deficient mice was distinct between the strong Tag neoantigen and the weakly immunogenic HY system. As immunization with the HY antigen lacks a strong inflammatory stimulus, the kinetics and potentially the magnitude of a T cell response is lengthened. The effector phase usually peaks at day seven after immunization in response to strong infection-associated antigens or neoantigens[176]. In contrast, a primary immune response against the HY antigen could be observed at day 11 (unpublished data). Thus, memory formation is seemingly dependent on the antigenic challenge and the inflammatory milieu. A possible reason for these differences in the

expression of transcriptional regulators might be the different kinetics of T cell fate decision upon strong or weak antigen challenge.

Altogether, the first part of this thesis showed that $CD8^+$ T cell programming is associated with the cytolytic strength. The increased cytolytic activity, due to the loss of EBAG9, favored the generation of an antigen-specific $CD8^+$ T cell memory pool orchestrated by different sets of memory-promoting transcription factors depending on the antigen stimulus.

## 6.2 RNAi-mediated targeting of the secretory pathway increases the cytolytic activity of mouse $CD8^+$ T cells

### 6.2.1 EBAG9 is a suitable target for RNAi-mediated T cell engineering

Genetic engineering of T cells prior to infusion into the patient provides the opportunity to enhance T cell function and overcome therapeutic obstacles such as poor tumor immunogenicity, limited *in vivo* survival and efficacy of transferred T cells. There have been numerous studies focusing on the suppressive influence of the tumor microenvironment on the functionality of tumor-specific T cells[166,190,191]. Yet, efficient ATT depends on the generation of high-avidity, long-lived, tumor-specific T cells. Therefore, to improve the therapeutical outcome, enhancing the functional avidity of these transferred effector T cells is desirable. The avidity of T cells refers to as the accumulated strength of multiple affinities. In other words, avidity integrates the combined effect of all affinities participating in the molecular interaction between the tumor and the T cell. The functional avidity of a T cell is, therefore, composed of all cellular responses in addition to antigen recognition as controlled by i) the structural avidity of a TCR or CAR with their antigen, ii) the transcriptional maturation of the T cell, iii) cytokine signaling and iv) costimulation[192]. Efforts to enhance the T cell avidity often focus on increasing TCR or CAR affinities[193-195]. However, the secretory pathway of T cells is also of importance for the functional avidity. The cytolytic efficiency of a T cell depends on the synthesis and storage of effector molecules, intracellular vesicle transport, as well as the maturation and secretion competence of secretory lysosomes. Therefore, targeting the secretory pathway of T cells might represent an alternative and universally applicable strategy to enhance the functional avidity of tumor-reactive T cells. In detail, this thesis focused on the RNAi-mediated downregulation of EBAG9. EBAG9 is a negative regulator of the regulated effector molecule secretion, therefore, EBAG9-deficiency increases the cytolytic activity of

$CD8^+$ T cells[64]. It was suggested that EBAG9 is associated with the immune escape of cancers as it negatively impacts host T cell cytotoxicity and further suppresses T cell infiltration into the tumor[196]. Moreover, Miyazaki and colleagues demonstrated that tumor formation and metastasis of transplanted bladder tumor cells were repressed, whereas there was an increased infiltration of the tumor with $CD8^+$ T cells in an EBAG9-deficient host[197]. Recently, Miyazaki *et al.* discovered EBAG9 expression in extracellular vesicles prepared from the supernatant of the prostate cancer cell line LNCaP by Western Blot analysis. These LNCaP-derived, EBAG9-containing extracellular vesicles decreased the *in vitro* cytotoxicity of T cell leukemia MOLT4 cells against LNCaP cells. Therefore, extracellular vesicles secreted by tumor cells are supposed to carry tumor-derived EBAG9 to the host T cells in order to negatively modulate immune cells in the tumor microenvironment[198]. As a novel aspect, the present thesis showed that loss of EBAG9 further favors the generation of a long-lived and antigen-specific memory $CD8^+$ T cell population. Collectively, these findings strongly suggest that EBAG9 qualifies as a prime target for enhancing the functional avidity and killing capacity of $CD8^+$ T cells.

### 6.2.2 EBAG9 knockdown using the RNAi pathway

The RNAi pathway can be induced by several dsRNA molecules. First, cells can be transfected with siRNAs that are useful for rapidly screening of the target gene knockdown phenotype[199]. However, one disadvantage is that the intracellular half-time is relatively short as siRNAs can be degraded by RNase A-like nucleases. More importantly, siRNAs can only mediate a transient silencing effect and are therefore limited in their applicability[200,201]. For long-term manipulation of gene expression, it is necessary to deliver dsRNA molecules by integrating gene transfer vectors. One possibility is the transfer of shRNAs that mimic the pre-miRNA stem-loop structure. Expression of these shRNAs is driven by the strong RNA polymerase III promoters that lead to high-level expression and stable gene knockdown[202-205]. However, there are concerns about this approach as shRNA overexpression was shown to mediate toxicity by saturation of the miRNA processing pathways. The considerable disruption of the cellular miRNA pathway was caused by the rate-limiting amounts of Ago2 and Exportin-5 and led to serious consequences such as brain damages, liver dysfunction, and death in animal models[206-208]. Furthermore, the toxicity of shRNA vectors in transduced human T cells has been reported[209]. In this thesis, artificial miRNAs were chosen to mediate a stable knockdown within primary T cells. These artificial miRNAs are analogous to the pri-miRNA and, therefore, are a step further towards mimicking

natural miRNA biology[210,211]. This has several advantages for potential clinical applications. Most importantly, using the endogenous miRNA processing machinery does not trigger cellular self-defense mechanisms such as interferon induction[212]. In addition, artificial miRNAs are transcribed by RNA polymerase II promoters comparable to most of the natural miRNAs. These promoters mediate regulated and tissue-specific expression and further enable the simultaneous expression of selector or therapeutic transgenes[201,213]. Moreover, it is possible to combine multiple miRNAs in one expression cassette to target regions in the same or different mRNAs, therefore, gaining an additive effect in target downregulation[199,211,214].

The risk of off-target effects is a critical aspect in using RNAi-mediated gene silencing and was described for the first time in 2003 by Jackson and colleagues[215]. Off-target effects are gene perturbations caused by unintended interactions between RNAi-inducing dsRNA molecules and cellular components. In addition to the aforementioned toxicity reliant on the saturation effect of the endogenous RNAi machinery, sequence-specific off-target effects are possible. As the RNA sequence loaded to the RISC can guide the complex to mRNAs with partial complementarity, sequence-specific off-target effects can occur[216]. For the recognition of targets by the endogenous miRNA, a complementary region of six to eight nucleotides within the 3'UTR of the mRNA is important[217]. Therefore, unique target regions should be selected in the process of dsRNA molecule design to avoid the unintentional regulation of several transcripts. Indeed, previously reported siRNA-mediated off-target effects were shown to be caused by sequence complementarity[215,218,219]. For efficient targeting of specific mRNAs, the AU content of the surrounding sequence and the presence of other miRNA target sites need be considered. In addition, the 3'UTR located binding motif is important[220]. Thus, the likelihood of sequence-specific off-target effects is quite low. To date, sequence-specific off-target effects were reported only for siRNAs and might be caused by high cytosolic siRNA concentrations. Recently, circular siRNAs were identified to increase the safety of siRNA-mediated gene silencing[221].

### 6.2.3 Silencing of EBAG9 increases the cytolytic activity of adoptively transferred mouse T cells

In the present thesis, EBAG9 silencing was achieved by the generation of a specific EBAG9-targeting miRNA. The knockdown efficiency of different miRNAs in cell lines and primary mouse T cells was quantified on an RNA level by qRT-PCR and on the

protein level by Western Blot analysis. Adoptively transferred mouse T cells with an engineered knockdown of EBAG9 showed an almost 2-fold higher cytolytic capacity compared to the GFP-transduced control T cell population. Differences in T cell engraftment or proliferation were excluded as the basis of the enhanced killing capacity. Interestingly, in the EBAG9 knockdown T cell population, the frequencies of $CD8^+$ T cells were modestly higher compared to the GFP control group. Although it cannot be excluded that this may have influenced the killing rate of the EBAG9 knockdown population, antigen-specific killing can also be mediated by $CD4^+$ CTLs. In addition to $CD8^+$ T cells, $CD4^+$ CTLs are also capable of secreting cytotoxic granules containing perforin and granzymes for the direct killing of target cells. $CD4^+$ CTLs were previously believed to be an *in vitro* artifact associated with long culturing times. However, they were also identified *in vivo,* and shown to play an important role in antiviral and antitumor responses[222,223].

Studies analyzing the siRNA-mediated knockdown of EBAG9 have so far focused on targeting EBAG9 in the tumor. Ogushi *et al.* reported of a tumor-promoting function of EBAG9 *in vivo* as the intratumoral administration of EBAG9-specific siRNA led to the regression of subcutaneously implanted renal cancer cell growth. They further concluded that EBAG9 does not function as an oncogene, but rather alters the tumor microenvironment by decreasing the local immune response[224]. In addition, siRNA-mediated silencing of EBAG9 within the highly malignant, spontaneously metastasizing 4T1 mouse mammary carcinoma was shown to suppress both tumor growth and metastasis. In mice that received the EBAG9-targeting siRNA, an enhanced specific cytotoxic activity of CTLs and enhanced IFN-$\gamma$ and IL-2 production was observed. In line with these observations, silencing EBAG9 prolonged the survival of tumor-bearing mice and induced intensive tumor infiltration of $CD8^+$ T cells[225]. As the consequences of the intratumoral EBAG9 silencing is more likely to modulate the host cytotoxic T cell activity instead of tumor cell intrinsic properties, the approach chosen within the scope of this thesis did not target EBAG9 in tumor cells themselves by a transient siRNA-mediated knockdown. Instead, the aim was to stably silence EBAG9 within cytotoxic $CD8^+$ T cells by using a specific miRNA to increase their killing capacity. Indeed, T cell avidity was shown to be enhanced due to the downregulation of EBAG9, therefore increasing the specific target cell killing capacity. Alternative molecular targets analyzed that modulate the cytotoxic activity of T cells are the E3 ubiquitin ligase Casitas B-lineage lymphoma b (Cbl-b) and the member of the suppressor of cytokine signaling family Cish[168,169]. Both are negative regulators of intracellular TCR signaling. Abrogation of Cbl-b was described by Stromnes *et al.*

to rescue IL-2 production and proliferation following target recognition[168]. However, it is known that genetically engineered Cbl-b-deficient mice have an increased susceptibility to autoimmunity[226,227]. Palmer *et al.* reported that the deletion of Cish enhanced $CD8^+$ T cell expansion, functional avidity, and polycytokine release[169]. Furthermore, by using an adoptive transfer model, they demonstrated a profound and durable regression of a poorly immunogenic established cancer following the loss of Cish[169]. Therefore, boosting the immune response by silencing cell-intrinsic negative regulators emerges as a promising approach for increasing the efficiency of ATT. However, to the best of our knowledge, the present thesis is the first study showing that targeting the secretory pathway of T cells leads to an increase of their cytolytic activity, an effect that is applicable to therapy.

## 6.3 EBAG9 knockdown increases the cytolytic activity of human CAR T cells

### 6.3.1 Simultaneous expression of EBAG9-targeting miRNAs and transgenes

One of the major advantages of using miRNA-based EBAG9 silencing is the potential to co-express the miRNA with a transgene because both are under the control of the polymerase II promoter[199]. Therefore, miRNA expression is tightly coupled to the appropriate transgene, which can be a selector or marker protein such as GFP, allowing for the enrichment of positively transduced cells. In addition, combining miRNA-mediated silencing with the expression of a specific TCR or CAR to confer antigen-specific target cell recognition is also possible. In this thesis, EBAG9-specific miRNA expression in mouse T cells was associated with GFP expression, whereas in human T cells, expression was combined with either a BCMA-targeting or a CD19-targeting CAR. Both CARs are of relevance in current clinical trials[228-230]. The expression of GFP and the BCMA-targeting CAR was observed to be markedly reduced by up to 50% upon the simultaneous expression of the miRNA. Co-expression of a miRNA and a transgene can lead to decreased transgene protein levels. This is caused by the γ-retroviral vector architecture used for transduction. To avoid the production of a truncated transgene mRNA due to miRNA processing, the miRNA is located within an intron. This intronic miRNA location usually allows for a robust co-expression of the linked transgene as an efficient splicing reaction segregates mRNA and miRNA maturation process[210,231,232]. However, there are limitations of transgene expression because retroviral vectors require the packaging

signal (Ψ) that ensures for the packaging of unspliced messages into the viral particles. The retroviral MP71 vector, that was used in the present thesis, encodes for an intron containing the miRNA and the packaging signal[233]. This intron is only weakly spliced and can partially restore the transgene expression. Using a more efficient intron could improve transgene expression but would simultaneously decrease the virus titer and is, therefore, not a suitable alternative. A possible way to increase the efficiency of transgene expression would be the use of a lentiviral vector system. In contrast to the retroviral system, the nuclear export of the unspliced mRNA and their translation is mediated through interaction of the viral Rev protein with the intronic-located Rev-responsive element. Thus, the presence of the Rev protein supports virus titers independently of the splicing efficiency[211,234,235]. Another strategy for the efficient co-expression of the miRNA and the transgene would be the use of bacterial plasmids instead of viral vectors as they would enable the use of strong introns. To overcome the problem of stable genomic integration, transposases such as Sleeping Beauty could be used[236-239]. Transposases are enzymes that can precisely excise a defined DNA region flanked by recognition sequences, integrating this region into the genome[240].

### 6.3.2 EBAG9 silencing enhances the capacity of human CAR T cells to eradicate tumor cells *in vitro* and *in vivo*

Functional validation of the human EBAG9-targeting miRNA revealed that the granzyme A secretion was increased substantially from transduced T cells harboring a silenced EBAG9 function, whereas the antigen-specific secretion of effector cytokines remained unaltered. Furthermore, *in vitro* cytotoxicity assays demonstrated that EBAG9 knockdown endowed CAR T cells with a higher cytolytic activity without causing antigen-independent T cell activation. Because this could be observed for BCMA and CD19 CAR T cells, it can be inferred that silencing EBAG9 to enhance the killing capacity of CAR T cells is a universally applicable principle that can be combined with any other CAR or TCR. Previously, Bluhm *et al.* performed *in vitro* cytotoxicity assays with the same BCMA CAR construct but revealed 2-fold higher cytotoxic activities against OPM-2, DOHH-2, and JeKo-1 target cells[154]. It should be noted that the different transduction rates in this thesis were normalized with untransduced T cells prior to functional *in vitro* assays. Transduction rates of only 20% to 30% were achieved, however, CAR T cells were not enriched, therefore, a heterogeneous population containing a large number of untransduced T cells was analyzed. The aforementioned study by Bluhm *et al.* used BCMA CAR T cells with a

transduction rate of approximately 50%-60%[154]. Although there is no linear correlation between transduction and the killing rate, it can be deduced that CAR T cell-mediated effects in the present thesis are relatively underestimated because of the presence of a large fraction of untransduced T cells. The target cell lines investigated expressed BCMA on their surface at different intensities. Bluhm *et al.* applied the Quantibrite quantification method to determine BCMA antigen density on the target cell surface. In accordance with the flow cytometry results, the MM cell line OPM-2 exhibited the highest density of BCMA molecules with approximately 5000 receptors per cell, whereas BCMA frequencies in the B-NHL cell lines DOHH-2 and JeKo-1 were in the range of 500 and less than 100 BCMA molecules, respectively[154]. BCMA CAR T cells killed all cell lines with similarly efficiency and largely independent from the antigen density. However, although EBAG9 silencing increased the cytolytic activity of BCMA CAR T cells against all applied cell lines, this effect was most pronounced when targeting OPM-2 and less distinctive when targeting JeKo-1. Thus, increasing the efficiency of the cytolytic activity of CAR T cells by the RNAi-mediated downregulation of EBAG9 appears to be dependent on the antigen density. However, additional low BCMA-expressing cell lines such as the follicular lymphoma cell line SC-1 may further confirm this observation and analyze the underlying mechanism.

Using an MM1.S xenotransplantation model, the *in vivo* efficacy of BCMA CAR-transduced T cells was compared to BCMA CAR T cells with a knockdown of EBAG9. The BCMA CAR used in the present thesis was generated and previously analyzed in our group. In this context, the xenotransplantation model has been proven to be suitable for analyzing BCMA-targeting CAR T cells[154]. MM1.S cells were transplanted to NSG mice and tumor location in the bone marrow was detected by bioluminescence. Furthermore, flow cytometry analysis was performed to determine tumor load and T cell persistence. BCMA CAR T cells with silenced EBAG9 were shown to control tumor growth with a considerably higher efficiency. Almost no tumor cells were detectable after BCMA CAR T cell transfer with an engineered loss of EBAG9. In contrast, tumor load in mice treated with BCMA CAR T cells was reduced compared to control mice with maximal tumor outgrowth; however, this did not lead to a complete tumor remission. Previously published data revealed a strong effect of this CAR in targeting MM cells within a xenotransplantation model similar to those applied in this thesis. In contrast to the data presented here, BCMA CAR T cells were able to control tumor growth within the first 21 days after CAR T cell transfer[154]. However, Bluhm *et al.* transferred 2-3 x $10^6$ $CAR^+$ T cells in contrast to the 1 x $10^6$ $CAR^+$ T cells used in this study. This reduced CAR T cell number might be the

cause for the modest activity of the BCMA CAR T cells. In line with this observation, the group of Michel Sadelain published a “CAR stress test” study. Applying CD19 CAR T cells in a pre-B ALL model, the authors lowered CAR T cell doses to levels in which CAR T cell therapy starts to fail. Tumor cell eradication efficacy decreased with the CAR T cell dose reduction[241]. In addition to tumor growth, BCMA CAR T cell persistence within the bone marrow was analyzed. Only modest numbers of CAR T cells were present. Surprisingly, the lowest cell number was detected for BCMA CAR T cells with silenced EBAG9, although these T cells exhibited the highest *in vivo* tumor eradication efficacy. This may be due to activation-induced cell death, a programmed cell death induced by repetitive antigen stimulation that is mediated by Fas/FasL-induced apoptosis and triggered by the expression of several signaling molecules[242,243]. However, BCMA CAR T cells with an engineered knockdown of EBAG9 modestly expressed the activation and exhaustion markers PD-1, LAG-3, and TIM-3. Indeed, their expression was similar to the control SP6 CAR T cells with silenced EBAG9. In contrast, not only higher numbers of BCMA CAR T cells could be detected, but the $CD8^+$ T cell population also expressed the highest levels of the exhaustion markers. It appears that the number of BCMA CAR T cells with silenced EBAG9 peaked at an early stage or the onset of contractions was faster. It would also imply that activation-induced cell death occurred earlier due to the higher cytolytic activity of these cells in comparison to the BCMA CAR T cells. Remaining T cells that have not undergone activation-induced cell death could still be activated following tumor eradication but express only low levels of the exhaustion markers. In contrast, the kinetics of BCMA CAR T cells may be delayed compared to CAR T cells with silenced EBAG9. From this perspective, the time point analyzed may reflect the peak of T cell expansion and exhaustion marker expression, just prior to activation-induced cell death. To investigate this hypothesis in more detail, kinetic studies and analysis of the characteristics of transferred CAR T cells at a higher frequency are required. Furthermore, analysis of FasL expression throughout the observation time period could provide further insight into the activation-induced cell death of CAR T cells. In addition, the recording of data regarding T cell contraction could be also informative.

In summary, EBAG9 silencing reduces the threshold for T cell activation, therefore, enhances the cytolytic activity of CAR T cells. The strategy of targeting the secretory pathway of T cells has several advantages in terms of increasing ATT efficacy. First, it offers the opportunity to reduce the number of CAR T cells in ATT and still achieve the same cytotoxic efficacy. This can be advantageous when limiting the risks of adverse side effects, the occurrence of which clearly correlates with effector cell

numbers. The most frequent and serious side effect of CAR T cells is cytokine release syndrome, a systemic inflammatory response especially characterized by the release of IL-6[244,245]. In an allogeneic setting, lowering the risk of graft-versus-host effects is important as it can lead to extensive tissue damage and life-threatening complications[246]. Furthermore, treatment of patients with the adoptive transfer of T cells is often performed after several rounds of chemotherapy. Therefore, because of a reduced regenerative potential of normal bone marrow cells, a limited number of T cells would be available that could be modified and reinfused into the patient. Another advantage of reducing CAR T cell numbers for ATT is accelerating the manufacturing process because shorter culture times and less effector T cells are required. The group of Nicholas Restifo reported that long *ex vivo* culturing times promote the differentiation of T cells to potent effector cells with increased antitumor response *in vitro*. Still, these cells are often less effective in triggering tumor regression *in vivo* as they exhaust their proliferative and survival capabilities and, therefore, disappear rapidly after adoptive transfer. The use of IL-2 to generate high numbers of tumor-reactive T cells appears rather problematic as T cells rapidly differentiate under IL-2 conditions[167]. Moreover, high capacity T cells would enable the targeting of tumor entities with low antigen density and could be able to compensate for low-affinity CARs or TCRs, particularly in the case of patient-derived low affinity but also tumor-reactive TILs that are, in part, dysfunctional *in vivo*.

### 6.3.3 *In vitro* long-term persistence of CAR T cells is not influenced by a loss of EBAG9

Inhibitory receptors associated with T cell exhaustion were identified and characterized during chronic viral infection models. Proving strong parallels, most of these receptors were also found in tumor-reactive T cells in cancer. For example, in the context of established progressing tumors, T cells exhibit an exhausted phenotype due to high tumor-antigen load and immunosuppressive factors within the tumor microenvironment. Isolated TILs are deficient in effector cytokine production and express inhibitory receptors such as PD-1, LAG-3, TIM-3, 2B4, and CTLA-4. Therefore, to achieve efficient tumor eradication, engineered T cells need to be generated that are persistent and remain functional[247-251]. T cells expressing high-affinity and high-avidity TCRs have been associated with reduced serial killing, leading to exhaustion or activation-induced cell death[252]. Because EBAG9 silencing enhances T cell avidity, the question arose whether this effect might be linked to an increased T cell exhaustion or an altered T cell persistence. Recursive antigen

stimulation was performed for five rounds with a total of 15 days. A similar experimental set up was performed for CD19 CAR T cells and revealed that serial antigen stimulation triggered activation-induced cell death[144]. In contrast, BCMA CAR T cells were shown to maintain their functionality over a period of 24 days[154]. In line with these results, this thesis demonstrated that BCMA CAR T cells with a knockdown of EBAG9 conserved their proliferative potential, viability, and capability of effector cytokine secretion. Accordingly, tumor cell clearance remained high and was associated with antigen-specific T cell proliferation. In the absence of FasL determination, direct conclusions concerning activation-induced cell death are not possible. Yet, the activation and exhaustion markers PD-1, LAG-3, and TIM-3 revealed an activation-induced expression pattern in $CD4^+$ and $CD8^+$ CAR T cells. The expression of these markers was not substantially altered throughout repetitive antigen stimulation and did not indicate increased cell death. Most importantly, increasing the cytolytic activity of BCMA CAR T cells by silencing EBAG9 did not influence the *in vitro* persistence or functionality of CAR T cells upon recursive antigen encounter.

In addition to CAR T cell functionality, the T cell subset composition was analyzed upon *in vitro* repetitive antigen stimulation. Surprisingly, the subset composition differed considerably between BCMA CAR T cells and BCMA CAR T cells with an engineered knockdown of EBAG9. Even at the beginning of the repetitive antigen stimulation, the $CD4^+$:$CD8^+$ ratio was higher within the BCMA CAR T cells. This further increased reaching an ratio of approximately 90% of $CD4^+$ to 10% of $CD8^+$ CAR T cells upon recursive stimulation with the tumor-antigen. In contrast, BCMA CAR T cells with silenced EBGA9 had a lower initial $CD4^+$:$CD8^+$ ratio of 60%:40%. Upon repetitive antigen stimulation, an equal distribution was reached. The transfer of a defined $CD4^+$:$CD8^+$ CAR T cell composition has recently become more important in ATT and has already been applied in clinical trials in adult B cell acute lymphoblastic leukemia patients[253,254]. As a 1:1 ratio of $CD4^+$:$CD8^+$ CAR T cells was shown to be remarkably potent, the BCMA CAR T cells with an engineered loss of EBAG9 might be superior as they inherently achieved this composition. Yet, it remains unclear how these differences in T cell subset composition develop and if the introduction of the EBAG9-targeting miRNA may be caused by a preferential $CD8^+$ CAR T cell proliferation or whether $CD4^+$ CAR T cell equipment is toxic to their persistence. A recent study showed CD19 CAR T cells to be differentially influenced by signals through the endogenous TCR in a syngeneic mouse model. While the presence of the TCR antigen led to a loss of $CD8^+$ CAR T cell efficacy that was

associated with exhaustion and apoptosis, $CD4^+$ CAR T cells retained their *in vivo* efficacy[255]. However, this model cannot be applied to the results of the present thesis as both CAR T cell populations were derived from the same donors and, therefore, equipped with the same endogenous TCR repertoire. Nonetheless, cell-intrinsic differences appear to be involved in transducing CAR T cell signaling in $CD4^+$ and $CD8^+$ T cells. This differences require a further elucidation to better understand the *in vivo* biology of engineered CAR T cells.

### 6.3.4 CAR T cells change their memory phenotype *in vitro* over time independently of EBAG9

In immunotherapy, an inverse correlation between T cell differentiation and antitumor efficacy has been described. The transfer of fully differentiated effector T cells was less effective and found to be linked to poor *in vivo* expansion and survival[167]. Instead, TCM and memory stem cells (TSCM) showed long-term persistence, exhibited enhanced metabolic fitness, and were more effective in their antitumor efficacy[256-259]. Thus, the application of a defined composition of T cell memory subsets is important for a long-lasting and successful tumor response. In the present thesis, the differentiation of BCMA CAR T cells and BCMA CAR T cells with an engineered knockdown of EBAG9 were analyzed upon *in vitro* repetitive antigen stimulation. While an equal distribution of TCM and TEM was initially present, TEM gained predominance and only minor amounts of TCM remained detectable. Of note, miRNA-mediated silencing of EBAG9 did not alter the memory phenotype differentiation of CAR T cells. However, these differentiation processes may be the result of culturing conditions. During T cell activation, transduction, and expansion, CAR T cells were cultured with IL-7 and IL-15. These are homeostatic cytokines that support T cell expansion and maintain a TCM phenotype[257,260,261]. Upon recursive antigen encounter, CAR T cells were co-cultured with tumor cells and only minor amounts of IL-7 and IL-15 were added. At the same time, activated CAR T cells were able to secrete the pro-proliferative cytokine IL-2, which favors effector differentiation[260,262]. To further control the impact of T cell culture conditions, it would be tempting to inhibit the IL-2R$\alpha$ signaling pathway using the mTOR inhibitor rapamycin[263].

## 6.4 Alternative silencing of EBAG9 by genome editing

Gene transfer for T cell engineering in ATT has been, to date, performed mainly in retroviral or lentiviral vectors leading to permanent integration into the genome. As the insertion sites cannot be controlled, this integration is rather random and might lead to side effects by oncogenic transformation, transcriptional silencing, or differences within transgene expression levels[264-266]. Although retroviral vectors have been used in clinical trials with a long-term safety record, alternative methods for sequence-specific interventions are currently under development[267-270]. Most recently, genome editing was used to specifically integrate a CAR into a defined locus within the genome. The group of Michel Sadelain used the CRISPR/Cas9 technology to insert a CD19 CAR gene into the *TRAC* locus encoding for the TCR$\alpha$ chain and gained consistent CAR expression in human T cells. Furthermore, through the analysis of different loci as sites of CAR integration, targeting the *TRAC* locus yielded greater antitumor potency in a mouse model of acute lymphoblastic leukemia, most likely caused by delayed effector differentiation and exhaustion[271]. In regard to targeting the secretory pathway of T cells to increase their cytolytic activity, this technique can be used to integrate a CAR with any desired specificity into the *EBAG9* locus. Thus, EBAG9 silencing could be accomplished without the need to induce the RNAi pathway or use of randomly integrating vectors. Although the benefits of using the *TRAC* locus in regard to increased antitumor efficacy would not be achieved, expression would, at least, be stable and no longer negatively influenced by the presence of miRNA. However, it remains to be shown whether the *EBAG9* locus is suitable for CAR expression as transcriptional configuration and expression levels are important for effective CAR activity.

## 6.5 Conclusions

In summary, the present study shows that targeting the secretory pathway of T cells is a promising strategy in improving ATT efficacy. As high-avidity and long-lived T cells are important for successful und remission-free immunotherapy, the negative regulator of effector molecule secretion EBAG9 is an attractive target. First, the fate of $CD8^+$ T cells was shown to be linked to their cytolytic strength in EBAG9-deficient mice because the loss of EBAG9 led to the preferential formation of an antigen-specific $CD8^+$ T cell memory pool. Second, the miRNA-mediated knockdown of EBAG9 in primary mouse and human T cells caused a substantially enhanced T cell avidity and therapeutic efficacy. Adoptive transfer of engineered mouse T cells with silenced EBAG9 increased antigen-specific cytotoxicity in *in vivo* killing assays.

Moreover, human CAR T cells were proven to kill their target cells *in vitro* and *in vivo* with enhanced efficiency due to the miRNA-mediated knockdown of EBAG9. Importantly, the effective CAR T cell numbers needed for efficient target cell killing could be decreased, which may lead to multiple advantages in terms of T cell manufacturing and reducing clinical adverse effects. The repetitive antigen stimulation assay *in vitro* ruled out that the engineered loss of EBAG9 altered functionality, persistence, or exhaustion of CAR T cells. Yet, to analyze memory formation and long-term *in vivo* persistence of T cells with miRNA-mediated silencing of EBAG9, a syngeneic mouse model is required.

Altogether, EBAG9 was found to be a novel type immune checkpoint inhibitor negatively regulating T cell memory formation and avidity. Therefore, targeting EBAG9 represents a feasible approach to increase the efficacy of adoptively transferred T cells by lowering the T cell activation threshold. Furthermore, this strategy provides the opportunity to overcome therapeutic limits due to the availability of low amounts or low-affinity T cells.

# 7. Literature


1 **Kimbrell, D. A. & Beutler, B. (2001).** „The evolution and genetics of innate immunity." *Nat Rev Genet* 2, 256-267.

2 **Turvey, S. E. & Broide, D. H. (2010).** „Innate immunity." *J Allergy Clin Immunol* 125, S24-32.

3 **Fearon, D. T. & Locksley, R. M. (1996).** „The instructive role of innate immunity in the acquired immune response." *Science* 272, 50-53.

4 **Ezekowitz, R. A. B. & Hoffmann, J. A. (1996).** „Innate immunity." *Curr Opin Immunol* 8, 1-2.

5 **Kaisho, T. & Akira, S. (2000).** „Critical roles of Toll-like receptors in host defense." *Crit Rev Immunol* 20, 393-405.

6 **Bonilla, F. A. & Oettgen, H. C. (2010).** „Adaptive immunity." *J Allergy Clin Immunol* 125, S33-40.

7 **den Haan, J. M., Arens, R. & van Zelm, M. C. (2014).** „The activation of the adaptive immune system: cross-talk between antigen-presenting cells, T cells and B cells." *Immunol Lett* 162, 103-112.

8 **Alcover, A., Alarcon, B. & Di Bartolo, V. (2018).** „Cell Biology of T Cell Receptor Expression and Regulation." *Annu Rev Immunol* 36, 103-125.

9 **Takaba, H. & Takayanagi, H. (2017).** „The Mechanisms of T Cell Selection in the Thymus." *Trends Immunol* 38, 805-816.

10 **Zhang, N. & Bevan, M. J. (2011).** „CD8(+) T cells: foot soldiers of the immune system." *Immunity* 35, 161-168.

11 **Luckheeram, R. V., Zhou, R., Verma, A. D. & Xia, B. (2012).** „CD4(+)T cells: differentiation and functions." *Clin Dev Immunol* 2012, 925135.

12 **Kaech, S. M. & Cui, W. (2012).** „Transcriptional control of effector and memory CD8+ T cell differentiation." *Nat Rev Immunol* 12, 749-761.

13 **Rutishauser, R. L. & Kaech, S. M. (2010).** „Generating diversity: transcriptional regulation of effector and memory CD8 T-cell differentiation." *Immunol Rev* 235, 219-233.

14 **Obar, J. J. & Lefrancois, L. (2010).** „Memory CD8+ T cell differentiation." *Ann N Y Acad Sci* 1183, 251-266.

15 **Buchholz, V. R., Graf, P. & Busch, D. H. (2013).** „The smallest unit: effector and memory CD8(+) T cell differentiation on the single cell level." *Front Immunol* 4, 31.

16 **Sallusto, F., Lenig, D., Forster, R., Lipp, M. & Lanzavecchia, A. (1999).** „Two subsets of memory T lymphocytes with distinct homing potentials and effector functions." *Nature* 401, 708-712.

17 **Stemberger, C. *et al.* (2007).** „A single naive CD8+ T cell precursor can develop into diverse effector and memory subsets." *Immunity* 27, 985-997.

18 **Gerlach, C. *et al.* (2010).** „One naive T cell, multiple fates in CD8+ T cell differentiation." *J Exp Med* 207, 1235-1246.

19 **Badovinac, V. P., Messingham, K. A., Jabbari, A., Haring, J. S. & Harty, J. T. (2005).** „Accelerated CD8+ T-cell memory and prime-boost response after dendritic-cell vaccination." *Nat Med* 11, 748-756.

20 **D'Souza, W. N. & Hedrick, S. M. (2006).** „Cutting edge: latecomer CD8 T cells are imprinted with a unique differentiation program." *J Immunol* 177, 777-781.

21 **Lanzavecchia, A. & Sallusto, F. (2002).** „Progressive differentiation and selection of the fittest in the immune response." *Nat Rev Immunol* 2, 982-987.

22 **Chang, J. T. *et al.* (2007).** „Asymmetric T lymphocyte division in the initiation of adaptive immune responses." *Science* 315, 1687-1691.

23 **Intlekofer, A. M. *et al.* (2005).** „Effector and memory CD8+ T cell fate coupled by T-bet and eomesodermin." *Nat Immunol* 6, 1236-1244.

24 **McLane, L. M. *et al.* (2013).** „Differential localization of T-bet and Eomes in CD8 T cell memory populations." *J Immunol* 190, 3207-3215.

25 **Bots, M. & Medema, J. P. (2006).** „Granzymes at a glance." *J Cell Sci* 119, 5011-5014.

26 **Kam, C. M., Hudig, D. & Powers, J. C. (2000).** „Granzymes (lymphocyte serine proteases): characterization with natural and synthetic substrates and inhibitors." *Biochim Biophys Acta* 1477, 307-323.

27 **Liu, C. C., Rafii, S., Granelli-Piperno, A., Trapani, J. A. & Young, J. D. (1989).** „Perforin and serine esterase gene expression in stimulated human T cells. Kinetics, mitogen requirements, and effects of cyclosporin A." *J Exp Med* 170, 2105-2118.

28 **Chowdhury, D. & Lieberman, J. (2008).** „Death by a thousand cuts: granzyme pathways of programmed cell death." *Annu Rev Immunol* 26, 389-420.

29 **Baumeister, S. H., Freeman, G. J., Dranoff, G. & Sharpe, A. H. (2016).** „Coinhibitory Pathways in Immunotherapy for Cancer." *Annu Rev Immunol* 34, 539-573.

30 **Bird, C. H. *et al.* (2005).** „Cationic sites on granzyme B contribute to cytotoxicity by promoting its uptake into target cells." *Mol Cell Biol* 25, 7854-7867.

31 **Shi, L. *et al.* (2005).** „Granzyme B binds to target cells mostly by charge and must be added at the same time as perforin to trigger apoptosis." *J Immunol* 174, 5456-5461.

32 **Motyka, B. *et al.* (2000).** „Mannose 6-phosphate/insulin-like growth factor II receptor is a death receptor for granzyme B during cytotoxic T cell-induced apoptosis." *Cell* 103, 491-500.

33 **Voskoboinik, I., Whisstock, J. C. & Trapani, J. A. (2015).** „Perforin and granzymes: function, dysfunction and human pathology." *Nat Rev Immunol* 15, 388-400.

34 **Martinvalet, D., Zhu, P. & Lieberman, J. (2005).** „Granzyme A induces caspase-independent mitochondrial damage, a required first step for apoptosis." *Immunity* 22, 355-370.

35 **Beresford, P. J. *et al.* (2001).** „Granzyme A activates an endoplasmic reticulum-associated caspase-independent nuclease to induce single-stranded DNA nicks." *J Biol Chem* 276, 43285-43293.

36 **Fan, Z., Beresford, P. J., Oh, D. Y., Zhang, D. & Lieberman, J. (2003).** „Tumor suppressor NM23-H1 is a granzyme A-activated DNase during CTL-mediated apoptosis, and the nucleosome assembly protein SET is its inhibitor." *Cell* 112, 659-672.

37 **Darmon, A. J., Nicholson, D. W. & Bleackley, R. C. (1995).** „Activation of the apoptotic protease CPP32 by cytotoxic T-cell-derived granzyme B." *Nature* 377, 446-448.

38 **Adrain, C., Murphy, B. M. & Martin, S. J. (2005).** „Molecular ordering of the caspase activation cascade initiated by the cytotoxic T lymphocyte/natural killer (CTL/NK) protease granzyme B." *J Biol Chem* 280, 4663-4673.

39 **Pham, C. T. & Ley, T. J. (1999).** „Dipeptidyl peptidase I is required for the processing and activation of granzymes A and B in vivo." *Proc Natl Acad Sci U S A* 96, 8627-8632.

40 **Sun, J. *et al.* (1996).** „A cytosolic granzyme B inhibitor related to the viral apoptotic regulator cytokine response modifier A is present in cytotoxic lymphocytes." *J Biol Chem* 271, 27802-27809.

41 **Phillips, T. *et al.* (2004).** „A role for the granzyme B inhibitor serine protease inhibitor 6 in CD8+ memory cell homeostasis." *J Immunol* 173, 3801-3809.

42 **Balaji, K. N., Schaschke, N., Machleidt, W., Catalfamo, M. & Henkart, P. A. (2002).** „Surface cathepsin B protects cytotoxic lymphocytes from self-destruction after degranulation." *J Exp Med* 196, 493-503.

43 **Schroder, K., Hertzog, P. J., Ravasi, T. & Hume, D. A. (2004).** „Interferon-gamma: an overview of signals, mechanisms and functions." *J Leukoc Biol* 75, 163-189.

44 **Tau, G. & Rothman, P. (1999).** „Biologic functions of the IFN-gamma receptors." *Allergy* 54, 1233-1251.

45 **Boehm, U., Klamp, T., Groot, M. & Howard, J. C. (1997).** „Cellular responses to interferon-gamma." *Annu Rev Immunol* 15, 749-795.

46 **Mach, B., Steimle, V., Martinez-Soria, E. & Reith, W. (1996).** „Regulation of MHC class II genes: lessons from a disease." *Annu Rev Immunol* 14, 301-331.

47 **Tannenbaum, C. S. & Hamilton, T. A. (2000).** „Immune-inflammatory mechanisms in IFNgamma-mediated anti-tumor activity." *Semin Cancer Biol* 10, 113-123.

48 **Buchmeier, N. A. & Schreiber, R. D. (1985).** „Requirement of endogenous interferon-gamma production for resolution of Listeria monocytogenes infection." *Proc Natl Acad Sci U S A* 82, 7404-7408.

49 **Pearl, J. E., Saunders, B., Ehlers, S., Orme, I. M. & Cooper, A. M. (2001).** „Inflammation and lymphocyte activation during mycobacterial infection in the interferon-gamma-deficient mouse." *Cell Immunol* 211, 43-50.

50 **van den Broek, M. F., Muller, U., Huang, S., Zinkernagel, R. M. & Aguet, M. (1995).** „Immune defence in mice lacking type I and/or type II interferon receptors." *Immunol Rev* 148, 5-18.

51 **Sedger, L. M. & McDermott, M. F. (2014).** „TNF and TNF-receptors: From mediators of cell death and inflammation to therapeutic giants - past, present and future." *Cytokine Growth Factor Rev* 25, 453-472.

52 **Salomon, B. L. *et al.* (2018).** „Tumor Necrosis Factor alpha and Regulatory T Cells in Oncoimmunology." *Front Immunol* 9, 444.

53 **Bertrand, F. *et al.* (2016).** „Targeting TNF alpha as a novel strategy to enhance CD8(+) T cell-dependent immune response in melanoma?" *Oncoimmunology* 5, e1068495.

54 **Ross, S. H. & Cantrell, D. A. (2018).** „Signaling and Function of Interleukin-2 in T Lymphocytes." *Annu Rev Immunol* 36, 411-433.

55 **Liao, W., Lin, J. X. & Leonard, W. J. (2013).** „Interleukin-2 at the crossroads of effector responses, tolerance, and immunotherapy." *Immunity* 38, 13-25.

56 **Russell, J. H. & Ley, T. J. (2002).** „Lymphocyte-mediated cytotoxicity." *Annu Rev Immunol* 20, 323-370.

57 **Huse, M., Lillemeier, B. F., Kuhns, M. S., Chen, D. S. & Davis, M. M. (2006).** „T cells use two directionally distinct pathways for cytokine secretion." *Nat Immunol* 7, 247-255.

58 **Jenkins, M. R., Tsun, A., Stinchcombe, J. C. & Griffiths, G. M. (2009).** „The strength of T cell receptor signal controls the polarization of cytotoxic machinery to the immunological synapse." *Immunity* 31, 621-631.

59 **van der Sluijs, P., Zibouche, M. & van Kerkhof, P. (2013).** „Late steps in secretory lysosome exocytosis in cytotoxic lymphocytes." *Front Immunol* 4, 359.

60 **Das, V. *et al.* (2004).** „Activation-induced polarized recycling targets T cell antigen receptors to the immunological synapse; involvement of SNARE complexes." *Immunity* 20, 577-588.

61 **Stenmark, H. (2009).** „Rab GTPases as coordinators of vesicle traffic." *Nat Rev Mol Cell Biol* 10, 513-525.

62 **Ghosh, P., Dahms, N. M. & Kornfeld, S. (2003).** „Mannose 6-phosphate receptors: new twists in the tale." *Nat Rev Mol Cell Biol* 4, 202-212.

63 **Lewin, D. A. *et al.* (1998).** „Cloning, expression, and localization of a novel gamma-adaptin-like molecule." *FEBS Lett* 435, 263-268.

64 **Ruder, C. *et al.* (2009).** „The tumor-associated antigen EBAG9 negatively regulates the cytolytic capacity of mouse CD8+ T cells." *J Clin Invest* 119, 2184-2203.

65 **Engelsberg, A. *et al.* (2003).** „The Golgi protein RCAS1 controls cell surface expression of tumor-associated O-linked glycan antigens." *J Biol Chem* 278, 22998-23007.

66 **Wherry, E. J. (2011).** „T cell exhaustion." *Nat Immunol* 12, 492-499.

67 **Zajac, A. J. *et al.* (1998).** „Viral immune evasion due to persistence of activated T cells without effector function." *J Exp Med* 188, 2205-2213.

68 **Wherry, E. J., Blattman, J. N., Murali-Krishna, K., van der Most, R. & Ahmed, R. (2003).** „Viral persistence alters CD8 T-cell immunodominance and tissue distribution and results in distinct stages of functional impairment." *J Virol* 77, 4911-4927.

69 **Moskophidis, D., Lechner, F., Pircher, H. & Zinkernagel, R. M. (1993).** „Virus persistence in acutely infected immunocompetent mice by exhaustion of antiviral cytotoxic effector T cells." *Nature* 362, 758-761.

70 **Blackburn, S. D. *et al.* (2009).** „Coregulation of CD8+ T cell exhaustion by multiple inhibitory receptors during chronic viral infection." *Nat Immunol* 10, 29-37.

71 **Crawford, A. & Wherry, E. J. (2009).** „The diversity of costimulatory and inhibitory receptor pathways and the regulation of antiviral T cell responses." *Curr Opin Immunol* 21, 179-186.

72 **Petrovas, C. *et al.* (2007).** „SIV-specific CD8+ T cells express high levels of PD1 and cytokines but have impaired proliferative capacity in acute and chronic SIVmac251 infection." *Blood* 110, 928-936.

73 **Blackburn, S. D. *et al.* (2010).** „Tissue-specific differences in PD-1 and PD-L1 expression during chronic viral infection: implications for CD8 T-cell exhaustion." *J Virol* 84, 2078-2089.

74 **Workman, C. J. *et al.* (2004).** „Lymphocyte activation gene-3 (CD223) regulates the size of the expanding T cell population following antigen activation in vivo." *J Immunol* 172, 5450-5455.

75 **Brooks, D. G. *et al.* (2006).** „Interleukin-10 determines viral clearance or persistence in vivo." *Nat Med* 12, 1301-1309.

76 **Ejrnaes, M. *et al.* (2006).** „Resolution of a chronic viral infection after interleukin-10 receptor blockade." *J Exp Med* 203, 2461-2472.

77 **Tinoco, R., Alcalde, V., Yang, Y., Sauer, K. & Zuniga, E. I. (2009).** „Cell-intrinsic transforming growth factor-beta signaling mediates virus-specific CD8+ T cell deletion and viral persistence in vivo." *Immunity* 31, 145-157.

78 **Punkosdy, G. A. *et al.* (2011).** „Regulatory T-cell expansion during chronic viral infection is dependent on endogenous retroviral superantigens." *Proc Natl Acad Sci U S A* 108, 3677-3682.

79 **Belkaid, Y. & Rouse, B. T. (2005).** „Natural regulatory T cells in infectious disease." *Nat Immunol* 6, 353-360.

80 **Wherry, E. J. *et al.* (2007).** „Molecular signature of CD8+ T cell exhaustion during chronic viral infection." *Immunity* 27, 670-684.

81 **Shin, H. *et al.* (2009).** „A role for the transcriptional repressor Blimp-1 in CD8(+) T cell exhaustion during chronic viral infection." *Immunity* 31, 309-320.

82 **Joshi, N. S. & Kaech, S. M. (2008).** „Effector CD8 T cell development: a balancing act between memory cell potential and terminal differentiation." *J Immunol* 180, 1309-1315.

83 **Leach, D. R., Krummel, M. F. & Allison, J. P. (1996).** „Enhancement of antitumor immunity by CTLA-4 blockade." *Science* 271, 1734-1736.

84 **Ishida, Y., Agata, Y., Shibahara, K. & Honjo, T. (1992).** „Induced expression of PD-1, a novel member of the immunoglobulin gene superfamily, upon programmed cell death." *EMBO J* 11, 3887-3895.

85 **Walunas, T. L. *et al.* (1994).** „CTLA-4 can function as a negative regulator of T cell activation." *Immunity* 1, 405-413.

86 **Chambers, C. A., Kuhns, M. S., Egen, J. G. & Allison, J. P. (2001).** „CTLA-4-mediated inhibition in regulation of T cell responses: mechanisms and manipulation in tumor immunotherapy." *Annu Rev Immunol* 19, 565-594.

87 **Hodi, F. S. *et al.* (2010).** „Improved survival with ipilimumab in patients with metastatic melanoma." *N Engl J Med* 363, 711-723.

88 **Ribas, A. & Wolchok, J. D. (2018).** „Cancer immunotherapy using checkpoint blockade." *Science* 359, 1350-1355.

89 **Pardoll, D. M. (2012).** „The blockade of immune checkpoints in cancer immunotherapy." *Nat Rev Cancer* 12, 252-264.

90 **Ribas, A. (2015).** „Adaptive Immune Resistance: How Cancer Protects from Immune Attack." *Cancer Discov* 5, 915-919.

91 **Met, O., Jensen, K. M., Chamberlain, C. A., Donia, M. & Svane, I. M. (2018).** „Principles of adoptive T cell therapy in cancer." *Semin Immunopathol*.

92 **Restifo, N. P., Dudley, M. E. & Rosenberg, S. A. (2012).** „Adoptive immunotherapy for cancer: harnessing the T cell response." *Nat Rev Immunol* 12, 269-281.

93 **Maus, M. V. *et al.* (2014).** „Adoptive immunotherapy for cancer or viruses." *Annu Rev Immunol* 32, 189-225.

94 **Schmidts, A. & Maus, M. V. (2018).** „Making CAR T Cells a Solid Option for Solid Tumors." *Front Immunol* 9, 2593.

95 **Louis, C. U. *et al.* (2011).** „Antitumor activity and long-term fate of chimeric antigen receptor-positive T cells in patients with neuroblastoma." *Blood* 118, 6050-6056.

96 **Rosenberg, S. A., Fox, E. & Churchill, W. H. (1972).** „Spontaneous regression of hepatic metastases from gastric carcinoma." *Cancer* 29, 472-474.

97 **Dudley, M. E. *et al.* (2005).** „Adoptive cell transfer therapy following non-myeloablative but lymphodepleting chemotherapy for the treatment of patients with refractory metastatic melanoma." *J Clin Oncol* 23, 2346-2357.

98 **Itzhaki, O. *et al.* (2011).** „Establishment and large-scale expansion of minimally cultured "young" tumor infiltrating lymphocytes for adoptive transfer therapy." *J Immunother* 34, 212-220.

99 **Radvanyi, L. G. *et al.* (2012).** „Specific lymphocyte subsets predict response to adoptive cell therapy using expanded autologous tumor-infiltrating lymphocytes in metastatic melanoma patients." *Clin Cancer Res* 18, 6758-6770.

100 **Andersen, R. *et al.* (2016).** „Long-Lasting Complete Responses in Patients with Metastatic Melanoma after Adoptive Cell Therapy with Tumor-Infiltrating Lymphocytes and an Attenuated IL2 Regimen." *Clin Cancer Res* 22, 3734-3745.

101 **Rosenberg, S. A. *et al.* (1988).** „Use of tumor-infiltrating lymphocytes and interleukin-2 in the immunotherapy of patients with metastatic melanoma. A preliminary report." *N Engl J Med* 319, 1676-1680.

102 **Dudley, M. E., Wunderlich, J. R., Shelton, T. E., Even, J. & Rosenberg, S. A. (2003).** „Generation of tumor-infiltrating lymphocyte cultures for use in adoptive transfer therapy for melanoma patients." *J Immunother* 26, 332-342.

103 **de Witte, M. A. *et al.* (2006).** „Targeting self-antigens through allogeneic TCR gene transfer." *Blood* 108, 870-877.

104 **Stanislawski, T. *et al.* (2001).** „Circumventing tolerance to a human MDM2-derived tumor antigen by TCR gene transfer." *Nat Immunol* 2, 962-970.

105 **Johnson, L. A. *et al.* (2009).** „Gene therapy with human and mouse T-cell receptors mediates cancer regression and targets normal tissues expressing cognate antigen." *Blood* 114, 535-546.

106 **Robbins, P. F. *et al.* (2011).** „Tumor regression in patients with metastatic synovial cell sarcoma and melanoma using genetically engineered lymphocytes reactive with NY-ESO-1." *J Clin Oncol* 29, 917-924.

107 **Kershaw, M. H. *et al.* (2006).** „A phase I study on adoptive immunotherapy using gene-modified T cells for ovarian cancer." *Clin Cancer Res* 12, 6106-6115.

108 **Davila, M. L. *et al.* (2014).** „Efficacy and toxicity management of 19-28z CAR T cell therapy in B cell acute lymphoblastic leukemia." *Sci Transl Med* 6, 224ra225.

109 **Maude, S. L. *et al.* (2014).** „Chimeric antigen receptor T cells for sustained remissions in leukemia." *N Engl J Med* 371, 1507-1517.

110 **Kochenderfer, J. N. *et al.* (2015).** „Chemotherapy-refractory diffuse large B-cell lymphoma and indolent B-cell malignancies can be effectively treated with autologous T cells expressing an anti-CD19 chimeric antigen receptor." *J Clin Oncol* 33, 540-549.

111 **Brudno, J. N. *et al.* (2018).** „T Cells Genetically Modified to Express an Anti-B-Cell Maturation Antigen Chimeric Antigen Receptor Cause Remissions of Poor-Prognosis Relapsed Multiple Myeloma." *J Clin Oncol* 36, 2267-2280.

112 **Gowrishankar, K., Birtwistle, L. & Micklethwaite, K. (2018).** „Manipulating the tumor microenvironment by adoptive cell transfer of CAR T-cells." *Mamm Genome*.

113 **Park, J. H. *et al.* (2018).** „Long-Term Follow-up of CD19 CAR Therapy in Acute Lymphoblastic Leukemia." *N Engl J Med* 378, 449-459.

114 **Porter, D. L. *et al.* (2015).** „Chimeric antigen receptor T cells persist and induce sustained remissions in relapsed refractory chronic lymphocytic leukemia." *Sci Transl Med* 7, 303ra139.

115 **Shankar, P., Manjunath, N. & Lieberman, J. (2005).** „The prospect of silencing disease using RNA interference." *JAMA* 293, 1367-1373.

116 **Lee, Y. *et al.* (2003).** „The nuclear RNase III Drosha initiates microRNA processing." *Nature* 425, 415-419.

117 **Wang, Y., Medvid, R., Melton, C., Jaenisch, R. & Blelloch, R. (2007).** „DGCR8 is essential for microRNA biogenesis and silencing of embryonic stem cell self-renewal." *Nat Genet* 39, 380-385.

118 **Ryan, B. M., Robles, A. I. & Harris, C. C. (2010).** „Genetic variation in microRNA networks: the implications for cancer research." *Nat Rev Cancer* 10, 389-402.

119 **Lund, E., Guttinger, S., Calado, A., Dahlberg, J. E. & Kutay, U. (2004).** „Nuclear export of microRNA precursors." *Science* 303, 95-98.

120 **Bartel, D. P. (2009).** „MicroRNAs: target recognition and regulatory functions." *Cell* 136, 215-233.

121 **Ji, Y., Hocker, J. D. & Gattinoni, L. (2016).** „Enhancing adoptive T cell immunotherapy with microRNA therapeutics." *Semin Immunol* 28, 45-53.

122 **Fabian, M. R., Sonenberg, N. & Filipowicz, W. (2010).** „Regulation of mRNA translation and stability by microRNAs." *Annu Rev Biochem* 79, 351-379.

123 **Meister, G. *et al.* (2004).** „Human Argonaute2 mediates RNA cleavage targeted by miRNAs and siRNAs." *Mol Cell* 15, 185-197.

124 **Pillai, R. S. *et al.* (2005).** „Inhibition of translational initiation by Let-7 MicroRNA in human cells." *Science* 309, 1573-1576.

125 **Humphreys, D. T., Westman, B. J., Martin, D. I. & Preiss, T. (2005).** „MicroRNAs control translation initiation by inhibiting eukaryotic initiation factor 4E/cap and poly(A) tail function." *Proc Natl Acad Sci U S A* 102, 16961-16966.

126 **Brummelkamp, T. R., Bernards, R. & Agami, R. (2002).** „A system for stable expression of short interfering RNAs in mammalian cells.“ *Science* 296, 550-553.
127 **Zeng, Y., Wagner, E. J. & Cullen, B. R. (2002).** „Both natural and designed micro RNAs can inhibit the expression of cognate mRNAs when expressed in human cells.“ *Mol Cell* 9, 1327-1333.
128 **Gregory, R. I. *et al.* (2004).** „The Microprocessor complex mediates the genesis of microRNAs.“ *Nature* 432, 235-240.
129 **Shen, L., Evel-Kabler, K., Strube, R. & Chen, S. Y. (2004).** „Silencing of SOCS1 enhances antigen presentation by dendritic cells and antigen-specific anti-tumor immunity.“ *Nat Biotechnol* 22, 1546-1553.
130 **Song, X. T. *et al.* (2008).** „A20 is an antigen presentation attenuator, and its inhibition overcomes regulatory T cell-mediated suppression.“ *Nat Med* 14, 258-265.
131 **Zhou, H. *et al.* (2006).** „Induction of CML28-specific cytotoxic T cell responses using co-transfected dendritic cells with CML28 DNA vaccine and SOCS1 small interfering RNA expression vector.“ *Biochem Biophys Res Commun* 347, 200-207.
132 **Rothlin, C. V., Ghosh, S., Zuniga, E. I., Oldstone, M. B. & Lemke, G. (2007).** „TAM receptors are pleiotropic inhibitors of the innate immune response.“ *Cell* 131, 1124-1136.
133 **Lu, Q. & Lemke, G. (2001).** „Homeostatic regulation of the immune system by receptor tyrosine kinases of the Tyro 3 family.“ *Science* 293, 306-311.
134 **Wallet, M. A. *et al.* (2008).** „MerTK is required for apoptotic cell-induced T cell tolerance.“ *J Exp Med* 205, 219-232.
135 **Huang, B., Mao, C. P., Peng, S., Hung, C. F. & Wu, T. C. (2008).** „RNA interference-mediated in vivo silencing of fas ligand as a strategy for the enhancement of DNA vaccine potency.“ *Hum Gene Ther* 19, 763-773.
136 **Liu, G. *et al.* (2004).** „Small interference RNA modulation of IL-10 in human monocyte-derived dendritic cells enhances the Th1 response.“ *Eur J Immunol* 34, 1680-1687.
137 **Dudda, J. C. *et al.* (2013).** „MicroRNA-155 is required for effector CD8+ T cell responses to virus infection and cancer.“ *Immunity* 38, 742-753.
138 **Pallandre, J. R. *et al.* (2007).** „Role of STAT3 in CD4+CD25+FOXP3+ regulatory lymphocyte generation: implications in graft-versus-host disease and antitumor immunity.“ *J Immunol* 179, 7593-7604.
139 **Hinterleitner, R. *et al.* (2012).** „Adoptive transfer of siRNA Cblb-silenced CD8+ T lymphocytes augments tumor vaccine efficacy in a B16 melanoma model.“ *PLoS One* 7, e44295.
140 **Stromnes, I. M. *et al.* (2012).** „Abrogation of SRC homology region 2 domain-containing phosphatase 1 in tumor-specific T cells improves efficacy of adoptive immunotherapy by enhancing the effector function and accumulation of short-lived effector T cells in vivo.“ *J Immunol* 189, 1812-1825.
141 **Karttunen, J., Sanderson, S. & Shastri, N. (1992).** „Detection of rare antigen-presenting cells by the lacZ T-cell activation assay suggests an expression cloning strategy for T-cell antigens.“ *Proc Natl Acad Sci U S A* 89, 6020-6024.
142 **Morita, S., Kojima, T. & Kitamura, T. (2000).** „Plat-E: an efficient and stable system for transient packaging of retroviruses.“ *Gene Ther* 7, 1063-1066.
143 **Valujskikh, A., Lantz, O., Celli, S., Matzinger, P. & Heeger, P. S. (2002).** „Cross-primed CD8(+) T cells mediate graft rejection via a distinct effector pathway.“ *Nat Immunol* 3, 844-851.
144 **Kunkele, A. *et al.* (2015).** „Functional Tuning of CARs Reveals Signaling Threshold above Which CD8+ CTL Antitumor Potency Is Attenuated due to Cell Fas-FasL-Dependent AICD.“ *Cancer Immunol Res* 3, 368-379.

145 **Oden, F. *et al.* (2015).** „Potent anti-tumor response by targeting B cell maturation antigen (BCMA) in a mouse model of multiple myeloma.“ *Mol Oncol* 9, 1348-1358.
146 **Sarkar, S. *et al.* (2008).** „Functional and genomic profiling of effector CD8 T cell subsets with distinct memory fates.“ *J Exp Med* 205, 625-640.
147 **Huster, K. M. *et al.* (2004).** „Selective expression of IL-7 receptor on memory T cells identifies early CD40L-dependent generation of distinct CD8+ memory T cell subsets.“ *Proc Natl Acad Sci U S A* 101, 5610-5615.
148 **Kaech, S. M. *et al.* (2003).** „Selective expression of the interleukin 7 receptor identifies effector CD8 T cells that give rise to long-lived memory cells.“ *Nat Immunol* 4, 1191-1198.
149 **Yang, C. Y. *et al.* (2011).** „The transcriptional regulators Id2 and Id3 control the formation of distinct memory CD8+ T cell subsets.“ *Nat Immunol* 12, 1221-1229.
150 **Gray, S. M., Kaech, S. M. & Staron, M. M. (2014).** „The interface between transcriptional and epigenetic control of effector and memory CD8(+) T-cell differentiation.“ *Immunol Rev* 261, 157-168.
151 **Velica, P. *et al.* (2015).** „Genetic Regulation of Fate Decisions in Therapeutic T Cells to Enhance Tumor Protection and Memory Formation.“ *Cancer Res* 75, 2641-2652.
152 **Engels, B. *et al.* (2003).** „Retroviral vectors for high-level transgene expression in T lymphocytes.“ *Hum Gene Ther* 14, 1155-1168.
153 **Shinkai, Y. *et al.* (1992).** „RAG-2-deficient mice lack mature lymphocytes owing to inability to initiate V(D)J rearrangement.“ *Cell* 68, 855-867.
154 **Bluhm, J. *et al.* (2018).** „CAR T Cells with Enhanced Sensitivity to B Cell Maturation Antigen for the Targeting of B Cell Non-Hodgkin's Lymphoma and Multiple Myeloma.“ *Mol Ther* 26, 1906-1920.
155 **Faitschuk, E., Hombach, A. A., Frenzel, L. P., Wendtner, C. M. & Abken, H. (2016).** „Chimeric antigen receptor T cells targeting Fc mu receptor selectively eliminate CLL cells while sparing healthy B cells.“ *Blood* 128, 1711-1722.
156 **Gattinoni, L. *et al.* (2011).** „A human memory T cell subset with stem cell-like properties.“ *Nat Med* 17, 1290-1297.
157 **Hamann, D. *et al.* (1997).** „Phenotypic and functional separation of memory and effector human CD8+ T cells.“ *J Exp Med* 186, 1407-1418.
158 **Picker, L. J. *et al.* (1993).** „Control of lymphocyte recirculation in man. II. Differential regulation of the cutaneous lymphocyte-associated antigen, a tissue-selective homing receptor for skin-homing T cells.“ *J Immunol* 150, 1122-1136.
159 **Picker, L. J. *et al.* (1993).** „Control of lymphocyte recirculation in man. I. Differential regulation of the peripheral lymph node homing receptor L-selectin on T cells during the virgin to memory cell transition.“ *J Immunol* 150, 1105-1121.
160 **Bosma, M. J. & Carroll, A. M. (1991).** „The SCID mouse mutant: definition, characterization, and potential uses.“ *Annu Rev Immunol* 9, 323-350.
161 **Shultz, L. D. *et al.* (2005).** „Human lymphoid and myeloid cell development in NOD/LtSz-scid IL2R gamma null mice engrafted with mobilized human hemopoietic stem cells.“ *J Immunol* 174, 6477-6489.
162 **Kalos, M. & June, C. H. (2013).** „Adoptive T cell transfer for cancer immunotherapy in the era of synthetic biology.“ *Immunity* 39, 49-60.
163 **Arens, R. & Schoenberger, S. P. (2010).** „Plasticity in programming of effector and memory CD8 T-cell formation.“ *Immunol Rev* 235, 190-205.
164 **Whiteside, T. L. (2006).** „Immune suppression in cancer: effects on immune cells, mechanisms and future therapeutic intervention.“ *Semin Cancer Biol* 16, 3-15.

165 **Rabinovich, G. A., Gabrilovich, D. & Sotomayor, E. M. (2007).** „Immunosuppressive strategies that are mediated by tumor cells." *Annu Rev Immunol* 25, 267-296.

166 **Gajewski, T. F., Schreiber, H. & Fu, Y. X. (2013).** „Innate and adaptive immune cells in the tumor microenvironment." *Nat Immunol* 14, 1014-1022.

167 **Gattinoni, L. *et al.* (2005).** „Acquisition of full effector function in vitro paradoxically impairs the in vivo antitumor efficacy of adoptively transferred CD8+ T cells." *J Clin Invest* 115, 1616-1626.

168 **Stromnes, I. M. *et al.* (2010).** „Abrogating Cbl-b in effector CD8(+) T cells improves the efficacy of adoptive therapy of leukemia in mice." *J Clin Invest* 120, 3722-3734.

169 **Palmer, D. C. *et al.* (2015).** „Cish actively silences TCR signaling in CD8+ T cells to maintain tumor tolerance." *J Exp Med* 212, 2095-2113.

170 **Opferman, J. T., Ober, B. T., Narayanan, R. & Ashton-Rickardt, P. G. (2001).** „Suicide induced by cytolytic activity controls the differentiation of memory CD8(+) T lymphocytes." *Int Immunol* 13, 411-419.

171 **Harty, J. T. & Badovinac, V. P. (2008).** „Shaping and reshaping CD8+ T-cell memory." *Nat Rev Immunol* 8, 107-119.

172 **Cui, W., Joshi, N. S., Jiang, A. & Kaech, S. M. (2009).** „Effects of Signal 3 during CD8 T cell priming: Bystander production of IL-12 enhances effector T cell expansion but promotes terminal differentiation." *Vaccine* 27, 2177-2187.

173 **Toubai, T. *et al.* (2012).** „Induction of acute GVHD by sex-mismatched H-Y antigens in the absence of functional radiosensitive host hematopoietic-derived antigen-presenting cells." *Blood* 119, 3844-3853.

174 **Bleakley, M. & Riddell, S. R. (2011).** „Exploiting T cells specific for human minor histocompatibility antigens for therapy of leukemia." *Immunol Cell Biol* 89, 396-407.

175 **Akatsuka, Y., Morishima, Y., Kuzushima, K., Kodera, Y. & Takahashi, T. (2007).** „Minor histocompatibility antigens as targets for immunotherapy using allogeneic immune reactions." *Cancer Sci* 98, 1139-1146.

176 **Joshi, N. S. *et al.* (2007).** „Inflammation directs memory precursor and short-lived effector CD8(+) T cell fates via the graded expression of T-bet transcription factor." *Immunity* 27, 281-295.

177 **Blair, D. A. *et al.* (2011).** „Duration of antigen availability influences the expansion and memory differentiation of T cells." *J Immunol* 187, 2310-2321.

178 **Sullivan, B. M., Juedes, A., Szabo, S. J., von Herrath, M. & Glimcher, L. H. (2003).** „Antigen-driven effector CD8 T cell function regulated by T-bet." *Proc Natl Acad Sci U S A* 100, 15818-15823.

179 **Pearce, E. L. *et al.* (2003).** „Control of effector CD8+ T cell function by the transcription factor Eomesodermin." *Science* 302, 1041-1043.

180 **Snyder, C. M. (2015).** „Front-Line Memory T Cells Think Outside the T-box... Mostly." *Immunity* 43, 1030-1032.

181 **Banerjee, A. *et al.* (2010).** „Cutting edge: The transcription factor eomesodermin enables CD8+ T cells to compete for the memory cell niche." *J Immunol* 185, 4988-4992.

182 **Paley, M. A. *et al.* (2013).** „Technical Advance: Fluorescent reporter reveals insights into eomesodermin biology in cytotoxic lymphocytes." *J Leukoc Biol* 93, 307-315.

183 **Juedes, A. E., Rodrigo, E., Togher, L., Glimcher, L. H. & von Herrath, M. G. (2004).** „T-bet controls autoaggressive CD8 lymphocyte responses in type 1 diabetes." *J Exp Med* 199, 1153-1162.

184 **Ji, Y. *et al.* (2011).** „Repression of the DNA-binding inhibitor Id3 by Blimp-1 limits the formation of memory CD8+ T cells." *Nat Immunol* 12, 1230-1237.

185 **Cannarile, M. A. *et al.* (2006).** „Transcriptional regulator Id2 mediates CD8+ T cell immunity." *Nat Immunol* 7, 1317-1325.

186 **Takemoto, N., Intlekofer, A. M., Northrup, J. T., Wherry, E. J. & Reiner, S. L. (2006).** „Cutting Edge: IL-12 inversely regulates T-bet and eomesodermin expression during pathogen-induced CD8+ T cell differentiation." *J Immunol* 177, 7515-7519.

187 **Xiao, Z., Casey, K. A., Jameson, S. C., Curtsinger, J. M. & Mescher, M. F. (2009).** „Programming for CD8 T cell memory development requires IL-12 or type I IFN." *J Immunol* 182, 2786-2794.

188 **Garcia, K. *et al.* (2014).** „IL-12 is required for mTOR regulation of memory CTLs during viral infection." *Genes Immun* 15, 413-423.

189 **Li, Q., Eppolito, C., Odunsi, K. & Shrikant, P. A. (2006).** „IL-12-programmed long-term CD8+ T cell responses require STAT4." *J Immunol* 177, 7618-7625.

190 **Rosenberg, S. A. *et al.* (2005).** „Tumor progression can occur despite the induction of very high levels of self/tumor antigen-specific CD8+ T cells in patients with melanoma." *J Immunol* 175, 6169-6176.

191 **Hodi, F. S. & Dranoff, G. (2010).** „The biologic importance of tumor-infiltrating lymphocytes." *J Cutan Pathol* 37 Suppl 1, 48-53.

192 **Alexander-Miller, M. A. (2005).** „High-avidity CD8+ T cells: optimal soldiers in the war against viruses and tumors." *Immunol Res* 31, 13-24.

193 **Zhao, Y. *et al.* (2007).** „High-affinity TCRs generated by phage display provide CD4+ T cells with the ability to recognize and kill tumor cell lines." *J Immunol* 179, 5845-5854.

194 **Malecek, K. *et al.* (2013).** „Engineering improved T cell receptors using an alanine-scan guided T cell display selection system." *J Immunol Methods* 392, 1-11.

195 **Jensen, M. C. & Riddell, S. R. (2014).** „Design and implementation of adoptive therapy with chimeric antigen receptor-modified T cells." *Immunol Rev* 257, 127-144.

196 **Suzuki, T. *et al.* (2001).** „EBAG9/RCAS1 in human breast carcinoma: a possible factor in endocrine-immune interactions." *Br J Cancer* 85, 1731-1737.

197 **Miyazaki, T. *et al.* (2014).** „EBAG9 modulates host immune defense against tumor formation and metastasis by regulating cytotoxic activity of T lymphocytes." *Oncogenesis* 3, e126.

198 **Miyazaki, T., Ikeda, K., Sato, W., Horie-Inoue, K. & Inoue, S. (2018).** „Extracellular vesicle-mediated EBAG9 transfer from cancer cells to tumor microenvironment promotes immune escape and tumor progression." *Oncogenesis* 7, 7.

199 **Park, T. S., Abate-Daga, D., Zhang, L., Zheng, Z. & Morgan, R. A. (2014).** „Gamma-retroviral vector design for the co-expression of artificial microRNAs and therapeutic proteins." *Nucleic Acid Ther* 24, 356-363.

200 **Tuschl, T. & Borkhardt, A. (2002).** „Small interfering RNAs: a revolutionary tool for the analysis of gene function and gene therapy." *Mol Interv* 2, 158-167.

201 **Herrera-Carrillo, E., Liu, Y. P. & Berkhout, B. (2017).** „Improving miRNA Delivery by Optimizing miRNA Expression Cassettes in Diverse Virus Vectors." *Hum Gene Ther Methods* 28, 177-190.

202 **Silva, J. M. *et al.* (2005).** „Second-generation shRNA libraries covering the mouse and human genomes." *Nat Genet* 37, 1281-1288.

203 **Chang, K., Elledge, S. J. & Hannon, G. J. (2006).** „Lessons from Nature: microRNA-based shRNA libraries." *Nat Methods* 3, 707-714.

204 **An, D. S. *et al.* (2006).** „Optimization and functional effects of stable short hairpin RNA expression in primary human lymphocytes via lentiviral vectors." *Mol Ther* 14, 494-504.

205 **Manjunath, N., Wu, H., Subramanya, S. & Shankar, P. (2009).** „Lentiviral delivery of short hairpin RNAs." *Adv Drug Deliv Rev* 61, 732-745.

206 **McBride, J. L. *et al.* (2008).** „Artificial miRNAs mitigate shRNA-mediated toxicity in the brain: implications for the therapeutic development of RNAi.“ *Proc Natl Acad Sci U S A* 105, 5868-5873.
207 **Grimm, D. *et al.* (2006).** „Fatality in mice due to oversaturation of cellular microRNA/short hairpin RNA pathways.“ *Nature* 441, 537-541.
208 **Grimm, D. *et al.* (2010).** „Argonaute proteins are key determinants of RNAi efficacy, toxicity, and persistence in the adult mouse liver.“ *J Clin Invest* 120, 3106-3119.
209 **Lo, H. L. *et al.* (2007).** „Inhibition of HIV-1 replication with designed miRNAs expressed from RNA polymerase II promoters.“ *Gene Ther* 14, 1503-1512.
210 **Du, G., Yonekubo, J., Zeng, Y., Osisami, M. & Frohman, M. A. (2006).** „Design of expression vectors for RNA interference based on miRNAs and RNA splicing.“ *FEBS J* 273, 5421-5427.
211 **Amendola, M. *et al.* (2009).** „Regulated and multiple miRNA and siRNA delivery into primary cells by a lentiviral platform.“ *Mol Ther* 17, 1039-1052.
212 **Bauer, M. *et al.* (2009).** „Prevention of interferon-stimulated gene expression using microRNA-designed hairpins.“ *Gene Ther* 16, 142-147.
213 **Lebbink, R. J. *et al.* (2011).** „Polymerase II promoter strength determines efficacy of microRNA adapted shRNAs.“ *PLoS One* 6, e26213.
214 **Snyder, L. L., Esser, J. M., Pachuk, C. J. & Steel, L. F. (2008).** „Vector design for liver-specific expression of multiple interfering RNAs that target hepatitis B virus transcripts.“ *Antiviral Res* 80, 36-44.
215 **Jackson, A. L. *et al.* (2003).** „Expression profiling reveals off-target gene regulation by RNAi.“ *Nat Biotechnol* 21, 635-637.
216 **Singh, S., Narang, A. S. & Mahato, R. I. (2011).** „Subcellular fate and off-target effects of siRNA, shRNA, and miRNA.“ *Pharm Res* 28, 2996-3015.
217 **Lai, E. C. (2002).** „Micro RNAs are complementary to 3' UTR sequence motifs that mediate negative post-transcriptional regulation.“ *Nat Genet* 30, 363-364.
218 **Jackson, A. L. *et al.* (2006).** „Widespread siRNA "off-target" transcript silencing mediated by seed region sequence complementarity.“ *RNA* 12, 1179-1187.
219 **Birmingham, A. *et al.* (2006).** „3' UTR seed matches, but not overall identity, are associated with RNAi off-targets.“ *Nat Methods* 3, 199-204.
220 **Grimson, A. *et al.* (2007).** „MicroRNA targeting specificity in mammals: determinants beyond seed pairing.“ *Mol Cell* 27, 91-105.
221 **Zhang, L. *et al.* (2018).** „Circular siRNAs for Reducing Off-Target Effects and Enhancing Long-Term Gene Silencing in Cells and Mice.“ *Mol Ther Nucleic Acids* 10, 237-244.
222 **Haabeth, O. A. *et al.* (2014).** „How Do CD4(+) T Cells Detect and Eliminate Tumor Cells That Either Lack or Express MHC Class II Molecules?“ *Front Immunol* 5, 174.
223 **Takeuchi, A. & Saito, T. (2017).** „CD4 CTL, a Cytotoxic Subset of CD4(+) T Cells, Their Differentiation and Function.“ *Front Immunol* 8, 194.
224 **Ogushi, T. *et al.* (2005).** „Estrogen receptor-binding fragment-associated antigen 9 is a tumor-promoting and prognostic factor for renal cell carcinoma.“ *Cancer Res* 65, 3700-3706.
225 **Hong, X. *et al.* (2009).** „EBAG9 inducing hyporesponsiveness of T cells promotes tumor growth and metastasis in 4T1 murine mammary carcinoma.“ *Cancer Sci* 100, 961-969.
226 **Krawczyk, C. *et al.* (2000).** „Cbl-b is a negative regulator of receptor clustering and raft aggregation in T cells.“ *Immunity* 13, 463-473.
227 **Krawczyk, C. M. *et al.* (2005).** „Differential control of CD28-regulated in vivo immunity by the E3 ligase Cbl-b.“ *J Immunol* 174, 1472-1478.
228 **Johnson, L. A. & June, C. H. (2017).** „Driving gene-engineered T cell immunotherapy of cancer.“ *Cell Res* 27, 38-58.

229 **Danhof, S., Hudecek, M. & Smith, E. L. (2018).** „CARs and other T cell therapies for MM: The clinical experience." *Best Pract Res Clin Haematol* 31, 147-157.

230 **Cohen, A. D. (2018).** „CAR T Cells and Other Cellular Therapies for Multiple Myeloma: 2018 Update." *Am Soc Clin Oncol Educ Book*, e6-e15.

231 **Chung, K. H. *et al.* (2006).** „Polycistronic RNA polymerase II expression vectors for RNA interference based on BIC/miR-155." *Nucleic Acids Res* 34, e53.

232 **Qiu, L., Wang, H., Xia, X., Zhou, H. & Xu, Z. (2008).** „A construct with fluorescent indicators for conditional expression of miRNA." *BMC Biotechnol* 8, 77.

233 **Hildinger, M., Abel, K. L., Ostertag, W. & Baum, C. (1999).** „Design of 5' untranslated sequences in retroviral vectors developed for medical use." *J Virol* 73, 4083-4089.

234 **Malim, M. H., Hauber, J., Le, S. Y., Maizel, J. V. & Cullen, B. R. (1989).** „The HIV-1 rev trans-activator acts through a structured target sequence to activate nuclear export of unspliced viral mRNA." *Nature* 338, 254-257.

235 **Dull, T. *et al.* (1998).** „A third-generation lentivirus vector with a conditional packaging system." *J Virol* 72, 8463-8471.

236 **Ivics, Z., Hackett, P. B., Plasterk, R. H. & Izsvak, Z. (1997).** „Molecular reconstruction of Sleeping Beauty, a Tc1-like transposon from fish, and its transposition in human cells." *Cell* 91, 501-510.

237 **Singh, H. *et al.* (2008).** „Redirecting specificity of T-cell populations for CD19 using the Sleeping Beauty system." *Cancer Res* 68, 2961-2971.

238 **Peng, P. D. *et al.* (2009).** „Efficient nonviral Sleeping Beauty transposon-based TCR gene transfer to peripheral blood lymphocytes confers antigen-specific antitumor reactivity." *Gene Ther* 16, 1042-1049.

239 **Yin, H. *et al.* (2014).** „Non-viral vectors for gene-based therapy." *Nat Rev Genet* 15, 541-555.

240 **Goodier, J. L. (2016).** „Restricting retrotransposons: a review." *Mob DNA* 7, 16.

241 **Zhao, Z. *et al.* (2015).** „Structural Design of Engineered Costimulation Determines Tumor Rejection Kinetics and Persistence of CAR T Cells." *Cancer Cell* 28, 415-428.

242 **Green, D. R., Droin, N. & Pinkoski, M. (2003).** „Activation-induced cell death in T cells." *Immunol Rev* 193, 70-81.

243 **Cencioni, M. T. *et al.* (2015).** „FAS-ligand regulates differential activation-induced cell death of human T-helper 1 and 17 cells in healthy donors and multiple sclerosis patients." *Cell Death Dis* 6, e1785.

244 **Chatenoud, L. *et al.* (1990).** „In vivo cell activation following OKT3 administration. Systemic cytokine release and modulation by corticosteroids." *Transplantation* 49, 697-702.

245 **Chatenoud, L. *et al.* (1989).** „Systemic reaction to the anti-T-cell monoclonal antibody OKT3 in relation to serum levels of tumor necrosis factor and interferon-gamma [corrected]." *N Engl J Med* 320, 1420-1421.

246 **Shlomchik, W. D. (2007).** „Graft-versus-host disease." *Nat Rev Immunol* 7, 340-352.

247 **Kim, P. S. & Ahmed, R. (2010).** „Features of responding T cells in cancer and chronic infection." *Curr Opin Immunol* 22, 223-230.

248 **Fourcade, J. *et al.* (2010).** „Upregulation of Tim-3 and PD-1 expression is associated with tumor antigen-specific CD8+ T cell dysfunction in melanoma patients." *J Exp Med* 207, 2175-2186.

249 **Fourcade, J. *et al.* (2012).** „CD8(+) T cells specific for tumor antigens can be rendered dysfunctional by the tumor microenvironment through upregulation of the inhibitory receptors BTLA and PD-1." *Cancer Res* 72, 887-896.

250 **Woo, S. R. *et al.* (2012).** „Immune inhibitory molecules LAG-3 and PD-1 synergistically regulate T-cell function to promote tumoral immune escape." *Cancer Res* 72, 917-927.

251 **Matsuzaki, J. *et al.* (2010).** „Tumor-infiltrating NY-ESO-1-specific CD8+ T cells are negatively regulated by LAG-3 and PD-1 in human ovarian cancer." *Proc Natl Acad Sci U S A* 107, 7875-7880.

252 **Valitutti, S. (2012).** „The Serial Engagement Model 17 Years After: From TCR Triggering to Immunotherapy." *Front Immunol* 3, 272.

253 **Sommermeyer, D. *et al.* (2016).** „Chimeric antigen receptor-modified T cells derived from defined CD8+ and CD4+ subsets confer superior antitumor reactivity in vivo." *Leukemia* 30, 492-500.

254 **Turtle, C. J. *et al.* (2016).** „CD19 CAR-T cells of defined CD4+:CD8+ composition in adult B cell ALL patients." *J Clin Invest* 126, 2123-2138.

255 **Yang, Y. *et al.* (2017).** „TCR engagement negatively affects CD8 but not CD4 CAR T cell expansion and leukemic clearance." *Sci Transl Med* 9.

256 **Sabatino, M. *et al.* (2016).** „Generation of clinical-grade CD19-specific CAR-modified CD8+ memory stem cells for the treatment of human B-cell malignancies." *Blood* 128, 519-528.

257 **Xu, Y. *et al.* (2014).** „Closely related T-memory stem cells correlate with in vivo expansion of CAR.CD19-T cells and are preserved by IL-7 and IL-15." *Blood* 123, 3750-3759.

258 **Wang, X. *et al.* (2016).** „Comparison of naive and central memory derived CD8(+) effector cell engraftment fitness and function following adoptive transfer." *Oncoimmunology* 5, e1072671.

259 **Hinrichs, C. S. *et al.* (2011).** „Human effector CD8+ T cells derived from naive rather than memory subsets possess superior traits for adoptive immunotherapy." *Blood* 117, 808-814.

260 **Hoffmann, J. M. *et al.* (2017).** „Differences in Expansion Potential of Naive Chimeric Antigen Receptor T Cells from Healthy Donors and Untreated Chronic Lymphocytic Leukemia Patients." *Front Immunol* 8, 1956.

261 **Kaneko, S. *et al.* (2009).** „IL-7 and IL-15 allow the generation of suicide gene-modified alloreactive self-renewing central memory human T lymphocytes." *Blood* 113, 1006-1015.

262 **Kaartinen, T. *et al.* (2017).** „Low interleukin-2 concentration favors generation of early memory T cells over effector phenotypes during chimeric antigen receptor T-cell expansion." *Cytotherapy* 19, 1130.

263 **Schmueck, M. *et al.* (2012).** „Preferential expansion of human virus-specific multifunctional central memory T cells by partial targeting of the IL-2 receptor signaling pathway: the key role of CD4+ T cells." *J Immunol* 188, 5189-5198.

264 **Ellis, J. (2005).** „Silencing and variegation of gammaretrovirus and lentivirus vectors." *Hum Gene Ther* 16, 1241-1246.

265 **Riviere, I., Dunbar, C. E. & Sadelain, M. (2012).** „Hematopoietic stem cell engineering at a crossroads." *Blood* 119, 1107-1116.

266 **von Kalle, C., Deichmann, A. & Schmidt, M. (2014).** „Vector integration and tumorigenesis." *Hum Gene Ther* 25, 475-481.

267 **Rosenberg, S. A., Restifo, N. P., Yang, J. C., Morgan, R. A. & Dudley, M. E. (2008).** „Adoptive cell transfer: a clinical path to effective cancer immunotherapy." *Nat Rev Cancer* 8, 299-308.

268 **Scholler, J. *et al.* (2012).** „Decade-long safety and function of retroviral-modified chimeric antigen receptor T cells." *Sci Transl Med* 4, 132ra153.

269 **Lombardo, A. *et al.* (2011).** „Site-specific integration and tailoring of cassette design for sustainable gene transfer." *Nat Methods* 8, 861-869.

270 **Sather, B. D. *et al.* (2015).** „Efficient modification of CCR5 in primary human hematopoietic cells using a megaTAL nuclease and AAV donor template." *Sci Transl Med* 7, 307ra156.

271 **Eyquem, J. *et al.* (2017).** „Targeting a CAR to the TRAC locus with CRISPR/Cas9 enhances tumour rejection.“ *Nature* 543, 113-117.

# 8. Appendix

## 8.1 Curriculum vitae

For reasons of data protection, the curriculum vitae is not included in the online version.

## 8.2 Presentations and posters

**Presentations**

"Modulation of the cytolytic strength in CTLs"
SFB TR36 "Principles and Applications of Adoptive T Cell Therapy", Retreat 2015, Döllnsee-Schorfheide, 22.-23.10.2015

"$CD8^+$ T cell memory formation is co-regulated by the cytolytic strength"
$20^{th}$ T Cell Meeting on T cell subsets and functions, Marburg, 29.-30.06.2017

"Immunological and translational consequences of an altered $CD8^+$ T cell cytolytic activity"
SFB TR 36 "Principles and Applications of Adoptive T Cell Therapy", Retreat 2017, Döllnsee-Schorfheide, 05.-06.10.2017

"Immunological and translational consequences of an altered $CD8^+$ T cell cytolytic activity"
SFB TR 36 "Principles and Applications of Adoptive T Cell Therapy", PhD Retreat 2017, Munich, 18.-20.10.2017

**Posters**

"Targeting the secretory pathway in T cells to enhance the cytolytic efficiency in adoptive T cell transfer"
FMP/MDC PhD Retreat, Bad Saarow, 15.-17.10.2015

"$CD8^+$ T cell memory formation under non-inflammatory conditions is co-regulated by the cytolytic strength"
$3^{rd}$ International Symposium on Adoptive T Cell Therapy, München, 17.-18.03.2016

"Targeting the secretory pathway in T cells to enhance the cytolytic efficiency in adoptive T cell transfer"
$10^{th}$ International PhD Student Cancer Conference, Cambridge (UK), 22.-24.06.2016

"Targeting the secretory pathway in T cells to enhance the cytolytic efficiency in adoptive T cell transfer"
FEBS $19^{th}$ International Summer School on Immunology, Hvar, Croatia 23.-30.09.2017

## 8.3 Acknowledgements

An dieser Stelle möchte ich einigen Menschen, die zum Gelingen dieser Arbeit beigetragen haben, meinen Dank aussprechen.

Allen voran möchte ich mich bei Dr. Armin Rehm für die Aufnahme in seine Arbeitsgruppe, die Vergabe des interessanten Arbeitsthemas und vor allem für die ausgezeichnete Betreuung bedanken. Er stand mir stets mit wissenschaftlichen Anregungen und auch praktischer Hilfe zur Seite und hat somit maßgeblich zum Entstehen dieser Dissertation beigetragen. Auch PD Dr. Uta E. Höpken möchte ich für die zahlreichen wissenschaftlichen Anregungen danken.

Vielen Dank an Prof. Dr. Oliver Daumke für seine Bereitschaft die Betreuung meiner Dissertation an der Freien Universität Berlin zu übernehmen und seine wertvollen Ratschläge in den Committee Meetings.

Im Rahmen des SFB TR36 sind viele wertvolle Diskussionen und Kooperationen entstanden, die im Laufe meiner Arbeit von Bedeutung waren. Hier möchte ich mich ausdrücklich bei Dr. Dana Hoser und Dr. Mario Bunse bedanken, die für alle theoretischen und praktischen Fragen ein offenes Ohr und aufschlussreiche Antworten hatten.

Ein besonders großer Dank gilt all meinen Kolleginnen und Kollegen aus der AG Rehm und AG Höpken für das angenehme Arbeitsklima und die große Hilfsbereitschaft im und außerhalb des Labors. Bei Kerstin Gerlach möchte ich mich für die umfassende Einführung in die neuen Methoden zu Beginn meiner Doktorarbeit und die fortwährende praktische Unterstützung bedanken. Mein Dank gilt ebenso Kerstin Krüger und Heike Schwede für die Unterstützung in praktischer Hinsicht und im Tierhaus. Besonders herzlich möchte ich mich hier bei Marleen Gloger bedanken, die manch langen Abend bereichert hat und mich stets aufzumuntern wusste. Auch Florian Scholz sei für viele anregende Gespräche und die schokoladige Unterstützung lieb gedankt.

Aus tiefstem Herzen möchte ich mich bei meinen Herzensmenschen, meiner Familie und meinen Freunden bedanken, deren bedingungslose Liebe, Unterstützung und endlose Geduld mir Kraft und Motivation gegeben haben.